Mannich base metal complexes and their thiocyanate analogues as catalysts in the oxidation of Catechol

A thesis submitted in fulfilment of the requirements
for the degree of

Doctor of Philosophy

In

Chemistry

By

AYENI AYOWOLE OLAOLU

M.Sc Hons (Obafemi Awolowo University, Nigeria)

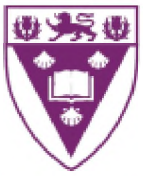

RHODES UNIVERSITY
Where leaders learn

Department of Chemistry
Grahamstown 6140, South Africa

April, 2018

ABSTRACT

The study focused on the design of new Cu(II) and Fe(III) complexes, with or without thiocyanate (NCS^-), as possible candidates of catechol oxidation using 3,5-di-tert-butylcatechol (3,5-DTBC) as substrate. Two classes of Mannich bases were studied depending on the active methylene group from which they were formed, being either p-cresol or acetaminophen. The ligands were characterised by ^1H and ^{13}C NMR spectroscopy. Crystal structures of three of the ligands are newly reported, along with detailed discussion of polymorphism observed in one of the ligands, and the nature of the hydrogen within the ligands in the solid state as well as in solution.

The Mannich bases behaved as bidentate (NO), tridentate (NNO) and tetradentate (NNOO) ligands on coordination to Cu(II) and Fe(III) ions in which the hydroxyl group may be protonated or deprotonated. Coordination was determined by IR spectroscopy, investigating shifts in νOH, νC-O and in νCNC of the Mannich bases. The νCNC stretching frequencies ν1 and ν2 of asymmetrical piperazine Mannich bases were observed to shift upward in few cases upon complexation and this is attributed to (chair-boat) conformational change. The mode of coordination of the thiocyanate was determined by IR spectroscopy. Of the forty metal complexes investigated, six groups of metal complexes were identified as follows: (i) $M_a(L^n)_aCl_b{\cdot}cH_2O$; (ii) $M_a(HL^n)_a(NCS)_aCl_b$; (iii) $M_a(L^n)_a(NCS)_aCl_b$; (iv) $M_a(HL^n)_aCl_b{\cdot}cH_2O$; (v) $M_a(L^n)_a(NCS)_a{\cdot}cH_2O$; (vi) $M_a(HL^n)_a(NCS)_a{\cdot}cH_2O$ where a = 1 - 2 ; b = 1 – 4, c = 1 – 8. Molar conductivity values of 4.38 – 161.77 $\Omega^{-1}.cm^2.mol^{-1}$ for the Cu(II) and Fe(III) complexes in DMSO showed that they range from non-electrolytes to 1:1 and 1:2 electrolytes.

Electronic spectra for the ligands and the complexes were conducted in DMF and DMSO. The ligands are characterised by $\pi\rightarrow\pi^*$ and $n\rightarrow\pi^*$ transitions. Intraligand charge transfer transitions peculiar to the nitro group were observed at about 430 nm for the nitro containing ligands. On coordination, these bands overshadowed the d-d transitions particularly for the nitro-Mannich

bases. On complexation, ligand to metal charge transfer transitions associated with the hydroxyl were observed between 320 – 420 nm. Charge transfer transitions associated with the thiocyanates were also observed and discussed. The d-d transitions for high spin Fe(III) complexes are spin forbidden and generally uninformative. Those of Cu(II) are spin allowed and allow tentative structural proposals. Square planar and octahedral geometry are generally prevalent in the Cu(II) complexes with trigonal bipyramidal observed in few instances. The Fe(III) complexes are generally octahedral.

Thirty-nine of the forty synthesised Cu(II) and Fe(III) complexes were catalytically active on the substrate (3,5-DTBC) in DMF with turnover rates (k_{cat}) reported in the range of 1.86 ± 0.09 to 112.32 ± 3.72 h^{-1}. From this pool of complexes, sixteen isostructural pairs were identified in terms of geometry, molecular formula and the source of the Mannich base and the following conclusions were made: The presence of thiocyanate in the metal complexes reduce catecholase activity; the Cu(II) complexes generally have better activity but the Fe(III) complexes become more relatively active with highly electron donating groups while the Cu(II) complexes become less; dinuclear complexes have greater activity than the mononuclear.

ACKNOWLEDGMENTS

Firstly, I use this medium to show my deepest gratitude to God Almighty, the Father of our Lord Jesus Christ for perfecting the good work He started in me.

My appreciation goes to my supervisor, Prof. Gareth Watkins who supervised this research work in a meticulous way for his scholarly and financial contributions towards attending the International Conference on Coordination Chemistry (ICCC42).

I also acknowledge Dr Eric Hosten of the Department of Chemical Science, Nelson Mandela Metropolitan University, Port Elizabeth, South Africa for his assistance towards obtaining the x-ray crystallography data of the novel Mannich bases in this study.

With a deep sense of appreciation, I acknowledge my dear wife Mrs Ayowande Ayeni and my son Tijesunimi for standing by me during the extended nights dedicated to the pursuit of this degree and for bearing the strain of being apart in the concluding part of this degree. Also to my parents Mr and Mrs Vincent Ayeni and all my siblings (Bukola, Seun, Bunmi, Sola and Damilola) and my in-laws of the family of Dr A. Adefioye for their prayers and encouraging words.

Due appreciation also goes to my sponsor Tertiary Education Trust Fund (TETFund) in Nigeria, my place of work; Obafemi Awolowo University (OAU Ife) for granting me study leave, the former Dean of the Faculty of Science (OAU Ife) Prof. A.O. Ogunfowokan for his enduring support and all staff of the Department of Chemistry (OAU Ife) especially my mentor Prof. G.O. Egharevba for taking care of the department while I pursue this degree.

To every member of the Redeemed Christian Church of God in Eastern Cape particularly House of Praise Parish here in Grahamstown including those from the early years Dr and Dr(Mrs) Komlan Agbedahin; Dr and Mrs Nelson Oghenekaro, Pastor Rotimi Adefehinti I say thank you all.

And to my amiable friends and lab mates (F12) including Thommas, Taffy, Vitalis, Siya, Magaji and my dear sister Bukola Oguntade among others I say *gracias*.

Finally, I express my gratitude to the Department of Chemistry especially Mr Francis Chindeka who carried out the elemental analysis and for conference attendance (ICCC42) and Rhodes University research bursary at very difficult times without which completing this work would have been tough.

CONFERENCE PARTICIPATION AND PUBLICATIONS

Conferences

(a) Symposium on Chemico- and Biomedical Research, October 27th, 2014, Rhodes University, Grahamstown, South Africa **(Oral and Poster Presentations).**

(b) The 17th South African Chemical Institute (SACI) Inorganic Chemistry Conference, 28th June – 2nd July 2015. Rhodes University, Grahamstown South Africa **(Poster Presentation).**

(c) 42nd International Conference on Coordination Chemistry (ICCC42), July 3rd – 8th, Brest, France. **(Poster Presentation).**

Publications

(a) **Ayeni A.O.**, Watkins G.M. (2018): Kinetic Studies of the impact of thiocyanate moiety on the catalytic properties of Cu(II) and Fe(III) complexes of a New Mannich base. Journal of Molecular Structure 1158 19 -25.

(b) **Ayeni A. O.**, Watkins G. M., Hosten E. C. (2018): Polymorphism of a new Mannich base [-4-methyl-2-((4-(4-nitrophenyl)piperazin-1-yl)methyl)phenol], Journal of Molecular Structure 1160 38 – 45.

(c) **Ayeni A. O.**, Watkins G. M., Synthesis and Evaluation of catecholase activities of metal complexes of 1, 4-substituted piperazine Mannich base of 4-acetamidophenol. Turkish Journal of Chemistry, DOI: 10.3906/kim-1710-20 (accepted).

(d) **Ayeni A. O.**, Watkins G. M., Impact of thiocyanate on the Catecholase activity of Cu(II) and Fe(III) complexes of 2-((4-(2-hydroxy-4-methylbenzyl)piperazin-1-yl)methyl)-5-methylphenol (a Mannich base). Acta Chemica Iasi (accepted).

TABLE OF CONTENTS

CHAPTER THREE

RESULTS

CHAPTER FOUR

DISCUSSION

LIST OF FIGURES

LIST OF SCHEMES

LIST OF TABLES

LIST OF ABBREVIATIONS

$CHCl_3$	Chloroform
DSC	Differential Scanning Calorimetry
DMF	dimethylformamide
DMSO	Dimethylsulphoxide
3,5-DTBC	3,5-di-tert-butylcatechol
3,5-DTBQ	3,5-di-tert-butylquinone
FT-IR	Fourier Transform Infrared
nm	nanometre
ppm	parts per million
cm^{-1}	per centimetre
dm^{-3}	per decimetre cube
h^{-1}	per hour
PXRD	powder x-ray diffraction

CHAPTER ONE

INTRODUCTION AND LITERATURE REVIEW

1.1 General introduction to catalysis

Catalysts are generally known as the workhorse of chemical transformations in the chemical industry. Approximately 85–90 % of the products of chemical industry are made by catalytic processes [1]. They provide an alternative, energetically favourable mechanism to the non-catalytic reaction, thus enabling processes to be carried out under industrially convenient conditions of pressure and temperature. The chemical industry cannot exist without catalysis, which is an indispensable tool in the production of fuels, bulk and fine chemicals. For scientists and engineers, the field of catalysis is a tremendously challenging, highly multidisciplinary field [1] because of the constant need for improvement on the catalytic abilities of existing catalysts and the introduction of more efficient candidates into the industry.

The interest in this study is homogenous catalysis where all participating species are present in the liquid phase. This is different from heterogeneous catalysis where solid support catalysts are used with the reactants/products present in other phases.

Table 1.1: Comparison of homogenous and heterogeneous catalysts [2].

Homogeneous catalysts	Heterogeneous catalysts
Good activity	Catalyst-product separation easy
Good selectivity	Recyclable
High atom efficiency	Low quantities of catalyst utilised
Require mild process conditions	High total turnover numbers achieved
Molecular structure of catalysts is known	
It allows the fine-tuning of catalysts	

Some comparable advantages of homogenous and heterogeneous catalysts are listed in Table 1.1 above.

The tremendous impact of enzymes on many catalytic reactions is notable as such reactions could not have been possible or could have taken place much slower. Enzymes can also be referred to as macro-molecular biological catalysts, they accelerate or catalyze chemical reactions. They act on molecules referred to as substrates and convert them into different molecules, called products. Almost all metabolic processes in the cell need enzymes in order to occur at rates fast enough to sustain life [3].

The field of enzyme kinetics deals with the investigation of how enzymes bind substrates and turn them into products. The rate data used in kinetic analyses are commonly obtained from enzyme assays. The theory (Michaelis–Menten kinetics) widely applied in studying enzymes was proposed in 1913 by Leonor Michaelis and Maud Leonora Menten [4]. This theory has been widely employed in the understanding of some of the parameters involved in homogenous catalysis. Catalytic processes that involve oxidation reactions are receiving great attention nowadays and this is where well designed coordination compounds possessing similar features to existing enzymes come in to play their role.

1.1.1 Catalytic activation of small molecules

The binding and activation of small molecules like dioxygen under mild operating conditions by enzymatic systems and biomimetic complexes is a very active research field connecting chemical synthesis and catalysis with the technological world.

Reactions involving the catalytic insertion of one or both atoms of dioxygen into an organic substrate are of importance in the synthesis of metabolic products and intermediates. Dioxygen also serves as an electron sink in the oxidation of a variety of small molecules including those of biological importance such as ascorbic acid, catechols and amino acids. The various binding modes of dioxygen found in the literature are presented in Scheme 1.1 [5, 6].

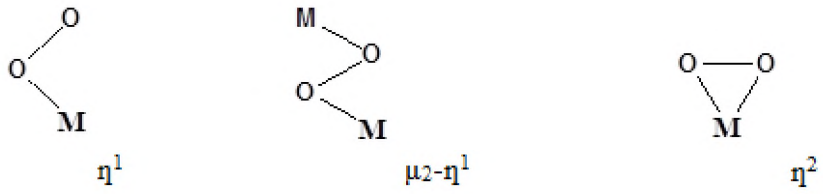

Scheme 1.1: Various coordination modes of O_2 to metal ions.

Apart from oxygen molecules, a few other small molecules are receiving attention as outlined below. A review was presented by Vigato *et al.* [7] on the ability of dinuclear copper(II) complexes to act as catalysts in oxidation processes and their analogous mononuclear analogues was carried out using the oxidation of the two well-known two-electron reducing agents, ascorbic acid and 3,5-di-tert-butylcatechol (DTBC), and N,N,N',N'-tetramethyl-p-phenylenediamine (TMPD) which is a one-electron reducing agent as model reactions.

Jayarathne *et al.* [8] also reported the activity of Cu-Fe bimetallic complexes towards CS_2 and N_2O. Research into activation of small molecules such as CO_2 is motivated by their role as greenhouse gases and their potential use in chemical synthesis of commercial products. Large kinetic barriers associated with the reactivity of such small-molecule substrates necessitates the use of catalysts [8]. In general, the activation of small molecules including oxygen has a wide application in the area of plant and fruit protection and environmental pollution clean-up. Enzymes and by extension metal complexes with biomimetic abilities can assist in bioremediation, biodegradation and general environmental clean-ups [9].

1.2 Catechol metabolism

Catechol (or 1,2-dihydroxybenzene) is widely used in the chemical industry as an important intermediate in manufacturing pesticides and medicines (e.g. L-dopa and methyl L-dopa used in the treatment of Parkinson's disease and hypertension) and can also be used to produce

perfumes -(e.g., piperonal), dyes, photosensitive material, special inks, antioxidants and polymerization inhibitors, promoters, light stabilizers, anticorrosive agents and fungicides [10]. Catechol is used in the manufacture of the artificial flavours vanillin, ethyl vanillin for use in food processing and also in the manufacture of the insecticides carbofuran and propoxur. The world production of catechol is more than 30,000 tonnes [11]. Overexposure to catechol and phenol vapour are known to cause irritation of the upper respiratory tracts [12].

Catechol metabolism is important both biologically and environmentally. Two major enzymes play the key role in these reactions, catechol dioxygenases and catechol oxidases as discussed below:

a. Catechol dioxygenases:

These are mononuclear non-heme iron enzymes that can be isolated from bacteria. They catalyze the insertion of dioxygen into catechols with simultaneous ring cleavage [13]. The possibility of enzyme promiscuity that makes these compounds mimic catechol oxidase has been highlighted by Carmago *et al.* [14]. These are mononuclear non-heme iron enzymes that catalyze the oxygenation of catechols to aliphatic acids via the cleavage of aromatic rings [15]. They incorporate oxygen molecules into their substrate. While the active site of catechol dioxygenases most frequently contains iron those possessing manganese have also been reported. Two types are highlighted herein:

Catechol 1, 2-dioxygenase which has Fe^{3+} as a prosthetic group and belongs to the enzymes that perform intradiol cleavage,

Catechol 2,3-dioxygenase which, belongs to the extra-diol cleaving enzyme class, has four identical subunits of 32KDa and contains a catalytic Fe^{2+} per subunit [16].

b. Catechol oxidase:

Catechol oxidase (which are found in bacteria, fungi, and plants) a type III copper enzyme and catalyzes the oxidation of a broad range of o-diphenols to o-quinones through the four-electron reduction of molecular oxygen to water. Catechol oxidase is often inferred to be involved in plant defence as highly reactive o-quinones auto polymerize to brown polyphenolic catechol melanins, a process that is thought to protect the damaged plant from pathogens or insects. Crystallographic characterizations of catechol oxidase from sweet potato (*Ipomoea batatas*) revealed the presence of a dinuclear copper center in accordance with that from other plant sources. Klabunde *et al.*,[17] isolated the first crystal structures of the catechol oxidase from *Ipomoea batatas* (sweet potato) in three catalytic states: the native *met* [Cu(II)Cu(II)] state, the reduced *deoxy* [Cu(I)Cu(I)] form, and in the complex with the inhibitor phenylthiourea [17].

In addition to tyrosinase, these two belong to a family of enzymes called polyphenol oxidase the key difference to catechol oxidase is that while tyrosinase can catalyse the hydroxylation of phenols to diphenols((monophenolase activity) as well as the oxidation of the o-diphenol to the o-quinone (diphenolase activity) , catechol oxidase only possesses diphenolase activity [18].

Most functional mimics of catechol oxidase are dinuclear Cu(II) complexes, although catalytically active complexes containing other transition metal ions such as Mn, Fe, Co, or Ni are also known [19]. However, the focus of this work is more attuned to mimicking catecholase oxidase employing Cu(II) and Fe(III) and that will be given attention onward.

1.2.1 Mechanism of catechol oxidation

There are two widely proposed mechanisms, one by Krebs and co-workers [20] and the other by Solomon and co-workers [21].

As proposed by Krebs and co-workers [20], the catalytic mechanism starts from the *met* form of catecholase enzyme Figure 1.1. Center of the *met* form dinuclear complex reacts with the catechol through monodentate binding of catechol to the CuB center. This results in the formation of quinone and *deoxy* form in which Cu(II) is reduced to Cu(I). Afterwards in the presence of oxygen, dioxygen and substrate bind simultaneously to the solvent bonded CuA center (by replacing the solvent molecule) and to the CuB center of *deoxy* form respectively [22].

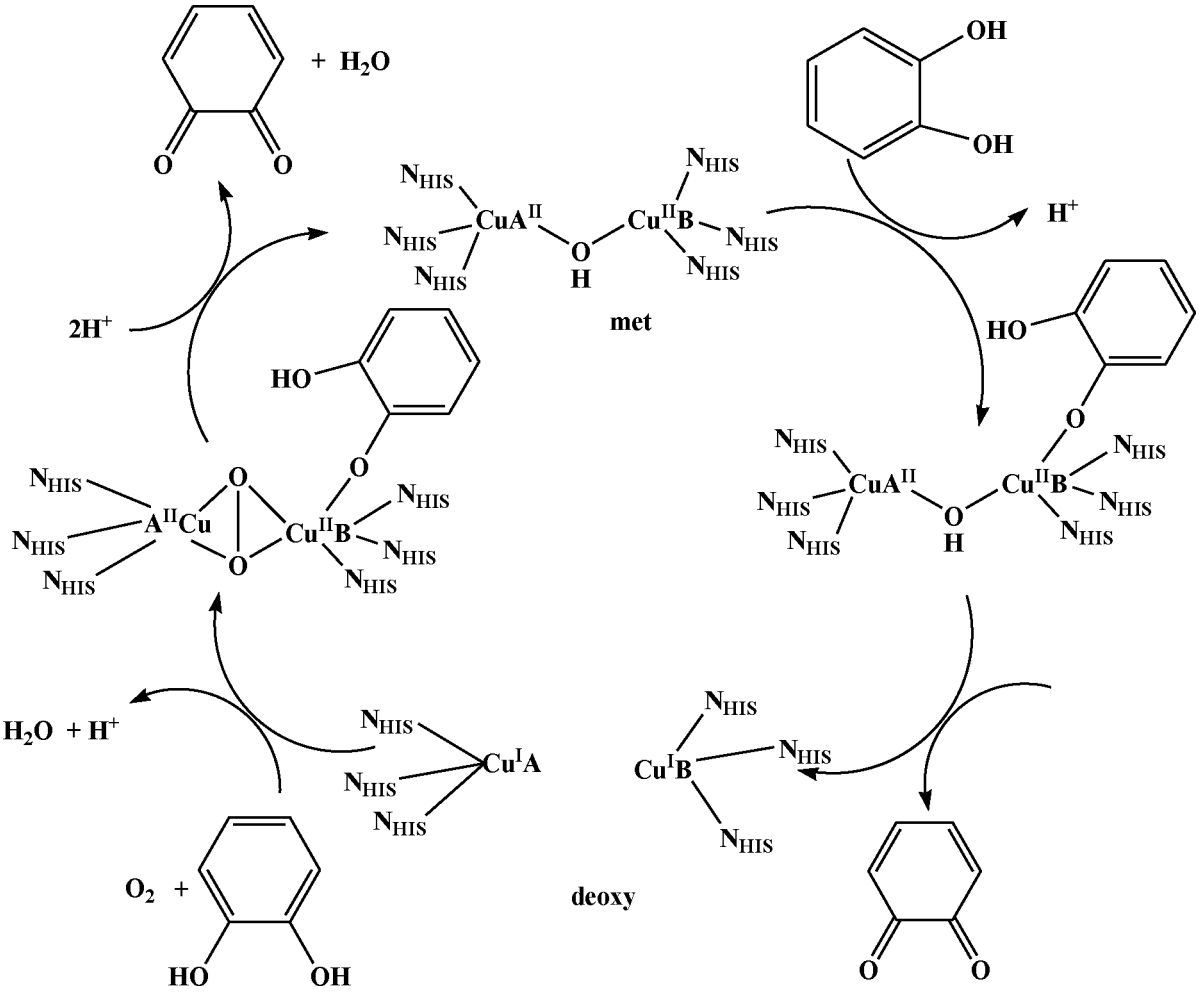

Fig. 1.1: Catalytic cycle of catechol oxidase from *Ipomoea batatas*, as proposed on the basis of structural, spectroscopic and biochemical data.

In this model, CuB is six-coordinated with a tetragonal planar coordination and the CuA site retains the square pyramidal geometry with a vacant sixth coordination site followed by the

cleavage of the O–O bond. This results in the formation of quinone with loss of a water molecule and restores the *met* form and thus completes the catalytic cycle.

A very similar catalytic mechanism had been proposed earlier by Solomon *et al.* for the catecholase activity of the structurally related type-3 protein tyrosinase. The cycle starts from the oxy and met states where a diphenol substrate binds to the met state (for example), followed by the oxidation of the substrate to the first quinone leading to the formation of the reduced state of the enzyme. The oxy state is formed after binding with oxygen, which subsequently receives the second diphenol molecule. Further oxidation to the second quinone yields the met state again and thereby ends the catalytic cycle. The second proposed mechanism lacks experimental support because the formation of bridging superoxide radical ion has never been reported for copper species [23].

1.2.2 Mimicking metalloenzymes

During studies of enzyme activity, it has been noted that certain enzymes contain metal ions that are essential to their function. The enzymes could be inactivated by removing the metal ions with a chelating agent, and reactivated by adding metal ions to the solution. These enzymes were termed metalloenzymes. The modern definition is that metalloenzymes are basically enzymes that contain one or more metal atoms. Usually this definition is restricted to those enzymes in which the metal ion is within the active site, and thus participates in the enzymatic reaction [24].

Metalloenzymes are of particular interest because their structure, which may be viewed as a metal centre with a complex ligand, resembles that of 'conventional' homogeneous catalysts. In addition almost all enzymes involved in reactions of small (2-5 atoms) molecules like oxygen are metalloenzymes, although not all metalloenzymes are involved in the reactions of small molecules. The oxidation of catechol to benzoquinone which involves dioxygen activation is also found in the category and the industrial importance of reactions involving

small molecules has increased the attention for designed or 'man-made' metalloenzymes [25]. Some of the metal complexes of interest are discussed below.

1.2.2.1 Cu complexes

Copper complexes with a wide variety of supporting ligands have so far been developed in the bioinorganic model chemistry area to replicate the active site structures and functions of copper proteins (enzymes). Particular attention has recently been focused on copper-dioxygen chemistry not only in bioinorganic chemistry but also in the field of catalytic oxidation reactions [26, 27].

Krebs and co-authors have also explored the function of the bridging hydroxo group in the catecholase activity [28]. In a series of dicopper(II) complexes with phenol-based ligands (shown below) the complex with the exogenous μ-hydroxo bridge found to have highest catalytic activity. The bridging by a hydroxyl group enforces the complex to adopt a very strained square pyramidal geometry, which makes it prone to exchange the μ-hydroxo bridged structural motif in favour of the bridging catechol coordination. In contrast to above alternative bridging, ligands with a larger bite distance lead to a relaxed conformation resulting in low activity.

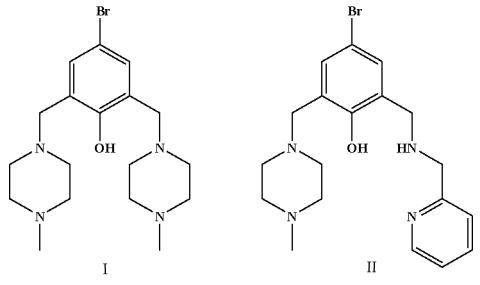

Fig. 1.2: Symmetrical and unsymmetrical Mannich bases of p-bromophenol.

The above explanation will suffice for observed differences in the catecholase activity observed for the metal complexes of the two ligands depicted in Figure 1.2 below. Activities in Cu(II) complex of I are higher than that of II [28].

So far, several types of mononuclear, dinuclear, trinuclear, and tetranuclear copper-dioxygen complexes have been structurally characterized, and their physicochemical properties and reactivities have been explored in detail, providing profound insights into the dioxygen activation mechanism by copper complexes [29].

From the isolated standpoint of catalysis, the general principles that should govern the construction of metal-containing active sites in enzymes are fairly clear. For example, a metal playing the role of Lewis acid needs to have an appropriate charge and coordination geometry, and the quality of its interactions with a substrate can be described via the HSAB (Hard –Soft-Acid-base) theory [30].

1.2.2.2 Fe complexes

Mono- and binuclear non-heme iron centers are frequently present in a variety of protein systems that perform important biological functions involving dioxygen. The mononuclear non-heme iron proteins that catalyze the oxidative cleavage of catechol or its derivatives with the incorporation of molecular oxygen are exemplified by catechol dioxygenases. The oxidative cleavage of catechol and other dihydroxy aromatics is a key step in the biodegradation by soil bacteria of naturally occurring aromatic molecules and many aromatic environmental pollutants [31, 32].

Mitra *et al.* synthesized a dinuclear Fe(III) complex, $[Fe_2(L)_2]$ using N,N' -bis(3-methoxysalicylaldimine)-1,3-diaminopropan-2-ol], which is an (N,O) donor trianionic Schiff base ligand. Kinetic experiments were performed spectrophotometrically with the complex using 3, 5-DTBC as the substrate in methanol, dichloromethane and acetonitrile [33]. The

kinetics parameters were moderately high with less coordinating solvents acting as the best medium for the experiment.

Although coordination compounds have been designed in order to mimic these catalytic properties, with few exceptions, most of the examples of synthetic catecholases described in the literature are related to dinuclear Cu(II) biomimetics, while di-iron systems have been rarely explored. One such interesting example has been recently reported by Neves and co-workers [34], in which it was possible to demonstrate that a dinuclear Fe(III)Fe(III) complex is able to catalyze both the cleavage of phosphodiester bonds and the oxidation of catechols to the corresponding quinones. In addition, it has also been reported that synthetic mononuclear iron(III) complexes show catalytic activity in the oxidative cleavage of 3,5-di-tert-butylcatechol by O_2 to yield specifically the intradiol product (1,2-dioxygenase activity) .

Furthermore, the unusual reactivity of molecular oxygen with the iron(III) catecholate complex of intradiol-cleaving catechol dioxygenases has been attributed to a partial transfer of electron density from the coordinated catecholate to the metal ion, whereby the active site is endowed with a partial iron(II) semiquinonate character, which is thought to be responsible for the reactivity [35].

Kalakhanov *et al*., have demonstrated that iron(III) complexes of pyridine, dihydroxylbenzoic acid and dihydroxylnaphthalenic acid are active in the hydroxylation of phenols to catechol [36].

Velusamy and coworkers in 2003 reported the synthesis of the following bis(phenolate) ligands displayed in Figure 1.3 utilizing the Mannich reaction [37]. The iron(III) complexes were thereafter synthesized and studied as structural and functional models for the intradiol cleaving catechol 1,2-dioxygenases (CTD). It was observed that the substituents on the bis(phenolate) ligands tend to tune the Lewis acidity of the iron(III) center and hence determine the course

and products of dioxygenase activity of the complexes, thereby providing support to the substrate activation mechanism of intradiol cleavage [38].

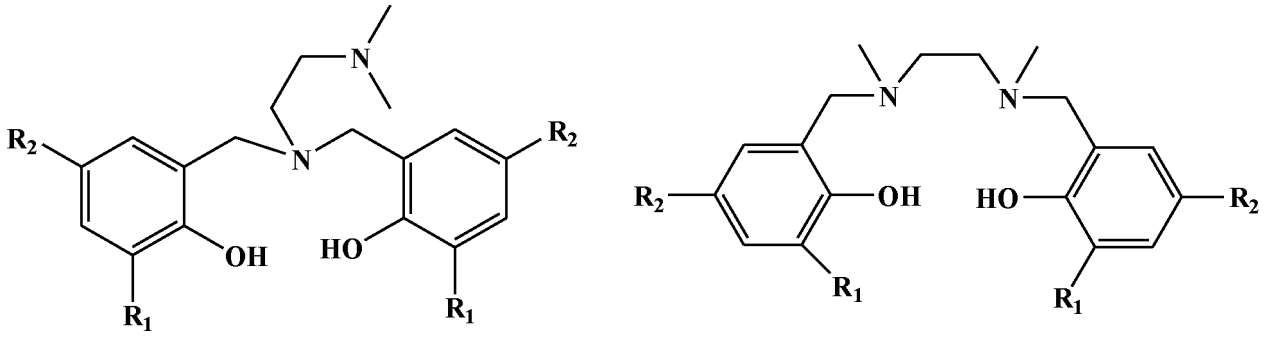

Fig. 1.3: Bis(phenolate) Mannich bases of 2,4-dimethylphenol.

Though Fe(III) complexes appear to mimic catechol dioxygenase better i.e cleaving the phenolic substrate rather than oxidizing it to catechol, catalytic promiscuity (a single catalytic site can catalyze more than one chemical transformation) is a common occurrence [39].

1.2.2.3 Ni complexes

It is noteworthy to mention nickel complexes as potential biomimetic compounds owing to their radical pathway mechanism for the oxidation of catechol. Biswas *et al.* reported studies on how reduced Schiff-base ligands with an N, N, O-donor set and containing a phenol group have been used to prepare dinuclear nickel(II) complexes, and their catechol oxidase-like activity has been examined and compared subsequently [40].

Consequently, research focused on the design of metal centres capable of bio-mimicking the activity of different enzymes is on the increase [41]. Such metal complexes (artificial enzymes) have same catalytic function but these are more stable and structurally less complex than enzymes. The naturally occurring enzymes with appropriate flexibility are more favourable to bind the substrate and transition state by an induced fit mechanism. A high activity is observed for the naturally occurring enzymes is attributed to their high flexibility as compared to synthetic models which are often too rigid or too flexible. Nevertheless, synthetic enzyme

models are helpful in understanding the mechanistic aspects of enzyme action. The biomimetic studies are necessary and must be continuously widened [19], as this current research seeks to do. Continuous research in this area is very useful and promising for the development of new, more efficient bio inspired, environment friendly catalysts which may find future applications in industrial synthesis.

1.3 Mannich reaction

The choice of reaction for the design of the ligands in this study is based on the fact that the Mannich reaction affords the two of the group of compounds that have featured extensively in the field of biomimetic activity (phenols and amines) to become linked together. This will allow the formation of an array of ligands and also the possibility of increased chelation with central metal ion owing to increase in ligand denticity.

The Mannich reaction (aminomethylation) consists of the condensation of a substrate (R-H) possessing at least one active hydrogen atom (alkyl ketones, phenols, NH-heterocycles, etc.) with formaldehyde/paraformaldehyde/dioxane (or, occasionally, other aldehydes) and a primary or secondary amine or occasionally, ammonia [42, 43].

The choice of starting materials is important and this includes:

- Formaldehyde, either as aqueous solution (formalin), paraformaldehyde or 1,3,5-trioxan is the aldehyde most frequently used.
- Amines are employed either as free bases or hydrochlorides.
- Most widely used solvents include ethanol, sometimes methanol and isopropyl alcohol [44].

The reaction conditions reportedly employed for some of the substrates of the active methylene group substrates employed in this study are:

Substituted phenols: substrate, secondary amine and aqueous formaldehyde (occasionally paraformaldehyde) in alcoholic solvents and heated for a short time (up to several hours) or are allowed to stand at room temperature for a longer time; up to a few days [45, 46]. More recently solvent free conditions are being employed in improving the yield and ease of formation of product [47].

Substituted acetophenones: substrate, secondary amine (sometimes amine hydrochloride) paraformaldehyde (or aqueous formaldehyde) are refluxed in alcoholic solvents for several hours or in form of microwave assisted reactions [48, 49].

Extensive studies have been carried out on the Mannich reaction and these have led to discussions on the mechanism. Various kinetic studies carried out on the reaction suggest that the mechanism widely acceptable and supported in this research can be represented as follows in Scheme 1.2.

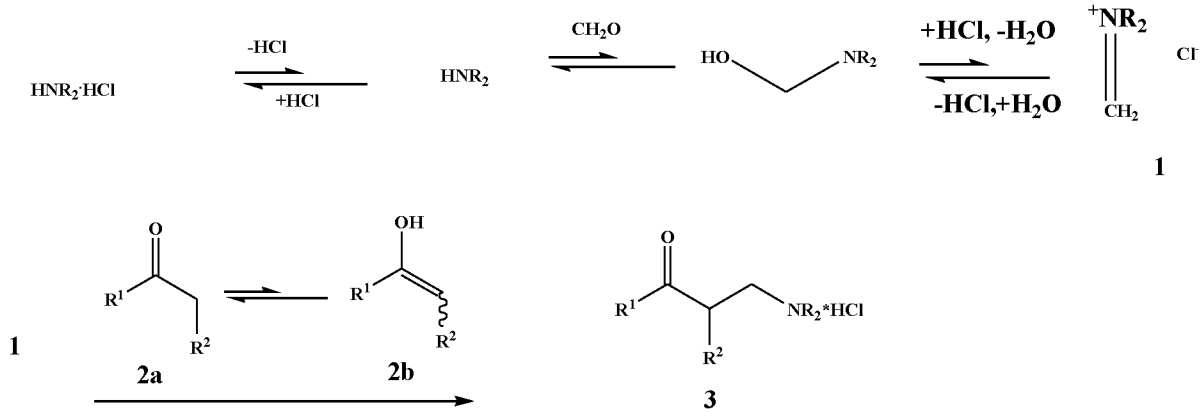

Scheme 1.2: Mechanism of Mannich reaction [46].

Sometimes, dibases are obtained alongside monoamino-methylated products and therefore extensive separation and purification will be required. Brycki *et al.* in 1991 estimated the amount of dibases formed in the aminomethylation of *p*-nitrophenol by studying on the (Ar-CH_2-N) signal using ^{1}H NMR spectroscopy [50].

Mannich bases are very reactive; in fact they can easily be transformed into numerous other compounds. The reactivity of the bases accounts for several interesting properties (mainly pharmacological). The possibilities of forming C- and N- Mannich bases have been highlighted by G. Roman [51] as outlined in Table 1.2, with the C-Mannich bases the most widely studied and reported.

1.3.1 Applications of Mannich reaction

Mannich bases are usually NO or NNO donor ligands because of their origin mainly from phenols and acetophenones, though various other conformations or donating groups can be obtained particularly with the use of bridging groups.

In phenol-based ''end-off'' complexes, in addition to the phenolate endogenous bridge the presence of one or two exogenous bridges made up of acetate, hydroxide, azide, cyanate etc. give favourable distance between the bimetal centers resembling biosites [52, 53].

1.3.1.1 Sources of Mannich bases

According to literature survey, Mannich bases of cresols (*ortho*-, meta- and para-) have received more attention than those of substituted acetamidophenols. In this work, the Mannich bases are from two sources as listed below:

1.3.1.1.1.1 *p*-Cresol

A wide variety of metal complexes of Mannich bases originating from p-cresol have been studied. The availability of the two *ortho*-positions to the hydroxyl group makes 2, 6-aminomethylation possible to give bis Mannich base in addition to monobases; the bis Mannich bases possess excellent coordination abilities to metal ions. The isolation of the desired product sometimes requires rigorous separation procedures [54, 55].

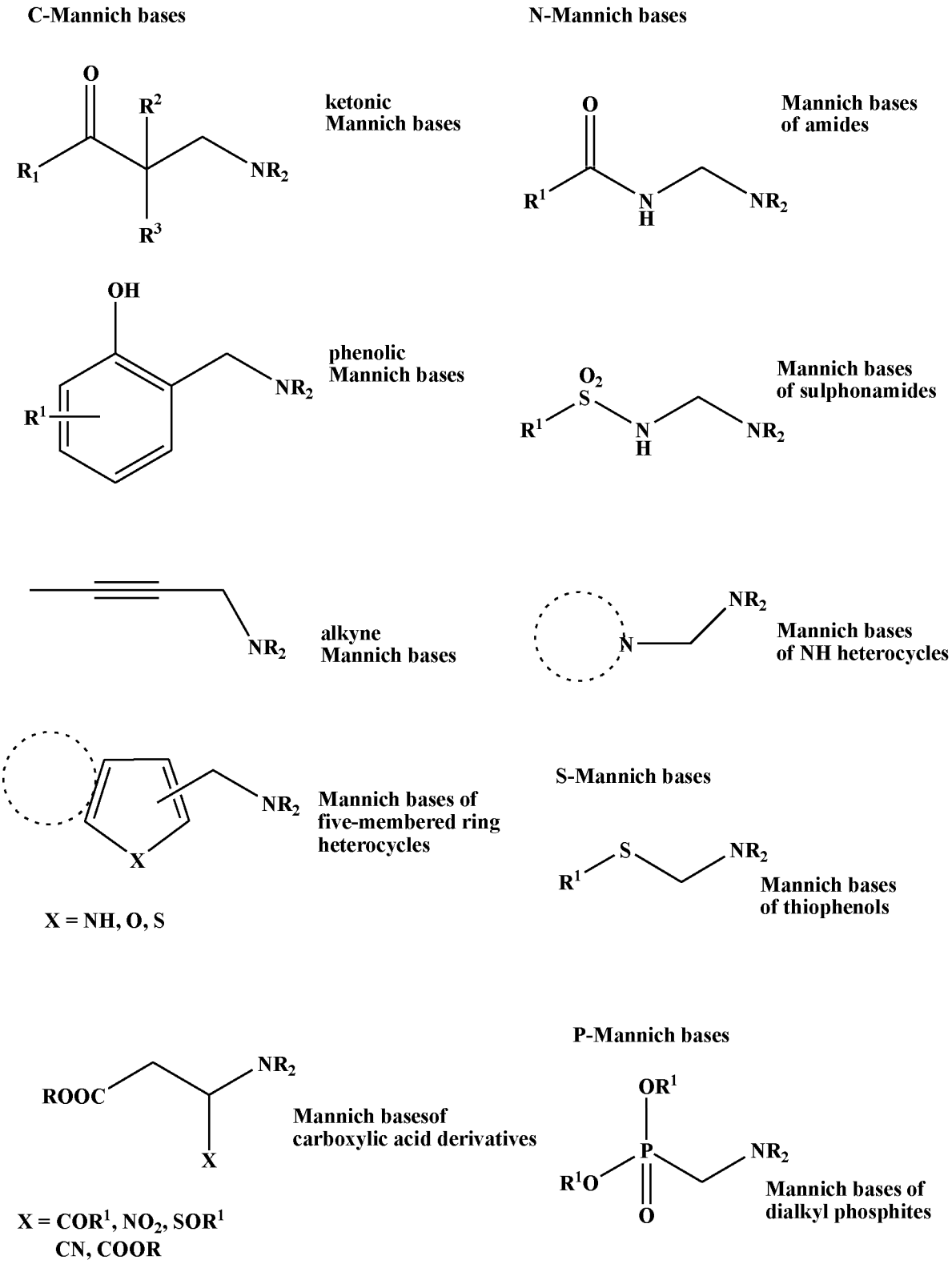

Table 1.2: Examples of various types of Mannich bases [51].

1.3.1.1.2 *p*-Acetamidophenol

Studies on the Mannich bases of 4-acetamidophenol have not received as much attention as those of 4-methylphenol. Also there is insufficient discussion on the coordination properties of Mannich bases of 4-acetamidophenol. One of the reasons proposed to be responsible for this is the tendency of reactions (substitution/complexation) to take place at the amide end of 4-acetamidophenol. Some idea can be obtained from reports on the metal complexes of azo dyes derived from 4-acetamidophenol [56, 57].

Blade-Font and Rocabayera [58] reported the synthesis of Mannich bases of 4-acetamidophenol with secondary amines like diethylamine, dimethylamine, piperidine and morpholine amongst other substituted phenols as starting material [58]. Rangisetty *et al.* [54], took the synthetic work a little further by reporting synthesis using 1-(2-pyridyl)piperazine as secondary amine. It must be stated that their synthetic works were enroute to the synthesis of dihydrobenzofurans and arylaminoquinoxalines (as antimalarials) respectively with no spectroscopic data reported for the Mannich reaction products. In both cases their studies were based on previous work reported by Burckhalter and co-workers [59] in 1948 and monoaminomethylation were successfully achieved. It must be noted that the possibility of the formation of dibases greatly exist when para-substituted phenols are employed and when this happens rigorous separation techniques are required. This unwanted side effect can be minimised by employing favourable reaction conditions and sometimes using an excess of the substituted phenols. The Mannich reaction is not new though there are new modifications in terms of substrate and stereochemistry, and it has been employed in the past in the synthesis of medicinal compounds as listed in Figure 1.4 including e.g. tolmetin and tramadol (anti-inflammatory drug), rolitetracycline (Mannich base of tetracycline), fluoxetine (anti-depressant) and azacyclophanes (anti-arthritic) [60, 61].

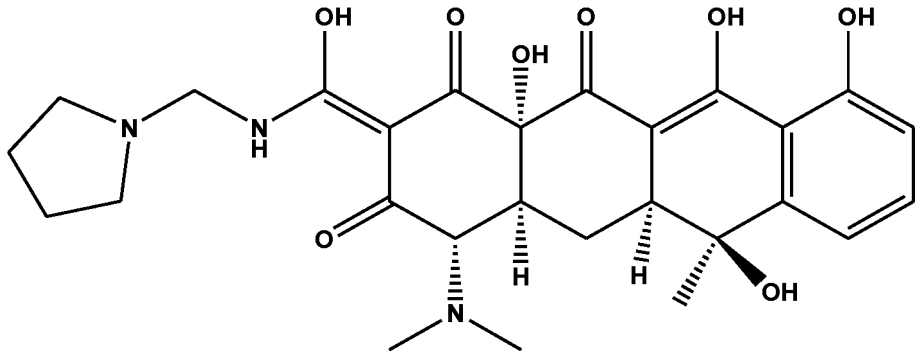

Rolitetracycline

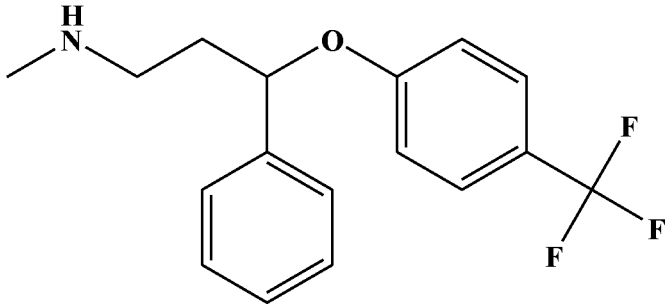

Fluoxetine

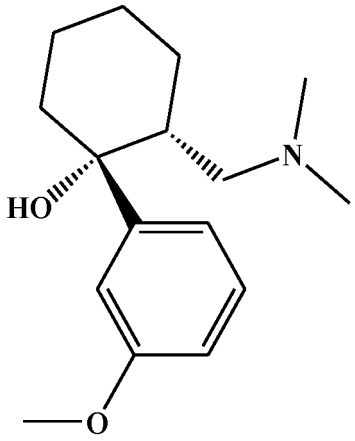

Tramadol

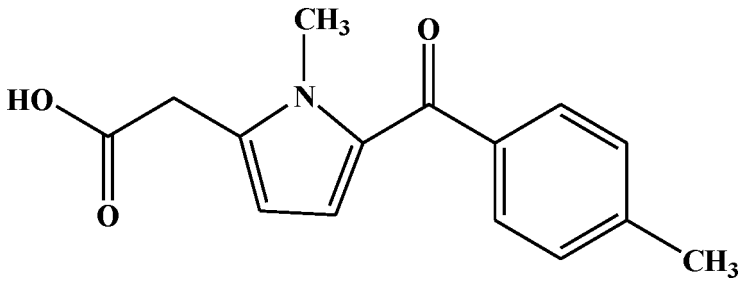

Tolmetin

Fig. 1.4: Some Mannich base medicinal compounds.

1.4 Thiocyanate

SCN is a small, strongly acidic pseudohalide thiolate, ambidentate ligand [62]. This has been referred to as a potentially useful therapeutic agent with host defense and antioxidant properties [63].

The linear thiocyanate group can be present in compounds as an anion or as a ligand acting as a monodentate ligand capable of coordination through the sulphur or nitrogen atoms, or as a bridging ligand. The great coordination ability of the thiocyanate group and a great variety of its bonding modes are responsible for the existence of a relatively great number of coordination compounds in liquid and solid state in which this group occurs [64].

Experimental evidence leads to the general conclusion on the bonding in certain group of metals as follows; class A metals (hard acids) tend to form *N*-bonded thiocyanate complexes, whereas class B metals (soft acids) tend to form *S*-bonded thiocyanate complexes [65].

The bridging ability of thiocyanate group has also resulted in the formation of multinuclear coordination compounds with interesting coordination properties. Though SCN has been administered in the past for various medical treatments ranging from hypertension to cystic fibrosis (CF), the correlation of increased SCN with better lung function is suggestive that there may indeed be a rational basis for SCN therapy in CF [66].

In addition, the thiocyanate-bridged metal-coordination complexes have received special attention because they exhibit interesting electrochemical, zeolitic, magnetic, and photomagnetic properties [67, 68].

1.4.1 Variation in bonding schemes of thiocyanate

According to Molecular Orbital calculations by Wagner [69], the π-electron structure of the thiocyanate ion may be represented as in Figure 1.5.

Where the numbers written over the atoms are the resulting electronic charges on the atoms, and the numbers written under the bonds are the π-bond orders.

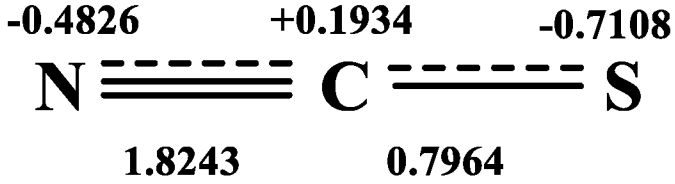

Fig. 1.5: Bond lengths and charge densities of NCS.

The difference in the charge densities of the N- and S- atoms is not very large [69]. This may be the reason why the NCS- exhibit a variety of coordination modes. The various bonding modes (including terminal and bridging) as highlighted in the literature [70, 71] are depicted below in Figure 1.6.

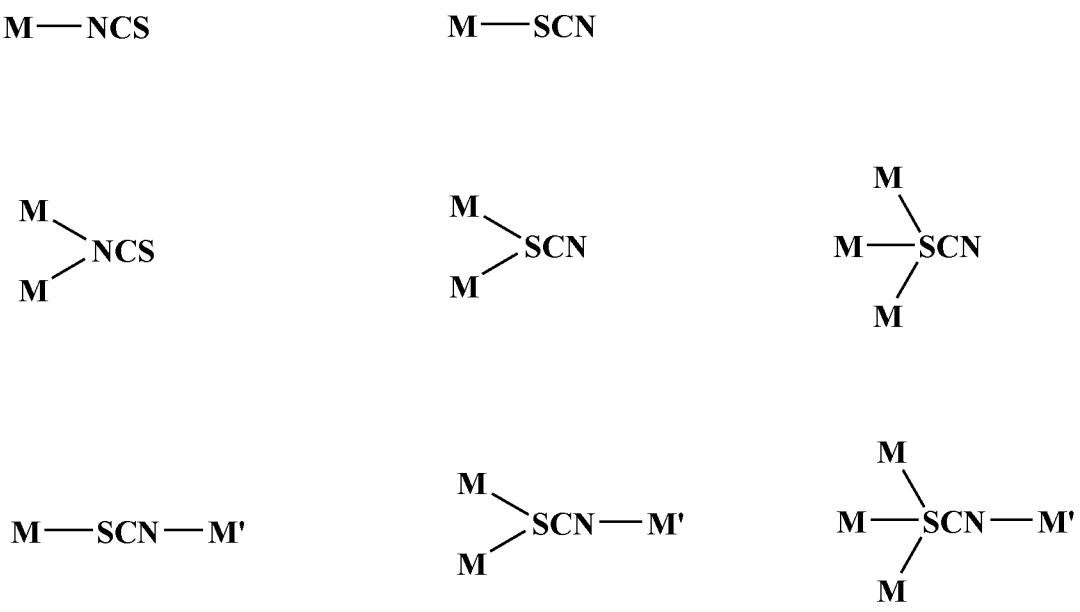

Fig. 1.6: Various bonding modes of NCS [70, 71].

1.4.2 Influence of thiocyanate in biological and chemical systems

The roles of thiocyanate (SCN^-) and its analogues in several biological and catalytic systems are well documented in the literature. In this section a brief description on some of them is given below:

Tahboub *et al.* [72] in 2005 reported investigations into the potential role of the co-substrate, thiocyanate (SCN^-), in modulating the activity some Fe(III) containing enzymes: myeloperoxidase (MPO) and other members of the mammalian peroxidase superfamily lactoperoxidase (LPO) and eosinophil peroxidase (EPO). They noted the presence of SCN^- can serve as a substrate or an inhibitor and this leads to an array of impact on the iron microenvironment [73].

The positive antimicrobial effects of increasing concentrations of thiocyanate (SCN^-) and H_2O_2 on the human peroxidase defence system are well known. For example, lactoperoxidase (a peroxidase enzyme) secreted from mammary, salivary, and other mucosal glands that functions as a natural antibacterial agent. Lactoperoxidase is a member of the heme peroxidase family of enzymes [74, 75]. The tested thiocyanate and H_2O_2 mixtures showed no relevant antimicrobial effect. However, by adding lactoperoxidase enzyme, the mixtures became not only an effective bactericidal (against *Streptococcus mutans* and *sanguinis*) but also a fungicidal (against *Candida albicans*) agent [76].

Anhydrotetracycline oxygenase is an enzyme that participates in tetracycline biosynthesis. Behal *et al.* [77] reported that the addition of benzyl thiocyanate increased the specific activity of the enzyme. The effect of the addition was most conspicuous in the growth phase and more pronounced in the low-production strain than in the producing variant.

Phenoxazinone synthase, is a multi-copper oxidase enzyme, found naturally in the bacterium *Streptomyces antibioticus*. It is known to catalyze the oxidative coupling of two molecules of

a substituted o-aminophenol to the phenoxazinone chromophore in the final step for the biosynthesis of actinomycin D [78, 79].

Guha *et al.*[80] also reported the synthesis and catalytic activities including catecholase activity of three new mono-manganese(II) complexes of a compartmental ligand shown below, one of which contains thiocyanate depicted (2), $[Mn(HL)(H_2O)_3]$ **(1)**, $[Mn(HL)(SCN)_2(H_2O)]$ **(2)**, and $[Mn(HL)\{N(CN)_2\}(H_2O)_2]$ **(3)**. The trend of catecholase activity is **1** > **2** > **3**, the presence of bulkier substituent in **3** compared to **2** brings about a more facile interaction between the substrate and the metal centre. The compartmental ligand (HL) is presented in Figure 1.7 below.

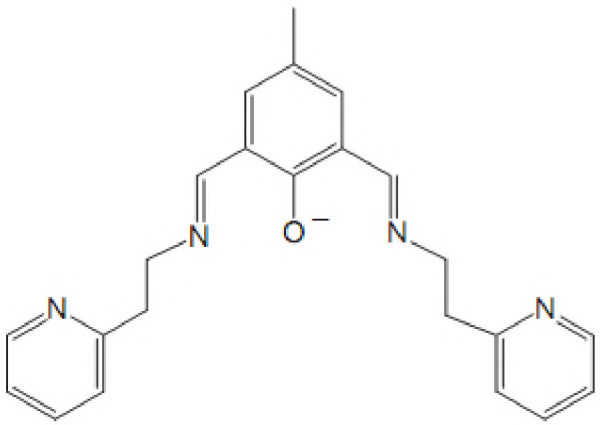

Fig. 1.7: Compartmental Schiff base in deprotonated form [80].

Ramadan *et al.* [81] carried out the synthesis, characterization, and ascorbic acid oxidase biomimetic catalytic activity of cobalt(III) oxime complexes of a new tetradentate tetraaza ligand which was prepared via Schiff-base condensation of 3, 4-diaminotoluene with 2,3-butandione monoxime in aqueous solution. A series of mixed ligands from Lewis bases like pyridine, thiophene, triphenylphosphine, or n-pentylamine were equally prepared and studied. Also the influence of thiocyanate, cyanate groups etc. on catalytic abilities was investigated and an interesting trend was observed [81]. Coordination of Lewis-base to cobalt(III) increases the strength of the axial ligand field and consequently increases the tetragonal splitting

parameter values, in agreement with the degree of irregularity of coordination geometry thereby increasing the catalytic activity of the corresponding metal complexes[Olive]. Summarily, their study showed that SCN is a good leaving group and thus easily makes available in solution a coordination site for an incoming substrate to occupy.

Also Adak *et al.*[82] in their quest to examine the comparative impact of bridging groups on catecholase activity compared thiocyanate and azide incorporated metal complexes of a Schiff base prepared from N, N-dimethylethylenediamine and 9-anthracenaldehyde. High turnover rates were recorded for the catecholase activity of these two metal complexes with marginal roles played by the bridging groups [82].

Studies on the biomimetic activity involving mononuclear cobalt(II) complexes of a group of Schiff bases of o-aminophenol showed that the presence of thiocyanate groups clearly reduce the catalytic efficiency. As the thiocyanate ion is a stronger binding ligand than chloride ion or water molecule in similar complexes, the coordination of substrate to the metal center also containing thiocyanate is less favourable [83].

In conclusion, from all the various reports outlined above; the ability of thiocyanate group to greatly alter the rate, course of biomimetic abilities of various metal complexes on vast number of enzymes is not in doubt with both positive and negative impacts on catalytic activity observed in the literature.

1.5 Designing Mannich base metal complexes

Multinuclear transition metal complexes have become a central theme of current research in biomimetics because of their potentially useful properties. They are involved in some notable catalytic processes. Their important use for modelling the metal active sites of metalloproteins and their recent applications in the area of nanoscale materials have drawn the focal point of

attraction of modern chemists towards the synthesis and characterization of such metal complexes.

A number of dinuclear complexes from various types of ligand systems (including Mannich bases) have been prepared and examined in terms of their oxygen uptake or redox processes of oxygen, their catalytic activity and at times their biological activities.

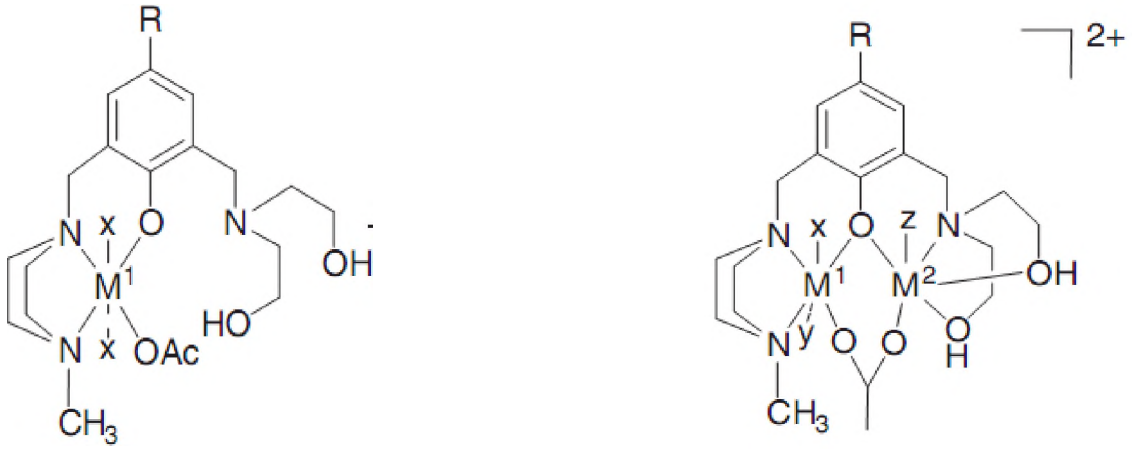

Fig. 1.8: Mononuclear and dinuclear Mannich base metal complexes with bridging groups [84].

Most popular with Mannich bases are mononuclear and binuclear complexes. Generally multinuclear (particularly binuclear complexes) have received greater attention because often the oxidation capabilities being studied e.g. the oxidation of catechol generally requires two-metal centres in close proximity.

Bharathi and coworkers studied the coordination of binuclear metal complexes [Cu(II), Ni(II), and Zn(II)] and reported the catecholase activity of only the Cu(II) complexes, although detailed kinetic study was not carried out [84]. The binuclear complexes are found to be more active than their mononuclear counterparts as shown in Figure 1.8 above.

Sanyal *et al.* [85] carried out studies on mononuclear and dinuclear zinc complexes of some Mannich bases containing halide groups as counter ions. Interestingly, the mononuclear

compounds are more reactive towards the oxidation of catechol than the dinuclear analogues. The complexes studied are depicted in Figure 1.9 below.

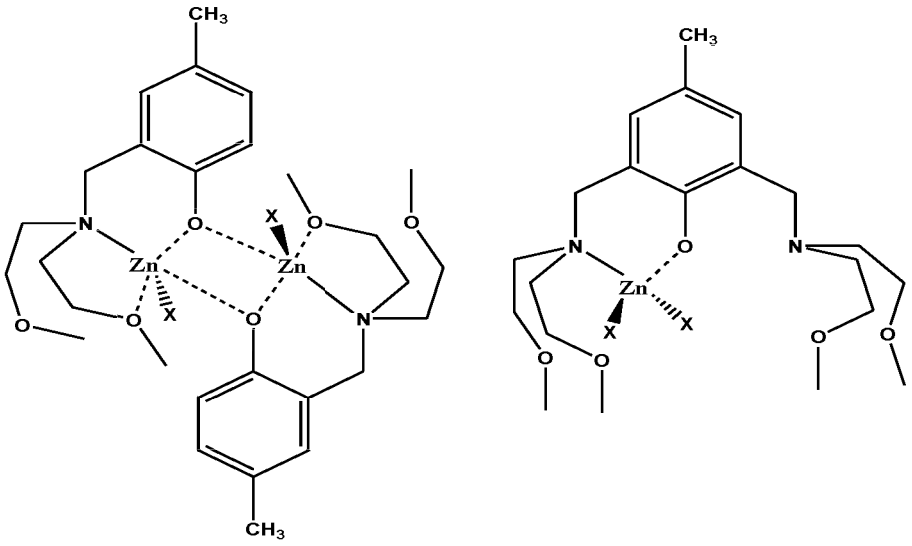

Fig. 1.9: Mononuclear and dinuclear Mannich base metal complexes without bridging groups (where x represents halogens Cl, Br and I) [85].

Mechanistic investigation in catecholase activity revealed the stability of phenoxyl radical generated from the system as the governing factor. The role of the halogen atom is also in turn related to the enhancement of phenoxyl radical stability which establishes finally that chlorine is the strongest oxidant followed by bromine and then iodine which ends up showing no activity [85].

Size appears to be the major difficulty associated with the modelling of metalloenzymes. The following modelling techniques in the field of computational chemistry are sometimes employed to provide insight into the dynamics of metalloenzymes/ substrate interaction:

- Molecular mechanics
- Semi-empirical quantum mechanics
- Ab initio quantum mechanics

Nevertheless, modelling the enzyme features using dinuclear complexes requires careful control of the interaction of the two metal centres along with structural parameter. Some previous observations have shown that redox-active metal ions such as Cu(II), Mn(II), Mn(III) catalyse the reaction neatly in a metal-centred redox pathway, while redox inactive metal ion such as Zn(II) (and also Ni(II)) takes a radical pathway for the same reaction (a few exceptions remain for Ni(II) systems) [86].

Reedijk and coworkers have put forward four approaches been used in the mechanistic studies on these model compounds for studying catecholase activity.

- Substrate-binding studies.
- Structure-activity relationship.
- Kinetic studies on catalytic reactions.
- Stoichiometric oxidation of catechol substrates by the peroxo- and oxo-dicopper complexes [87].

Out of these, the approach of structure activity has been more frequently employed by various groups. Under this approach the relationships between metal-metal distance, steric factor, exogenous bridging ligand; ligand structure, solvent properties and pH of the solution, with the catecholase activity have been exploited. The conditions above have to be strictly met particularly in the case of binucleating ligands. Various literature based on these consideration above have reported catecholase activity of many metal complexes acting as metalloenzymes [88, 89].

1.5.1 Geometry, conductivity, solvent, pH consideration in Catecholase activity

The synthetic models studied on the reactivity of copper(II) complexes towards catechols implicated geometry around the copper ions as the most dominant feature in determining the catalytic activity of the complexes [90]. Non-planar mononuclear complexes and binuclear complexes with the two coppers separated by ca. 3 - 4 Å catalyse the oxidation process, while

square-planar mononuclear complexes and dinuclear complexes with a large Cu-Cu distance (>5 Å) are generally unreactive towards catechol [91 - 93]. In model systems, some authors observed better activity if the coordination geometry is a trigonal bipyramidal, while some others observed better activity for square pyramidal or even square planar [94 - 97].

It has been previously observed that planar mononuclear copper(II) complexes are not active catalysts toward oxidation of catechols, supposedly due to the lack of effective steric match between the substrate and the catalyst [98]. However, the results in the literature show that square-planar complexes can be effective catalysts [99, 100] and that geometrical effects are only one facet of the activity determinants. Although five-coordinate trigonal bipyramidal and tetrahedral have redox potential values approaching the four-coordinate square planar the latter exhibits lower reactivity, again suggesting the difference in reactivity of these chelates is not dependent only on electrochemical character of copper(II) [101]

Also, a strong equatorial ligands field opposes the interaction of copper ion with a substrate, disfavouring formation of the intermediate copper-substrate adduct [102]. A strong field also disfavours reduction from copper(II) to copper(I) during the catalytic cycle. Das *et al.* [103], studied the biomimetic abilities of four Ni(II) complexes of oxime based Schiff base in acetonitrile and found out that octahedral complexes exhibited catecholase like activity, but square planar species were inactive. The octahedral complexes contain water molecules that are easily removed to create free coordination sites for 3,5-DTBC unlike their square planar counterparts where binding to substrate was not evidenced [103].

The x-ray crystal structure of this catechol dioxygenase reveals a trigonal bipyramidal geometry around the iron(III) core [104, 105]. This similar geometry to the iron(III) centre in catechol dioxygenases may have also favoured trigonal bipyramidal or distorted octahedral complexes Fe(III) in biomimetic activity [106, 107].

Conductivity of solutions of metal complexes which is dependent on the presence of counter ions outside the coordination sphere has shown this to also play a minimally appreciable role in catalytic activity. Studies on three Ni(II) complexes of aminoethylpiperazine Schiff bases showed that the presence of Cl^- within the coordination sphere (low conductivity) brings about the neutralization of the effective positive charge on nickel(II) to a greater extent compared to complexes where all chloride ions are outside the coordination sphere. In conclusion, lower conductivity values can influence biomimetic abilities negatively [108].

The influence of solvent properties (e.g. polarity), pH and use of buffer systems have been shown to play a huge role in the catecholase activity studies of metal complexes with the results well documented [109, 110]. Literature search has revealed studies where relative rates of oxidation were compared in methanol, dichloromethane, acetonitrile, DMSO; results show that protic-medium viscous solvents like acetonitrile and methanol are the best solvents.

It has also been reported that metal complexes in solvents with high coordinating abilities like DMF and DMSO may display relatively lower catecholase activity because the possibility of catechol–substrate adduct formation is retarded [111, 112]. Neves *et al.*, also observed that the addition of a small amount of an aqueous buffer TRIS pH 8 solution to the oxygen saturated methanol solution increases significantly the reaction rates observed for the catalytic behaviour of the metal complexes studied [113].

1.6 Enzyme kinetics

It is important to understand the mechanisms of enzymatic reactions to be able to design new catalysts, both modified proteins and completely synthetic molecules, and also to design inhibitors for those reactions that have pharmacological significance [114].

In general, enzymes are known for their high efficiency and specificity but, cases exist where a single catalytic site can bring about more than one chemical transformation. This is called

catalytic promiscuity and this is a phenomenon reasonably well described for biological systems [38]. For example, the aminopeptidase isolated from *Streptomyces griseus* with a dinuclear Cu(II) active site is capable of hydrolysing phosphate esters and peptides, while also possessing oxidative properties on catechols. The values obtained for it activity is close to those observed for the native enzyme-gypsywort catechol oxidase [115].

One clear focus in catalysis is to carry out kinetic study and examine how the rate of the reaction changes as the concentration off substrate is varied with the enzyme concentration kept constant. Firstly, the initial rate (V_o), and thereafter the plot of V_o versus substrate concentration [S], will give the following nonlinear regression curve, called a Michaelis-Menten curve as shown in Figure 1.10 below.

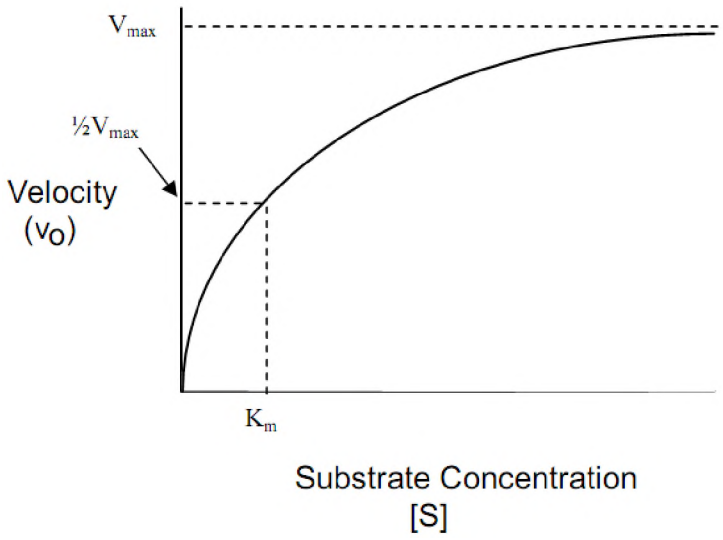

Fig. 1.10: Michaelis-Menten plot.

The Michaelis-Menten equation is represented below:

$$V = \frac{d[P]}{dt} = \frac{V_{max}[S]}{K_M + [S]}$$

Where p = product

As [S] increases, V_o eventually becomes independent of [S]. The velocity at which this occurs is called V_{max}, and it is the fastest that the given amount of enzyme can operate (the maximum

rate at saturated concentration). The [S] that yields $^1/_2V_{max}$ is another important kinetic parameter called the Michaelis-Menten constant, designated K_m. K_m is important in that it indicates the [S] at which the enzyme is most effective at altering the rate of the reaction. The derivation of the equation relies on the concept of free diffusion, thus the equation may not be readily applicable in very concentrated systems owing to limited mobility and so creating some limitations [116]. Consequently, some slight variations to these equations (like employing integrated forms of Michaelis-Menten equations through the use of nonlinear least squares) in fitting the behaviour of some enzymes have been reported [117, 118].

1.6.1 Lineweaver-Burk plots

The Lineweaver-Burk plot (also referred to as the **double reciprocal plot**) is a graphical representation of the Lineweaver–Burk equation of enzyme kinetics. It was described by Hans Line Weaver and Dean Burk in 1934 [119]. It provides a useful graphical method for the analysis of the Michaelis-Menten equation. The double reciprocal plot is given in Figure 1.11 below.

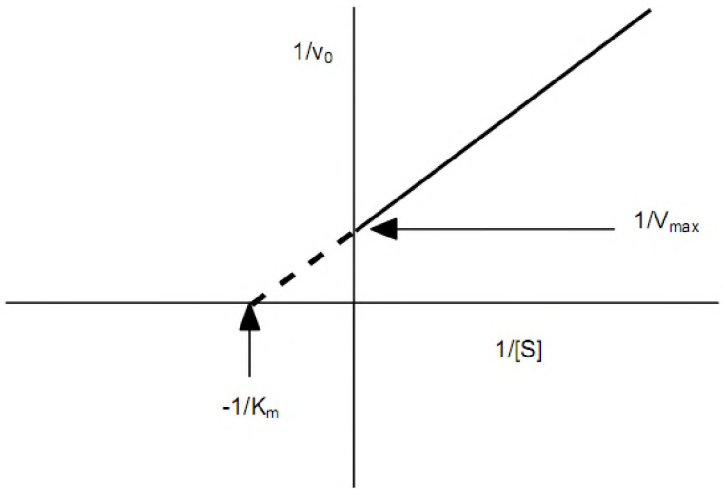

Fig. 1.11: Lineweaver-Burk plot.

Some of the concerns or limitations associated with Lineweaver-Burk plots include error in the calculating the reciprocal of the rate of reaction, extrapolation, solubility issues and the uneven

weighing of data points [120]. However the method remains popular because it allows for a reasonable estimation of K_m and V_{max} [121, 122]. An alternative to the above method is the Eadie – Hofstee plot.

1.6.2 Methods of measuring Catecholase activity

A number of laboratory techniques are used in the evaluation of catecholase activities of biomimetic molecules. For example, catecholase activity of tyrosinase is evaluated by either of the following, measurement of oxygen uptake during enzymatic reaction; the reduction of the oxidized phenolic substrate by ascorbic acid or on the spectrophotometric determination of the oxidation products [123].

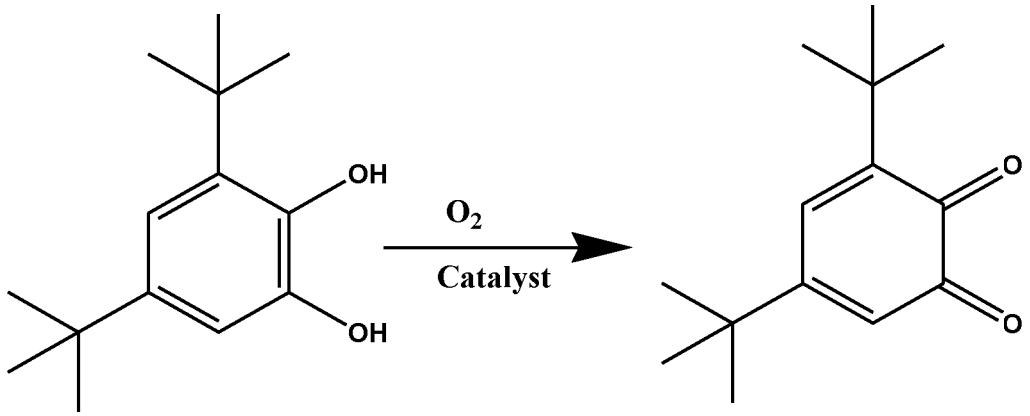

Scheme 1.3: The basic reaction for the oxidation of catechol.

The reaction showing the oxidation of 3, 5-di-tert butyl catechol employed as the substrate is shown above in scheme 1.3.

Another method widely used is to isolate the product 3, 5-DBTQ after the completion of the spectrophotometric determination of the product (i.e scanning within the region of the λ_{max} of the product) followed by the isolation and examination of the product by ^1H NMR spectroscopy. The following NMR data were reported for 3, 5-DBTQ by Mitra *et al.* [124] ^1H NMR ($CDCl_3$, 400 MHz): δH = 1.16 (s, 9H), 1.20 (s, 9H), 6.15 (d, J = 2.4 Hz, 1H), 6.86(d, J =

2.4 Hz, 1H). Similar data have been also reported from another experiment with heterogeneous catalysts by Louloudi *et al.* [125].

Within our research group, a technique previously adopted is one whereby the reaction mixture is prepared in substrate: complex ratios of 100:1 in the appropriate solvent (e.g. DMF) while adding some triethylamine in order to prevent complex decomposition. The reaction mixture is then aerated by stirring vigorously for 1-5 days. At the conclusion of the reaction, the mixture was concentrated to dryness in vacuo and the residue analysed by ^{1}H NMR spectroscopy to determine the substrate: product ratio. Data for conversion (%) and recyclability (%) of the metal complex are reported [126, 127].

1.7 A Review of physical methods

1.7.1 UV-Visible spectroscopy

There exist a number of different possible origins for the electronic absorption spectra of complexes. The intense bands are highlighted below:

1.7.1.1 Ligand spectra

Organic molecules frequently occur as ligands in transition metal complexes, and particularly if these molecules already contain π-electron systems, they will themselves possess characteristic absorption spectra, which will usually be located in the ultraviolet region. Where such organic molecules are bonded to a metal in a complex ion, it generally seems that only small alterations occur in the ligand spectrum. Thus thiocyanate and many other polyatomic ions commonly possess very intense bands in the region of 50,000cm^{-1} (200 nm) and once again little significant change seems to occur to these upon co-ordination. In Mannich bases, intraligand transitions (e.g $\pi \rightarrow \pi^*$) occurs around 250 nm and undergo usually hypsochromic or bathochromic shifts in the spectra of the metal complexes [128, 129].

1.7.1.2 Charge-transfer spectra

Due to the close environment of the metal atom and the ligands, and the bonding between them, the likelihood exists of new transitions occurring, these involving the transfer of an electron from the ligand to the metal or vice-versa. The position of the CT band is reported as transition energy and depends on the solvating ability of the solvent. A shift to lower wavelength (higher frequency) is observed when the solvent has high solvating ability [130].

Another very interesting transition commonly observed and very structurally diagnostic are the d-d transitions. Insights into the electronic properties of interest of the metal ions studied in this research work as observed in solution are briefly discussed below.

1.7.1.3 Cu(II) complexes

The commonest oxidation state in most copper complexes is (+2). Copper(II) complexes are mostly blue or green, however the nature of the ligand does influence the colour of the isolated complexes. The origin of the colour is due to the presence of an absorption band in the 600 – 900 nm region of the spectrum of the complexes [131]. Jahn-Teller distortion is a common occurrence in non-linear degenerate orbitals that are not symmetrically occupied and this result in the lowering of the energy. The usual coordination numbers adopted by Cu(II) are 4, 5 and most commonly 6. The crystal field splitting pattern is given in Figure 1.9.

In octahedral crystal field, the ground state electronic distribution of Cu^{2+} is $t_{2g}^6e_g^3$ which yields ^2E_g term. The excited electronic state is $t_{2g}^5e_g^4$ which corresponds to $^2T_{2g}$ term. Thus only one single electron transition, i.e., $^2E_g \rightarrow {}^2T_{2g}$, is expected in an octahedral crystal field with the difference of about 10Dq. Octahedral coordination is distorted either by elongation or compression of octahedron leading to tetragonal symmetry. Normally, the ground ^2E_g state is split due to Jahn-Teller effect and hence lowering of symmetry is expected for Cu(II) ion [132].

The five coordinated system of Cu(II) complexes is not commonly observed and in few cases documented, a distorted square pyramidal geometry commonly results. In penta-coordinating ligand (N_4S), Bhattacharya *et al.* attributed the band at 608 nm to d-d transition in a square pyramidal geometry [133]. A similar observation has been made in some dinuclear Cu(II) complexes of Mannich base [84, 134]. By changing to coordinating solvents (e.g from chloroform to acetonitrile) Neves *et al.* reported a slight shift in the d – d transition to higher wavelength [135]. The Crystal field splitting of the d-orbitals of a central ion depicting various geometries is given in Figure 1.12 below.

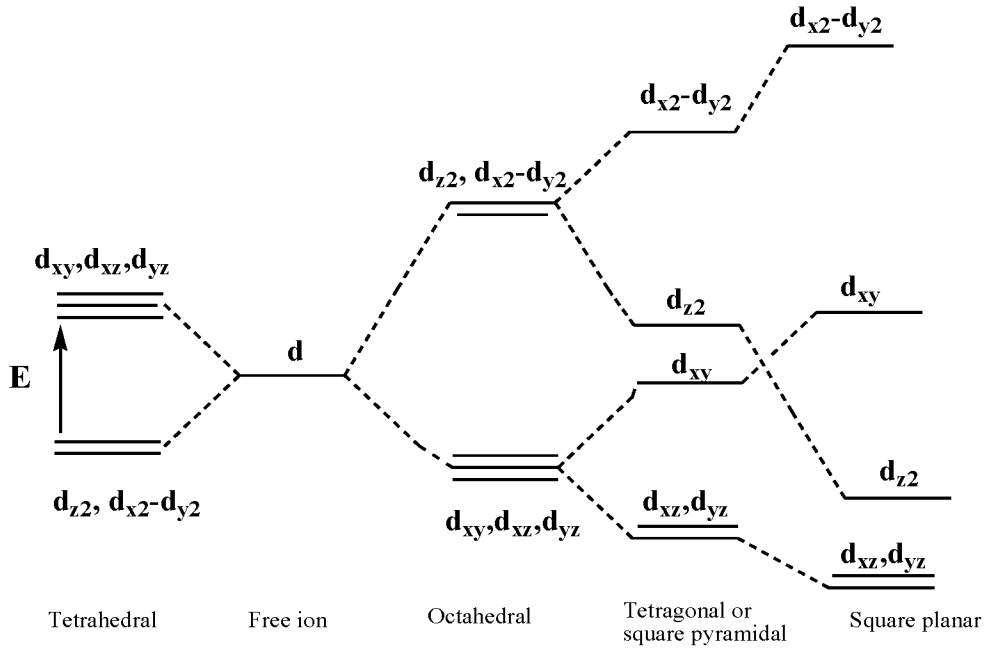

Fig. 1.12: Crystal field splitting of the d-orbitals of a central ion in complexes of various geometries.

In the four coordinate system, square planar geometry appear to be the more favoured and the distortion in the system usually leads to the observation of three transition which are $^2B_2 \rightarrow {}^2A_2$; $^2B_2 \rightarrow {}^2B_1$ and $^2B_2 \rightarrow {}^2A_1$ with characteristic transitions ranging from 480 nm to above 1000 nm [136]. Some of the Cu(II) complexes of Mannich bases highlighted in the literature displayed

a single transition in the range 530 – 660 nm and this is attributed to $^2A_{1g} \rightarrow {}^2B_{1g}$ transition in square planar geometry [137, 138].

Copper(II) complexes are likely to undergo ligand-solvent exchange or the possibility of more than one species in equilibrium, this observation is dependent on the coordination number involved [139].

1.7.1.4 Fe(III) complexes

In general, electronic spectral measurements on iron(III) complexes are not the most sensitive probe for the understanding of their electronic and molecular structure. The spectra, at least of solutions, are generally dominated by strong ligand or metal-ligand charge-transfer bands [140]. Trivalent iron has the electronic configuration of $3d^5$ which corresponds to a half-filled d-sub-shell and is particularly most stable. In crystalline fields, the usual high spin configuration is $t_{2g}^3 e_g^2$ with one unpaired electron in each of the orbitals and the low spin-state has the t_{2g}^5 configuration with two pairs of paired electrons and one unpaired electron.

The ground state of d^5 ion, ^6S transforms into $^6A_{1g}$ - a singlet state. The d-d transitions for S = 5/2 iron(III), which has a $^6A_1$ ground term are both spin and Laporte forbidden and hence very weak. For Fe^{3+}, there are three transitions: $^6A_{1g}(S) \rightarrow {}^4T_{1g}$ (G) (ν1), $^6A_{1g}(S) \rightarrow {}^4T_{2g}$ (G) (ν2). ν1 occurs at about 10525 cm^{-1} (975 nm) and ν2 occurs between 15380 cm^{-1} (650 nm) to 18180 cm^{-1} (550 nm) usually as a shoulder. The bands corresponding to $^6A_{1g}(S) \rightarrow {}^4A_{1g}$ (G), ^4E_g (G) (ν3) appear around 22000 cm^{-1} (454 nm). The last transition is field independent. The ligand field spectrum of ferric iron appears as if the first (ν1) and the third (ν3) bands of octahedral symmetry are only present [141].

The masking of the d-d transition by the intense charge transfer band makes it difficult to have any structure correlation from the spectral data [142]. Characteristic phenolate to Fe^{3+} charge

transfer transitions are observed as broad absorption band centred at ~500 nm as previously reported and is responsible for the reddish-brown colour observed [143].

1.7.2 Infrared spectroscopy

It has been shown from infrared data; dipole moment measurements, and X-ray diffractions, that ortho Mannich bases are a class of compounds characterized by stable intramolecular hydrogen bonds as seen in Figure 1.13. These bonds possess all of the spectroscopic features typical of intermolecular bonds and are characterized by a rigid conformation and high stability [144].

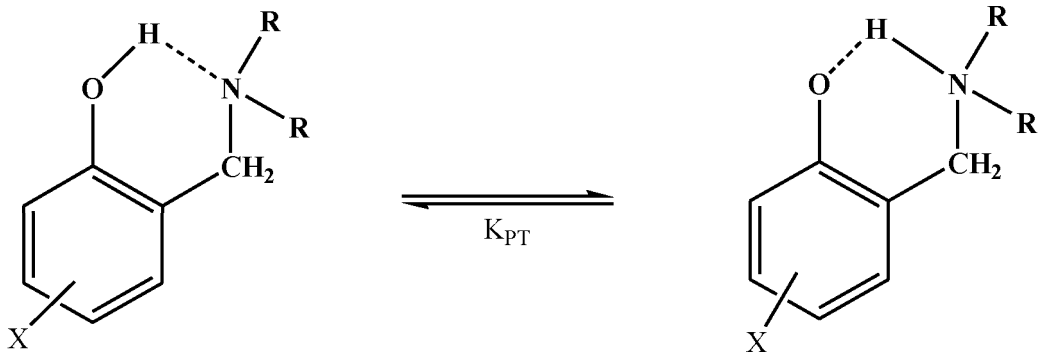

Fig. 1.13: Mannich bases strong intramolecular H-bonds.

Infrared spectroscopy has further corroborated this observation by the effects on the vibrational properties of the hydroxyl group of Mannich bases. Absorption of energy in the infrared region (ν = 4000 - 200 cm^{-1}) arises from changes in the vibrational energy of the molecules [145]. For example, the impact of hydrogen bonding on the stretching frequency of the hydroxyl group has also been widely reported for other class of compounds. For example, studies have reported shift in the vOH of the oxime ligand from 2846 cm^{-1} to between (2330 – 2360) cm^{-1} in the various cobalt(III) oxime complexes previously studies. Strong intramolecular and intermolecular forms of hydrogen bonding have been observed in different classes of Mannich bases previously studied [15], Kim and Ishida reported the observation of the νOH stretching

frequency of a series of Mannich base dimers at 2500 – 3300 cm^{-1}. These bands are assigned to –OH···N intramolecular H-bonding. [146]. This observation has been complimented by measurements of bond lengths in Mannich bases carried out on their crystalline structures and the lengthening of the OH bond was observed [147].

Also, the values from νC-O of the phenol are known to compliment the observation of downwards shifts due to hydrogen bonding [148] and also complexation with metal ions [149].

In addition, Mannich bases possess tertiary amine components, which are highly nucleophilic and capable of binding to a complexing ion. Harbatsevich *et al.* [149] studied Cu(II) of Mannich bases, ν(C–N) vibration of the Cu(II) complexes are observed at 1360 – 1250 cm^{-1} and it undergoes a bathochromic shift of (15 – 60) cm^{-1} with the band appearing weaker. A similar observation for also made for the Mn(II) complexes of the same set of ligands [149]. These downward shifts are commonly observed during complexation, however these two bands νOH and νCNC can also be shifted to higher frequencies as reported below.

Bands due to CN asymmetric and symmetric vibrations of the amine component of the Mannich base do undergo positive shift indicating the involvement of nitrogen atoms in the formation of complexes as observed by Bhat and Tabassum [150], in Schiff bases containing piperazine. Also, N,N'-bis[(2-hydroxybenzilideneamino)-propyl]-piperazine (a Schiff base) exhibited νCNC as medium intense bands at 1278 cm^{-1} while those of the Co and Zn complexes were at 1254 and 1282 cm^{-1}. The upward shift was attributed to the boat-chair conformation change of piperazine [151].

Generally upward shifts in νC-O is an indication of complexation through deprotonated phenol [152, 153]. Several literature searches are available for these observations with Schiff bases but very scanty information is available on Mannich bases.

The vibrations for the thiocyanato group may be described approximately as a C-N stretch ν(CN), a C-S stretch ν(CS) and a S-C-N bend δ(SCN) and are recorded in the mid and far-infrared region [46, 154] as given in Table 1.3 below. The various bonding modes are highlighted in Figure 1.6.

Table 1.3: Infra-red data for various bonding modes of thiocyanate (cm^{-1}) [155, 156].

Mode of coordination	ν(CN)	ν(CS)	δ(NCS)
$(NCS)^-$	2053	746	486 – 471
M-NCS	2100 – 2050 (s,b)	870 - 820 (w)	485 – 475
M-SCN	2130 – 2085 (s,sp)	760 – 700 (b)	470 – 430
M-NCS-M	2165 - 2065	800 - 750	470 – 440

s = strong, b = broad, sp = split, w = weak

It has been known for many years that infrared spectroscopy presents a good method for the determination of the mode of bonding between a metal ion and the thiocyanate ion. The linear triatomic ion SCN- has four normal vibrations of which two are degenerated. They are all infrared active. On coordination, all these shift in frequencies and the shifts are characteristic of the mode of bonding.

It is possible to correlate the frequencies of the M--NCS, C--S, C--N stretching vibrations and the NCS bending vibration and determine the geometry of the coordination compound for example a clear distinction between tetrahedral and octahedral compounds can be made. For the compounds studied by Clarke and Williams [157], both the C--N and C--S stretching frequencies increase on coordination of the thiocyanate ion to the metal. However, for tetrahedral complexes of a given metal, the C--S stretching frequencies are higher (by 40 - 65 cm^{-1}) than for octahedral complexes, whereas the C--N stretching frequencies are very similar for compounds of each type [157].

In spite of the fact that the most reliable data on bonding modes of thiocyanate ligand can be obtained from single crystal X-ray diffraction analysis, infrared spectroscopy is often used for approximate estimation of bonding modes.

1.7.3 Nuclear magnetic resonance spectroscopy (NMR)

Nuclear Magnetic Resonance (NMR) is a powerful non-selective, non-destructive analytical tool that enables you to ascertain molecular structure including relative configuration, relative and absolute concentrations, and even intermolecular interactions of an analyte [158].

It is a vastly used tool in elucidating the structure of molecules e.g. ligands in coordination chemistry. It has also found use in the understanding of the nature of coordination in metal complexes containing diamagnetic metal (e.g. Zn). ^{1}H and ^{13}C are not the only nuclei susceptible to NMR experiments though those are the only ones reported in this thesis. The technique could not be employed for Cu(II) and Fe(III) complexes because of their paramagnetic properties - d^9 and d^5 respectively which leads to broadening of signals and ultimately make coupling difficult to resolve [159].

NMR is based on interactions between an externally applied magnetic field (B_o) and the electron densities around NMR active nuclei. This technique essentially translates the different environments of the individual NMR active nuclei that make up a compound/species into a spectrum, which is characteristic of that species.

1.7.3.1 Chemical shift

The chemical shift is the resonant frequency of an atom relative to a standard in a magnetic field. Often the position and number of chemical shifts are diagnostic of the structure of a molecule [160]. The detected frequencies (in Hz) for ^{1}H and ^{13}C nuclei are usually referenced against tetramethylsilane (TMS). The convention used in NMR spectroscopy to describe

spectra is based on the frequency of the energy required to promote the nuclei to the higher energy state.

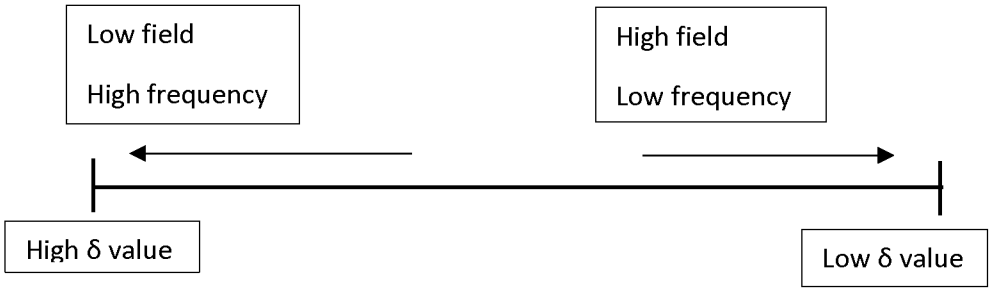

Fig. 1.14: Representation of chemical shifts nomenclature.

Energy is required to promote the nuclei to the higher energy state. That is chemical shifts of high δ values (large and positive) are described as being deshielded, requiring higher frequency radiation, hence appearing low or down field at the high frequency end of the spectrum, conversely, low δ values (small and positive) are shielded appearing high or upfield, at the low frequency end of the spectrum (Figure 1.14). This nomenclature is maintained throughout the thesis.

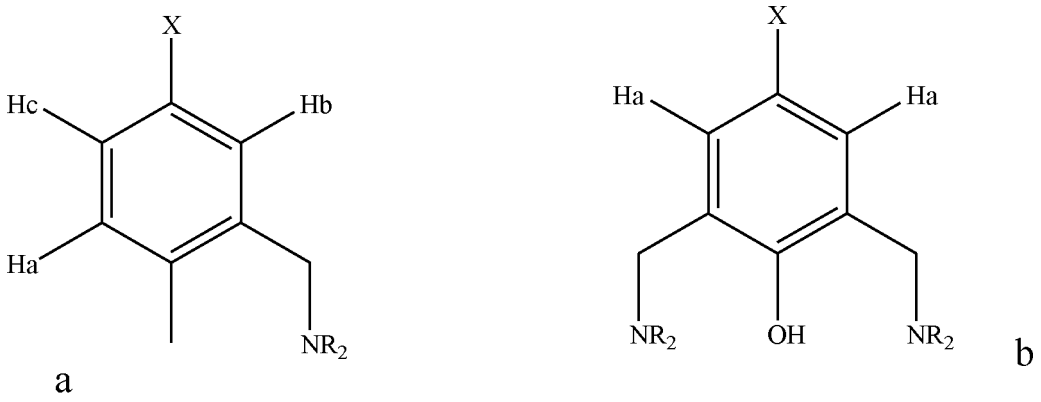

Fig. 1.15: Some basic description of ^{1}H and $^{13}CNMR$ spectra of Mannich mono and dibases.

In the aromatic region (6.5 – 8.0 ppm) of Mannich bases that is mono- or di-substituted with non-aromatic containing amines, three protons in 3 different environments will be observed while a di-substituted Mannich base will display a single peak with an integration equal to two

protons due to the two protons being occupied in the same electronic environment. In addition, 6 carbon environments will be observed in (a) while compound (b) will display 4 show four signals due to equivalent carbon atoms.

The ease of evaluation Ar-**CH_2**-N (probably the most important signal in the NMR spectra of Mannich bases) from ^1H NMR makes it possible to differentiate mono- from di-Mannich bases and therefore characterisation by NMR is not in doubt [50]. This knowledge has been employed in this work and the structures are well supported by the elemental analysis. And finally an article by Hansen and Spanget-Larsen [161] has summarised the IR and NMR spectroscopic data of strong H-bonded Mannich bases as [2800 > νOH > 1800 cm^{-1}, and 19 ppm > δOH > 15 ppm]. This was part of their review work on theoretical advances diketone enols, Mannich bases and quinoline N-oxides. These range of values particularly for the NMR data are largely disagreed with in this work.

1.7.4 Conductivity measurements

The measurement of conductivity for coordination compounds and the interpretation of such data in terms of possible structures dates back to the commencement of serious studies in the field of coordination chemistry. Some of the earliest studies reported in the literature were carried out in aqueous medium. However, except for the simplest complexes of (usually) inorganic compounds, the use of water as a solvent for conductance purposes is often undesirable because of problems of hydrolysis, and is impracticable because of the metal complexes in this work are largely insoluble in water [162]. This has generally led to a decline in studies involving conductivity in aqueous medium and the use of organic solvents has increased rapidly, particularly over the last few years. The expected ranges of molar conductivities, Λm, for different electrolytes in 10^{-3} M solutions in common solvents are listed in Table 1.4.

In qualitative terms, a solvent with a high dielectric constant and low viscosity will be preferred for conductivity purposes, and on this basis acetonitrile and methanol may be selected as particularly useful.

Table 1.4: Some properties of non-aqueous solvents relevant to their use for conductivity measurements [162].

Solvents	Dielectric constant	Viscosity ($g^{-1}.sec^{-1}$)	Specific conductivity ($ohm^{-1}.\ cm^{-1}$)
Acetone	20.7	0.295	5.80×10^{-8}
Nitromethane	35.9	0.595	6.56×10^{-7}
Nitrobenzene	34.8	1.634	9.10×10^{-7}
Methanol	32.6	0.545	1.50×10^{-9}
Ethanol	24.3	1.078	1.35×10^{-9}
Acetonitrile	36.2	0.325	5.90×10^{-8}
Dimethylformamide	36.7	0.796	$0.60 - 2.00 \times 10^{-7}$
Dimethylsulphoxide	46.6	1.960	3.00×10^{-8}
Pyridine	12.3	0.829	4.00×10^{-8}

The little disadvantages associated with use of both nitrobenzene and dimethylsulfoxide are high viscosity and odour. DMSO has a high Trouton constant (29.5) [163] evidence that it is a coordinating solvent. The structural aspects of dimethylsulfoxide indicate that it should function as an electron-donor solvent; hence, its solutions might be expected to exhibit solute- solvent interactions similar to those which have been observed for solutions of the same solutes in dimethylformamide, acetone or pyridine.

Although information on the use of DMSO in conductivity are not widely available compared to other solvents like DMF and methanol due to viscosity considerations, few references are cited in here. The standard paper often consulted on the conductivity of non-complex 1:1 electrolytes in this solvent is that of Sears *et al.* [164] and this has been relied upon until

the contributions of Ali *et al.*[165] further expanded the discussion to include detailed data from water and DMSO as solvents . Ali *et al.* provided the most recent update on conductivity measurements (Table 1.5) and these values are relied upon in this study.

Table 1.5: The ranges of molar conductivity ($\Omega^{-1}cm^2mol^{-1}$) of metal complexes with different ratios of cationic and anionic species.

Solvents	Electrolyte types				References
	1:1	1:2	1:3	1:4	
Nitromethane	75–95	150–180	220-260	290–330	[162]
Nitrobenzene	20–30	50–60	70-82	90–100	[162]
Acetonitrile	120–160	220–300	340-420	>500	[162]
Acetone	100–140	160–200	270-330	>360	[162]
DMF	65–90	130–170	200-240	>300	[162, 166]
Methanol	80–122	160–220	290-350	>450	[162,167]
Ethanol	35–45	70–90	120-140	>160	[162]
DMSO	50–90	110–195	200-240	—	[162,168, 169]
Water	118-131	145-273	408-435	540-560	[170, 171]

Other reports include: an approximate value of Λ_m at 10^{-3} M for the solutes given as 35 $ohm^{-1}cm^2mol^{-1}$, with individual values ranging from ~23 (potassium octadecyl-sulphate) to 42 $ohm^{-1}cm^2mol^{-1}$ (potassium thiocyanate). Values published for complexes $[MCl_2(en)_2]Cl$ (M = Ru, Co) also fall into this range. A value of 37.8 $ohm^{-1}cm^2mol^{-1}$ published for $[(C_6H_5)_4P]NO_3$ also supports this range, and is in contrast to the value of 73.2 $ohm^{-1}cm^2mol^{-1}$ for the corresponding hydrogen dinitrate salt $[NO_2OHONO_2]$. Values of 50 – 70 $ohm^{-1}cm^2mol^{-1}$ have been reported for 1:1 electrolyte solutions of Tellurium (IV) halides in DMSO [131, 172].

1.8 Aim of the study

As noted above kinetic studies on biomimetic abilities of binuclear copper complexes compared to those of catecholase oxidase; an enzyme famous for the oxidation of catechol to o-benzoquinone has received great attention. In general binuclear complexes are reputed to be better at this catalytic process compared to their mononuclear counterparts. Reports have shown increased catecholase activities in the presence of bridging groups or substituents capable of back-bonding to the centre metal iron. The influence of bridging modes of thiocyanate to copper and iron complexes of Mannich bases is yet to be explored in great details.

The aim of this study therefore is to synthesise copper(II) and iron(III) complexes of new mono-Mannich (aminomethylated) bases based on p-methylphenol and p-acetamidophenol, also using thiocyanate as a bridging ligand to obtain various configuration and consequently evaluate the catecholase activity alongside the kinetics using 3,5-di-tert-butyl catechol as substrate.

1.9 Scope of the study

Two substituted phenols (p-methylphenol and p-acetamidophenol) possessing ortho-active methylene groups were selected for this study. Five secondary amines were also selected to study the influence on the secondary amine functional group and these include piperidine, 1-(2-pyridyl)piperazine, 1-(4-nitrophenyl)piperazine, diethylamine hydrochloride and piperazine.

1.10 Objectives

The objectives of the study are stated as follows:

- Synthesis of p-cresol mono-aminomethylated Mannich bases from piperidine, piperazine, diethylamine, 1-(2-pyridyl)piperazine as well as their copper(II) and iron(III) complexes.

- Synthesis of p-acetamidophenol mono-aminomethylated Mannich bases from piperidine, piperazine, diethylamine, 1-(2-pyridyl)piperazine as well as their copper(II) and iron(III) complexes.
- Evaluation of the catecholase activity of the metal complexes using 3,5-ditertbutylcatechol as substrate.
- Determination of the various kinetic parameters of catecholase activity (V_{max}, K_{cat} and K_m).
- Identification of the oxidation products and to provide insight into the catalytic pathway.

Though the synthesis of few of the Mannich bases in this work have been previously reported, the syntheses and the evaluated of the catecholase activity of their thiocyanate metal complexes are yet to be reported according to literature review.

References

1. I. Chorkendorff, J. W. Niemantsverdriet, (2003). Introduction to Catalysis, in Concepts of Modern Catalysis and Kinetics, Wiley-VCH Verlag GmbH & Co. KGaA, Weinheim, FRG.
2. H. P. Dijkstra, G. P. M. van Klink, G. van Koten, Acc. Chem. Res., **2002**, 35, 798 – 810.
3. L. Styrer, J.M. Berg, J. L. Tymoczko, (2002). Biochemistry (5th ed.), San Francisco: W.H. Freeman.
4. A. K. Johnson, R. S. Goody, Biochemistry, **2011**, 50, 8264−8269.
5. E.L. Mutterties, T.N. Rhodin, E. Band, G.F. Brucker, W.R. Pretzer, Chem. Rev., **1979,** 79, 91 - 137.
6. E.C. Niederhoffer, J.H. Timmons, A.G. Martell, Chem. Rev., **1984**, 84, 137 – 203.
7. P. A. Vigato, S. Tamburini, D. E. Fenton, Coord. Chem. Rev., **1990**,106, 25 - 170.
8. U. Jayarathne, S. R. Parmelee, N. P. Mankad, Inorg. Chem., **2014**, 53, 7730−7737.
9. A. S. da Silva, R. J.S. Jacques, R. Andreazza, F.M. Bento, F. A. de Oliveira Camargo, Sci. Agric., **2013**, 70,68-73.
10. V. B. Megadi, P. N. Tallur, S. I. Mulla, H. Z. Ninnekar, J. Agric. Food Chem., **2010**, 58, 12863–12868.
11. H. Fiegel, H. W. Voges, T. Hamamoto, S. Umemura, T. Iwata, H. Miki, Y. Fujita, H.J. Buysch, D. Garbe, W. Paulus, (2002). 'Phenol Derivatives' in Ullmann's Encyclopedia of Industrial Chemistry; Wiley-VCH: New York.
12. I. Hiroshawa, G. Asaeda, H. Arizono, S. Shimbo, M. Ikeda, Int. Arch. Occup. Environ. Hlth., **1976**, 37, 107-114.
13. M. Merkel, D. Schnieders, S. M. Baldeau, B. Krebs, Eur. J. Inorg. Chem., **2004**, 783-790.
14. T. P. Camargo, F. F. Maia, C. Chaves, B. de Souza, A. J. Bortoluzzi, N. Castilho, T. Bortolotto, H. Terenzi, E. E. Castellano, W. Haase, Z. Tomkowicz, R. A. Peralta, A. Neves, J. Inorg. Biochem. **2015**,146, 77–88.
15. R. Yamahara, S. Ogo, H. Masuda, Y. Watanabe, J. Inorg. Biochem., **2002**, 88, 284–294.
16. S. Harayama, Ann. Rev. Microbiol., **1992**, 46, 565 – 601.
17. T. Klabunde, C. Eicken, J.C. Sacchettini, B. Krebs, Nat. Struct. Biol., **1998,** 5, 1084 – 1090.

18. H. Jyotsnabaran, T. Prodia, A.N. Bhaduri, J. Nutri. Biochem., **1998**, 9, 75 – 80.
19. S. Anbu, M. Kandaswamy, B. Varghese, Dalton Trans., **2010**, 39, 3823 – 3832.
20. C. Eicken, F. Zippel, K. B. Karentzopoulos, B. Krebs, FEBS Lett. **1998**, 436, 293 – 299.
21. E.I Solomon, U. M. Sundaram, T. E. Machonkin, Chem. Rev., **1996**, 96, 2563 –2605.
22. S. A. Kuby, (1991). A Study of Enzymes, Vol. 1, pp. 283–300, CRC Press, Boca Raton, FL.
23. P.E. M. Siegbahn, J. Biol. Inorg. Chem., **2004**, 9, 577 – 590.
24. S.T. Prigge, R.E. Mains, B.A. Eipper, L.M. Amzel, Cell. Mol. Life Sci., **2000**, 57, 1236 – 1259.
25. D.F. Shriver, P.W. Atkins, C.H. Langford, (1994). Inorganic Chemistry, 2nd edition, ELBS (Oxford Univ. Press).
26. K.D. Karlin, Science, **1993**, 261, 701 – 708.
27. K.D. Karlin, Z. Tyeklar, (1993). Eds. Bioinorganic Chemistry of Copper; Chapman & Hall: New York.
28. J. Reim, B. Krebs, J. Chem. Soc., Dalton Trans., **1997**, 3793 – 3804.
29. T. Osako, Y. Ueno, Y. Tachi, S. Itoh, Inorg. Chem., **2003**, 42, 8087−8097.
30. C. E. Valdez, Q. A. Smith, M. R. Nechay, A. N. Alexandrova, Acc. Chem. Res., **2014**, 47, 3110−3117.
31. E.I. Solomon, Inorg. Chem., **2001**, 40, 3656 – 3669.
32. L. Que, R.Y.N. Ho, Chem. Rev., **1996**, 96, 2607 - 2624.
33. M. Mitra , A. K. Maji , B. K. Ghosh , P. Raghavaiah , J. Ribas, R. Ghosh, Polyhedron, **2014**, 67, 19 – 26.
34. A. P. Neves, C. C. Barbosa, S. J. Greco, M. D. Vargas, L. C. Visentin, C. B. Pinheiro, A. S. Mangrich, J. P. Barbosae, G. L. da Costa, J. Braz. Chem. Soc., **2009**, 20, 712-727.
35. A.L. Feig, S. Lippard, Chem. Rev., **1994**, 94, 759 – 805.
36. E. A. Karakhanov, A. L. Maximov, Y. S. Kardasheva, V. A. Skorkin, S. V. Kardashev, E. A. Ivanova, E. Lurie-Luke, J. A. Seeley, S. L. Cron, App Cat. A, **2010**, 385, 62 – 72.
37. M. Velusamy, M. Palaniandavar, R. S. Gopalan, G. U. Kulkarni, Inorg. Chem., **2003**, 42, 8283 – 8293.
38. T. P. Camargo, Fernanda F. Maia ,C. Chaves, B. de Souza, A. J. Bortoluzzi, N. Castilho, T. Bortolotto, H. Terenzi, E. E. Castellano, W. Haase , Z. Tomkowicz, R. A. Peralta, A. Neves, J. Inorg. Biochem., **2015**, 146, 77–88.

39. A. Biswas, L.K. Das, M. G. B. Drew, G. Aromí, P. Gamez, A. Ghosh, Inorg. Chem., **2012**, 51, 7993 – 8001.
40. P. Molenveld, J.F.J. Engbersen, D.N. Reinhoudt, Chem. Soc. Rev., **2000**, 29, 75 – 86.
41. F. F. Blicke, Organic Reactions, Wiley, New York, **1942**, 1, 303.
42. H. Hellmann, G. Opitz, angew. Chem., **1956**, 68, 265 – 272.
43. B.B. Thompson, J. Pharm. Sci., **1968**, 57, 715 – 733.
44. M. Tramontini, Synthesis, **1971**, 703 – 775.
45. S. S. S. Raj, M. N. Ponnuswamy, G. Shanmugam, M. Kandaswamy, J. Chem. Cryst., **1994**, 24, 83 – 87.
46. M. S. Singh, S. Chowdhury, RSC Advances, **2012**, 2, 4547 – 4592.
47. H. I. Gul, J. Vepsalainen, M. Gul, E. Erciyas, O. Hanninen, Pharma. Acta Helv., **2000**, 74, 393 – 398.
48. F. Lehmann, A. Pilotti, K. Luthman, Mol. Diversity, **2003**, 7, 145 – 152.
49. E. R. Alexander, E. J. Underhill, J. Am. Chem. Soc., **1949,** 71, 4014 – 4019.
50. B. Brycki, H. Maciejewska, B. Brzezinski, J. Mol. Structure, **1991**, 246, 61-71.
51. G. Roman, Eur. J. Med. Chem., **2015,** 89, 743 – 816.
52. M. Suzuki, H. Furutachi, H. Okawa. Coord. Chem. Rev., **2000**, 200, 105 - 129.
53. T.N. Sorrell, C. O'Connor, O.P. Anderson, J.H. Reibenspies, J. Am. Chem. Soc., **1985**, 107, 4199 – 4206.
54. J. B. Rangisetty, C. N. V. H. B. Gupta, A. L. Prasad, P. Srinivas, N. Sridhar, P. Parimoo, A. Veeranjaneyulu, J. Pharm. Pharmacol, **2001**, 53, 1409 – 1413.
55. R. Sanyal, X. Zhang, P. Chakraborty, F. A. Mautner, C. Zhao, D. Das, RSC Adv., **2016**, 6, 73534 - 73546.
56. S.M. Abdallah, Arabian J. Chem., **2012**, 5, 251 – 256.
57. G. G. Mohamed, Z. M. Zaki. Syth. React. Inorg. Met. Org. Chem., **2004**, 34, 1497 – 1516.
58. A. Blade-Font, T. de Mas Rocabayera JCS Perkin, **1982**, 1, 841 – 848.
59. J.H. Burckhalter, F.H. Tendick, E. Jones, P.A. Jones, W.F. Hol-comb, A.L. Rawlins, J. Am. Chem. Soc., **1948**, 70, 1363 – 1372.
60. A. Rivera, R. Quevedo, Tetrahedron Lett., **2004**, 45, 8335 – 8338.
61. R. Quevedo, B. Moreno-Murillo, Tetrahedron Lett., **2009**, 50, 936 – 938.
62. T.D.B. Morgan, G. Stedman, P.A.E. Whincup, J Chem. Soc., **1965**, 4813 – 4822.
63. J. D. Chandlera, B. J. Day, Biochem. Pharmacol., **2012**, 84(11), 1381 – 1387.

64. N.N. Greenwood, E. Alan, (1997). Chemistry of Elements, Butterworth-Heinemann, p. 326
65. A. H. Norbury, Advan. Inorg. Chem. Radiochem., **1975**, 17, 231 – 386.
66. D. Lorentzen , L. Durairaj, A.A. Pezzulo, Y. Nakano, J. Launspach, D.A. Stoltz, Free Radic. Biol Med., **2011,** 50, 1144 – 1150.
67. A. Rodriguez, H. Sakiyama, N. Masciocchi, Inorg. Chem., **2005**, 44, 8399 - 8406.
68. P. Kulkarni, S. Padhye, E. Sinn, Inorg. Chim. Acta, **2002**, 332, 167 – 175.
69. E.L Wagner, J. Chem. Phy., **1965**, 43, 2728 – 2733.
70. H. Zhang, X. Wang, K. Zhang, B. K. Teo, Coord. Chem. Rev., **1999**,183, 157–195.
71. J. Lin, Z. Li, J. Li, S. Du, Polyhedron, **2007**, 26, 107–114.
72. Y. R. Tahboub, S. Galijasevic, M. P. Diamond, H. M. Abu-Soud, J. Biol. Chem., **2005**, 280, 26129 – 26136.
73. J.O. Tenuvuo, (1985). The peroxidase system in human secretions, New York Dekker, p. 272.
74. K.M. Pruitt, B. Reiter (1978), Biochemistry of peroxidase systems: antimicrobial effects. New York: Marcel Dekker, p 143 – 177.
75. A. Welk, Meller, R. Schubert, Schwahn, A. Kramer, H. Below, BMC Microbiology **2009**, 9, 134 – 142.
76. C.E. Barry, P.G. Nayar, T.P. Begley, Biochemistry, **1989**, 28, 6323 - 6333.
77. V. Behal, J. G. Prusakova, Z. Hostalek, Folia Miorobiol., **1982**, 27, 102 – 106.
78. A.W. Smith, A. Camara-Artigas, M. Wang, J.P. Allen, W.A. Francisco, Biochemistry, **2006**, 45, 4378 - 4387.
79. C.E. Barry, P.G. Nayar, T.P. Begley, J. Am. Chem. Soc., **1988**, 110, 3333 - 3334.
80. A. Guha, K. S. Banu, A. Banerjee, T. Ghosh, S. Bhattacharya, E. Zangrando, J. Mol. Cat. A: Chemical, **2011**, 1, 51–57.
81. A. M. Ramadan, S. Y. Shaban, M. M. Ibrahim, J. Coord. Chem., **2011**, 64, 3376 –3392.
82. P. Adak, C. Das , B. Ghosh, S. Mondal, B. Pakhira, E. Sinn, A. J. Blake, A. E. O'Connor, S. K. Chattopadhyay, Polyhedron, **2016**, 119, 39 – 48.
83. A. Panja, Polyhedron, **2014**, 80, 81–89.
84. K. S. Bharathi, S. Sreedaran, Hema Priya, A. K. Rahiman, K. Rajesh, L. Jagadish, V. Kaviyarasan, V. Narayanan, J. Coord. Chem., **2009**, 62, 1356 – 1372.
85. R. Sanyal, S. K. Dash, P. Kundu, D. Mandal, S. Roy, D. Das, Inorg. Chim. Acta, **2016**, 453, 394 – 401.

86. R. Sanyal, S.K. Dash, S. Das, S. Chattopadhyay, S. Roy, D. Das, J. Biol. Inorg. Chem., **2014,** 19, 1099 – 1111.
87. I.A. Koval, P. Gamez, C. Belle, K. Selmeczib, J. Reedijk, Chem. Soc. Rev., **2006**, 35, 814 – 840.
88. S. Majumder, S. Sarkar, S. Sasmal, E. C. Sanudo, S. Mohanta, Inorg. Chem., **2011**, 50, 7540–7554.
89. T. Ghosh, J. Adhikary, P. Chakraborty, P. K. Sukul, M. S. Jana, T. K. Mondal, E. Zangrando, D. Das, Dalton Trans., **2014**, 43, 841 - 852.
90. S. Kida, H. Okawa, Y. Nishida (1983). In Copper Coordination Chemistry: Biochemical and Inorganic Perspectives, eds. K. D. Karlin, J. Zubieta, Adenine, Guilderland, New York, p, 425.
91. M. R. Malachowski, M. G. Davidson, J. N. Hoffman, Inorg. Chim. Acta, **1989**,157, 91 - 94.
92. J. Chyn, F. L. Urbach, Inorg. Chim. Acta, **1991**,189, 157 – 163.
93. A. Latif, C. Woods, E. Bogas, G. LeGuenniou, Inorg. Chim. Acta, **1992**, 195, 67 – 71.
94. J. Reim, B. Krebs, J. Chem. Soc., Dalton Trans., **1997**, 3793–3804.
95. C. Belle, C. Beguin, I. Gautier-Luneau, S. Hamman, C. Philouze, J.L. Pierre, F. Thomas, S. Torelli, Inorg. Chem., **2002**, 41, 479–491.
96. D. Ghosh, T.K. Lal, S. Ghosh, R. Mukherjee, J. Chem. Soc. Chem. Comm., **1996**,13–14.
97. D. Ghosh, R. Mukherjee, Inorg. Chem., **1998**, 37, 6597–6605.
98. M. M. Rogic, M.D. Swerdloff, T.R. Demmin, (1983). In Copper Coordination Chemistry: Biochemical and Inorganic Perspectives, K.D. Karlin, J. Zubieta (Eds), Adenine, Guilderland, NY, pp. 167 – 425.
99. M. Tumer, N. Deligonul, A. Golcu, E. Akgun, M. Dolaz, H. Demirelli, M. Dıgrak, Transition Met. Chem., **2006**, 31, 1 – 12.
100. N. I. Jakab, A. Jancso, T. Gajda, B. Gyurcsik, A. Rockenbauer, J. Inorg. Biochem., **2008**, 102, 1438–1448.
101. A. M. Ramadan, M. M. Ibrahim, I. M. El-Mehasseb, J. Coord. Chem., **2012**, 65, 2256 – 2279.
102. R.P. Bonomo, E. Conte, R. Marcelli, A.M. Sontoro, G.J. Tabi, J. Inorg. Biochem., **1994**, 53, 172 - 178.
103. L. K. Das, A. Biswas, J. S. Kinyon, N. S. Dalal, H. Zhou, A. Ghosh, Inorg. Chem., **2013**, 52, 11744−11757.

104. H. G. Jang, D. D. Cox, L. Que Jr, J. Am. Chem. Soc., **1991**, 113, 9200 - 9204.
105. J. Adhikary, P. Chakraborty, S. Das, T. Chattopadhyay, A. Bauza, S.K. Chattopadhyay, B. Ghosh, F. A. Mautner, A. Frontera, D. Das, Inorg. Chem., **2013**, 52, 13442−13452.
106. D. H. Ohlendorf, J. D. Lipscomb, P. C. Weber, Nature, **1988**, 336, 403 - 405.
107. D. H. Ohlendorf, A. M. Orville, J. D. Lipscomb, J. Mol. Biol., **1994**, 244, 586 - 608.
108. R. Singh, A. Banerjee, K. K. Rajak, Inorg. Chim. Acta, **2010**, 363, 3131–3138.
109. P. Combo, H. Wadepohl, S. Wunderlich, Eur. J. Inorg. Chem., **2011**, 5242–5249.
110. M. Mitra, P. Raghavaiah, R. Ghosh, New J. Chem., **2015**, 39,200 - 205.
111. M. Mitra , A. K. Maji, B.K. Ghosh, P. Raghavaiah, J. Ribas, R. Ghosh, Polyhedron, **2014** ,67, 19–26.
112. P. Chakraborty, I. Majumder, H. Kara, S. K. Chattopadhyay, E. Zangrando, D. Das, Inorg. Chim. Acta, **2015**, 436, 139 –145.
113. A. Neves, L. M. Rossi , A. J. Bortoluzzi , A. S. Mangrich, W. Haase, R. Werner, J. Braz. Chem. Soc., **2001**, 12, 747-754.
114. I.A. Koval, P. Gamez, C. Belle, K. Selmeczi, J. Reedijk, Chem. Soc. Rev., **2006**, 35, 814 – 840.
115. G.F.Z. da Silva, L. J. Ming, J. Am. Chem. Soc., **2005**, 127, 16380–16381.
116. H. X. Zhou, G. Rivas, A. P. Minton, A.P. Annu. Rev. Biophys., **2008**, 37, 375–397.
117. C. M. Hill, R. D. Waight, W. G. Bardsley, Mol. Cell. Biochem., **1977**, 15, 173 – 178.
118. R. M. F. Bezerra, A. A. Dias, App. Biochem. Biotech., **2004**, 112, 173 - 184.
119. H. Lineweaver, D. Burk, J. Am. Chem. Soc., **1934**, 56, 658 – 666.
120. R. B. Martin, J. Chem. Edu. **1997**, 74 - 76.
121. R. J. Ritchie, T. Prvan, Biochem. Edu., **1996**, 24, 196 - 206.
122. S. Schnell, P. K. Maini, Comm. Theoret. Biol., **2003**, 8, 169–187.
123. P.G. Pifferi, L. Baldassari, Anal. Biochem., **1973**, 53, 325 - 335.
124. M. Mitra, P. Raghavaiah, R. Ghosh, New J. Chem., **2015**, 39, 200 – 205.
125. M. Louloudi, K. Mitopoulou, E. Evaggelou, Y. Deligiannakis, N. Hadjiliadis, J. Mol. Catalysis A: Chemical, **2003**, 198, 231 – 240.
126. P. T. Kaye, T. Nyokong, G. M. Watkins, K. W. Wellington, Arkivoc, **2009**, 9, 9 – 18.
127. P. T. Kaye, G. M. Watkins, K. W. Wellington, S. Afr. J. Chem., **2005**, 58, 1 – 3.
128. M. J. Al-Jeboori, A. J. Abdul-Ghani, A. J. Al-Karawi, Transition Met. Chem., **2008**, 33, 925–930.
129. R. Sanyal, X. Zhang, P. Kundu, T. Chattopadhyay, C. Zhao, F. A. Mautner, D. Das, Inorg. Chem., **2015**, 54, 2315−2324.

130. D. Sutton, (1969). Electronic spectra of transition metal complexes, McGraw-Hill, London, p. 13.
131. W. E. Hatfield, R. Whyman, Transition Met. Chem., **1969**, 5, 47 – 179.
132. D. Nicholls, (1973). In J. C. Bailer, H.J. Emeleaus, R. Nyholm, A.F. T. Dickenson (eds), Comprehensive Inorganic Chemistry, Pergamon Press. Oxford, p. 3.
133. S. Bhattacharyya, S. B. Kumar, S. K. Dutta, E. R. T. Tiekink, M. Chaudhury, Inorg. Chem., **1996**, 35, 1967-1973.
134. R. Sanyal, P. Kundu, E. Rychagova, G. Zhigulin,S. Ketkov, B. Ghosh, S.K. Chattopadhyay, E. Zangrando, D. Das, New J. Chem., 2016, 40, 6623 - 6635.
135. A.P. Neves, K. C.B. Maia, M. D. Vargas, L. C. Visentin, A. Casellato, M. A. Novak, A. S. Mangrich, Polyhedron, 29, **2010**, 2884–2891.
136. J. Ferguson, J. Chem. Phys., **1964**, 40, 3406 -3410.
137. A. Neves, A.J. Bortoluzzi, R. Jovito, R.A. Peralta, B.D. Souza, B. Szpoganicz, A.C. Joussef, H. Terenzi, P.C. Severino, F.L. Fischer, G. Schenk, M.J. Riley, S.J. Smith, L.R. Gahan, J. Braz. Chem. Soc., **2010**, 21, 1201–1212.
138. N. Buyukkidan, S. Ozer, Turk. J. Chem., **2013**, 37, 101 – 110.
139. C. Battistoni, G. Mattogno, A. Monaci, F Tarli, J. Inorg. Nucl. Chem., **1971**, 33, 3815 – 3832.
140. K.S Murray, Coord. Chem. Rev., **1974**, 12, 1 – 35.
141. D. P. Graddon, (2017). An Introduction to coordination chemistry: International series of Monographs, Inorganic Chemistry Volume 3, Second Edition, Pergamon Press, p 47.
142. C.J. Ballhausin (1967). Introduction to ligand field theory. New York: Mc Graw Hill.
143. N. Brot, J. Goodwin, H. Fales, Biochem. Biophys. Res. Comm., **1966**, 25, 454 – 461.
144. A. Koll, M. Rospenk, L. Sobczyk, T. Glowiak, Can. J. Chem., **1986**, 64, 1850 - 1854.
145. B.P. Gaber, V. Miskowski, T.G. Spiro, J. Am. Chem. Soc., **1974**, 96, 6868 – 6873.
146. Ho-Dong Kim and Hatsuo Ishida, J. Phys. Chem. A, **2002**, 106, 3271- 3280.
147. A. Koll, P. Wolschann, Monatshefte fiir Chemie, **1996**, 127, 475 – 486.
148. A. Rivera, D. Quiroga, J. Ríos-Motta, V. Eigner, M. Dušek, Chem. Cent. J., **2013**, 7, 100
149. H. I. Harbatsevich, N. V. Loginova, T. V. Kovalchuk, N. P. Osipovich, A. T. Gres, I. I. Azarko,G. I. Polozova, J. Appl. Spec., **2015**, 82, 713 - 718.
150. I. Bhat, S. Tabassum, Spectrochim. Acta, A, **2009**, 72, 1026 – 1033.

151. C. Cretu, R. Tudose, L. Cseh, W. Linert, E. Halevas, A. Hatzidimitriou, O. Costisor, A. Salifoglou , Polyhedron, **2015**, 85, 48 – 59.
152. K. Pothiraj, T. Baskaran, N. Raman, J. Coord. Chem., **2012**, 65, 2110 – 2126.
153. R. C. Maurya, R. Verma, T. Singh, Synth. React. Inorg. Met-org. Chem., **2003**, 33, 309 – 325.
154. A. Miezi, Acta Chem. Scand., **1973**, 27, 3746 – 3760.
155. J. Tercero, C. Diaz, J. Ribas, E. Ruiz, J. Mahia, M. Maestro, Inorg. Chem., **2002**, 41, 6780−6789.
156. M. Kabesova, J. Gazo, Chem. Zvesti, **1980**, 34, 800 - 841.
157. R. J. H. Clark, C. S. Williams, Spectrochim. Acta, **1966**, 22, 1081 - 1090.
158. A.E. Derome (1987), Modem NMR Techniques for Chemistry Research, Silverstein; Bassler; Morrill.
159. F.H. Kohler, (2007). Paramagnetic Complexes in Solution: The NMR Approach, in eMagRes, 2007, John Wiley.
160. J.A. Pople, Mol. Phys., **1964**, 301 – 306.
161. P. E. Hansen, J. Spanget-Larsen, Molecules, **2017**, 22, 552 – 573.
162. W.J. Geary, Coord. Chem. Rev., **1971**, 7, 81 – 122.
163. T. B. Douglas, J. Am. Chem. Soc., **1948**, 70, 2001 – 2002.
164. P. G. Sears, G. R. Lester, L. R. Dawson, J. Phys. Chem., **1956**, 60, 1433 – 1436.
165. I. Ali, W. A. Wani, K. Saleem, Synth. React. Inorg. Met.-Org. Chem., **2013**, 43, 1162–1170.
166. H. F. A. El-Halima, G.G. Mohamed, M.M.I. El-Dessoukya, W.H. Mahmoud, Spectrochim. Acta A, **2011**, 82, 8 – 19.
167. H.A. Hussain, A.A. Ansari, K. Iftikhar, Spectrochim. Acta A, **2004**, 60, 873 – 884.
168. O.H. Shehab, A.A. R.H Al-Hiti, Am. Chem. Sci. J., **2012**, 2, 1–11.
169. R. Kumara, S. Chandra, P. Mishra, Spectrochim. Acta A, **2007**, 68, 1250 – 1255.
170. S.N. Shukla, P. Gaury, R. Mehrotray, M. Prasad, H. Kaury, M. Prasady, R.S. Srivastava, J. Coord. Chem., **2009**, 62, 2556 – 2568.
171. F.H. Fry, G.D. Fallon, L. Spiccia, Inorg. Chim. Acta, **2003**, 346, 57 – 66.
172. R. K. Boggess, D. A. Zatko, J. Chem. Edu., **1975**, 52, 649 - 652.

CHAPTER TWO

EXPERIMENTAL

2.1 Reagents

All reagents and chemicals obtained from Sigma-Aldrich or Merck were of Analar grade and used without further purification. Chemicals and solvents used in the synthesis of the Mannich bases and the metal complexes include: p-cresol, p-acetamidophenol, piperidine, piperazine, diethylamine, 1-(2-pyridyl)piperazine, 1-(4-nitrophenyl)piperazine, paraformaldehyde, formaldehyde, L-proline, absolute ethanol, absolute methanol, isopropyl alcohol, n-hexane, chloroform, dimethylformamide (DMF), dimethyl sulfoxide (DMSO), copper(II) chloride dihydrate, iron(III) chloride hexahydrate, trimethylamine, deuterated chloroform (d_1) and deuterated dimethyl sulfoxide (d_6). Also, 3,5-di-tert-butyl catechol was purchased from Sigma-Aldrich and used as received.

2.2 Physical and analytical methods

The Mannich bases with their copper(II) and iron(III) complexes prepared in this study have been characterized using a combination of elemental, titrimetric and spectroscopic techniques. Structural elucidation was carried out through ^{1}H and ^{13}C Nuclear Magnetic Resonance. Also carried out was single crystal x-ray diffraction crystallography for some of the ligands. Bonding modes of the ligands to the metal ions were studied using Infra-red spectroscopy. Also conductivity and UV/Visible spectroscopic studies were carried out to support the proposed structures.

2.2.1 Nuclear magnetic resonance spectroscopy (NMR)

The ^{1}H and ^{13}C NMR spectra were recorded on a Bruker 300MHz spectrometer in deuterated chloroform (d_1) or deuterated dimethyl sulfoxide (d_6) with tetramethylsilane as internal

standard. All spectra were recorded at ambient temperature with the chemical shifts measured in parts per million (ppm) downfield to the reference signal.

2.2.2 Infrared spectroscopy (MIR)

Infrared spectra were recorded on a Perkin-Elmer 100 ATR-IR spectrometer in the region 4000 – 650 cm^{-1} with 4 scans at an average resolution of 8 cm^{-1}. The spectrometer was fitted with universal attenuated total reflectance accessory (ZnSe crystal/diamond) and thus requires no sample preparation.

2.2.3 UV-Visible spectroscopy

UV spectra were obtained from Perkin Elmer Lambda 25 spectrophotometer. All solutions were prepared to approximately a concentration of 10^{-3} M in DMF and DMSO within the range of 200 – 1000 nm.

2.2.4 Microanalysis

Carbon, hydrogen, nitrogen and sulphur combustion microanalysis were carried out on a Vario MICRO VI.6.2 elemental analysen systemme GmbH by Mr Francis Chindeka of the Department of Chemistry, Rhodes University.

2.2.5 Molar conductivity

Molar conductivity measurements for the complexes were carried out in dimethyl sulfoxide depending on the solubility of the complexes, using Az® 86555 pH/mV/Cond./TDS/Temp apparatus at a concentration of 1 x 10^{-3} M. An alternative solvent is dimethylformamide.

2.2.6 Melting point

The melting points of the compounds were determined using Galenkemp melting point apparatus. The values were uncorrected.

2.2.7 X-ray diffraction

Single crystals of the four ligands suitable for X-ray diffraction were obtained via slow evaporation of the appropriate solvent systems. The single crystal X-ray diffraction was done at Nelson Mandela Metropolitan University, Port Elizabeth, South Africa by Dr Eric Hosten. The data was collected using a Bruker KAPPA APEX II single crystal X-ray diffractometer, with a 4-circle Kappa goniometer and sensitive CCD detector. The instrument used a Molybdenum fine focus sealed X-ray tube as an X-ray source and an Oxford Cryostream 700 system for sample temperature control. Bruker's APEX2 software [1] was used for instrument control.

The structure was solved using SHELXT-2014 [2] and refined by least square procedures using SHELXL-2016 [3] with SHELXLE [4] as a graphical interface. Data were recorded for absorption effects using the numerical method implemented in SADABS [1].

2.2.8 Powder X-ray diffraction (PXRD)

X-ray powder diffraction patterns were recorded on a Bruker D8 Discover (Billercica, MA, USA) equipped with a proportional counter, using Cu-Kα radiation (λ = 1.5405 Å, Nickel filter). Data were collected in the range from 2θ = 10° to 100 °, scanning at 1.5 ° min^{-1} with a filter time constant of 0.38 s per step and a slit width of 6.0 mm. samples were placed on a silicon slide. The x-ray diffraction data were treated using Eva (evaluation curve fitting) software. Baseline correction was performed on each diffraction pattern by subtracting a spline function fitted to the curved background. Crystallography data were run at Rhodes University, Grahamstown, South Africa with the assistance of Dr Jonathan Britton of the Centre for Nanotechnology Innovation.

2.2.9 Differential scanning calorimetry (DSC)

Differential Scanning Calorimetry was carried out using a Perkin-Elmer DSC 6000 calorimeter under N_2 gas at a flow rate of 19.28 $cm^{-3}min^{-1}$. The weighted samples were heated from 30 to 445 °C at a heating rate of 10 °C min^{-1} using Al pans.

2.3 Synthesis of the ligands

The Mannich bases were synthesized according to the general synthetic procedures in the literature while making few modifications to some of the existing protocols in the literature [5-8]. Absolute ethanol and isopropyl alcohol are used as solvents for most of the synthesis. A three-component condensation of a substituted phenol, secondary amine and formaldehyde achieved the desired ligands.

2.3.1 p-Cresol based ligands

10 mmol (1.0815 g) of p-cresol in 5 mL of absolute methanol was added to a 5 mL solution containing 10 mmol (1.03 mL) of diethylamine and 0.754 mL of formaldehyde solution were stirred at room temperature for one hour and warmed on a steam bath for two hours. The progress of the reaction was monitored by TLC. Column chromatography was carried out with chloroform: methanol (9:1) to achieve the desired mono-aminomethylated product (HL^1).

Other Mannich bases in this class were obtained by refluxing the three components for between 6 – 24 hours using ethanol as solvent and recrystallizing the products from chloroform and ethanol or DMSO/ toluene mixture. Scheme 2.1 below depicts the synthesis of the ligands.

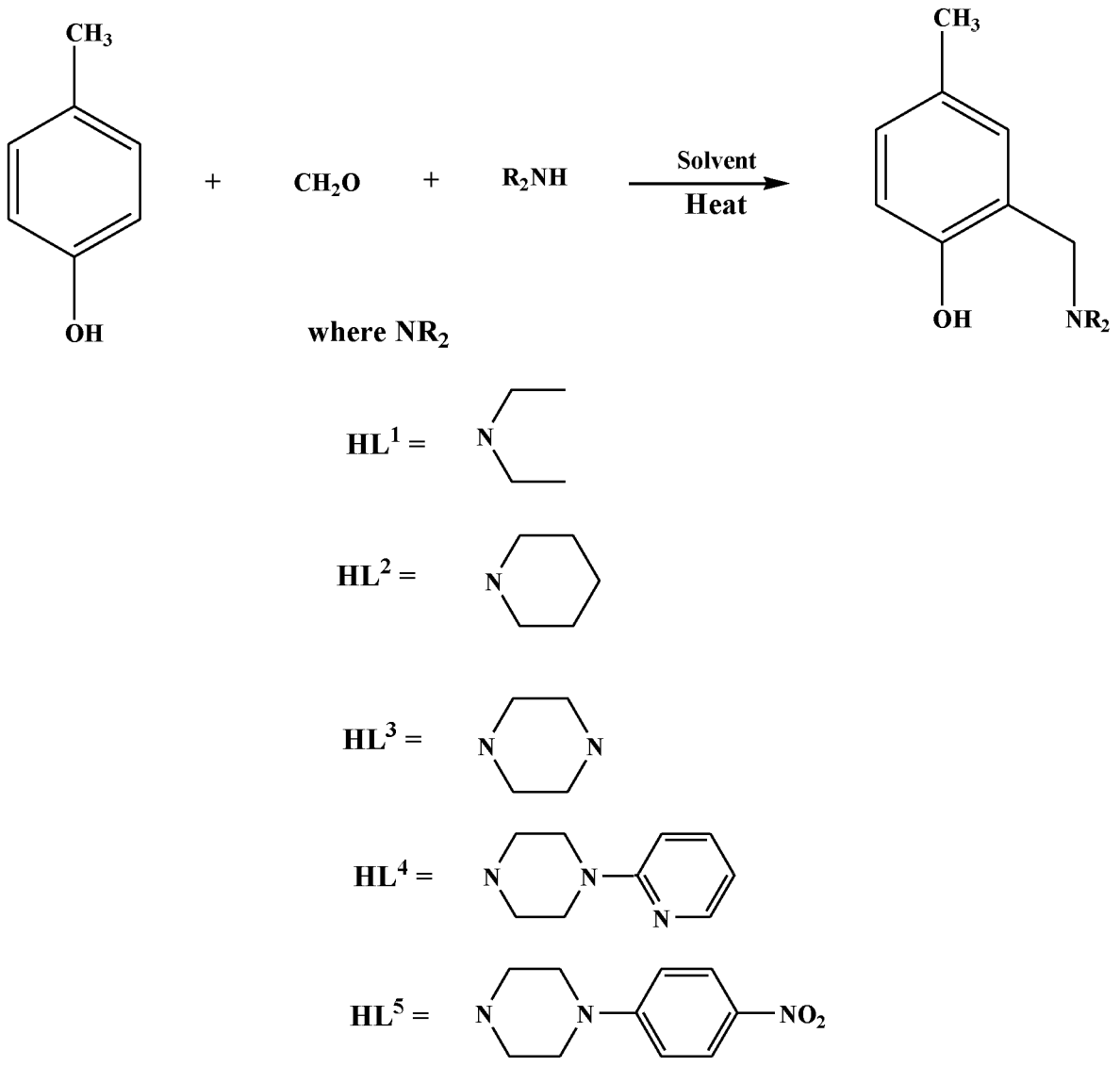

Scheme 2.1: Synthesis of Mannich bases of p-cresol (HL^{1-5}).

2.3.2 p-Acetamidophenol based ligands

The synthetic route for the ligands has previously been encountered in the synthesis of aromatic amino analogues of artemisinin [8]. A mixture of equivalent amounts (10 mmol) of acetamidophenol and formaldehyde were taken along with the excess amount of secondary amines suspended in 10 mL of isopropyl alcohol and heated in a steam bath for 3 hours. Upon cooling, a crystalline mass formed in the case of HL^{7-9}, which was washed with acetone or alcohol, recrystallized from chloroform and ethanol and then allowed to dry.

In certain cases, when a crystalline product could not be readily obtained by the above-mentioned procedure, the volatile materials were removed under reduced pressure and the residue taken into ether and treated with excess alcoholic hydrogen chloride as is the case of HL^6. The synthesis of HL^{10} was achieved by refluxing for 36 hours while monitoring the progress of the reaction by TLC. At completion, the solvent was removed under vacuum and column chromatography was carried out using chloroform and methanol (9:1) mixture to give a yellow solid.

It is worth noting here that ligand HL^6 has been synthesized previously and the crystal structure reported by Latif *et al.*, [9]. However, the synthesis of the ligand was achieved in this study by a simpler and greener route as the use of hydrochloric acid was not involved with a moderately high yield recorded.

The synthesis of the ligands is shown in scheme 2.2.

The synthesis of HL^3 and HL^8 involved aminomethylation using the two ends of the piperazine and the structures were confirmed by NMR and elemental analysis and the expected products are depicted in Figure 2.1.

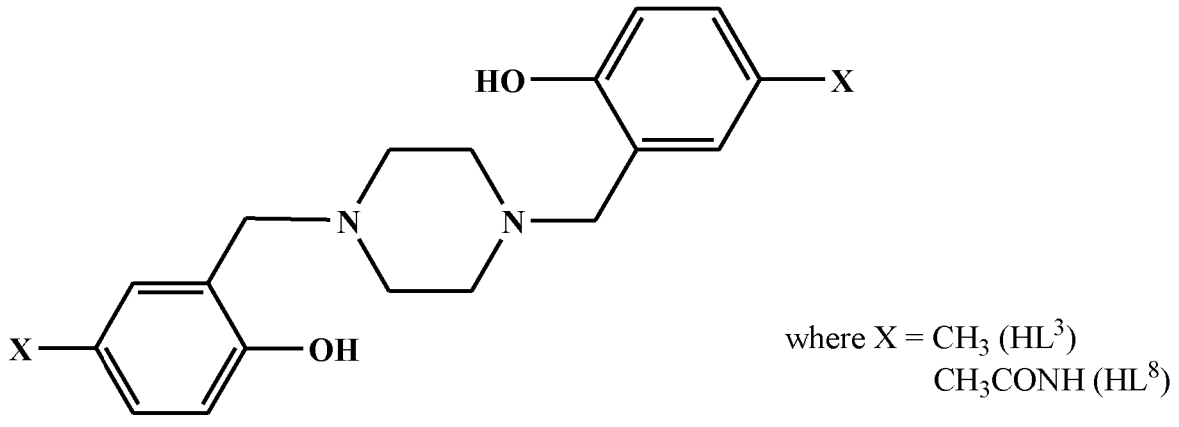

Fig. 2.1: Structural representation of HL^3 and HL^8.

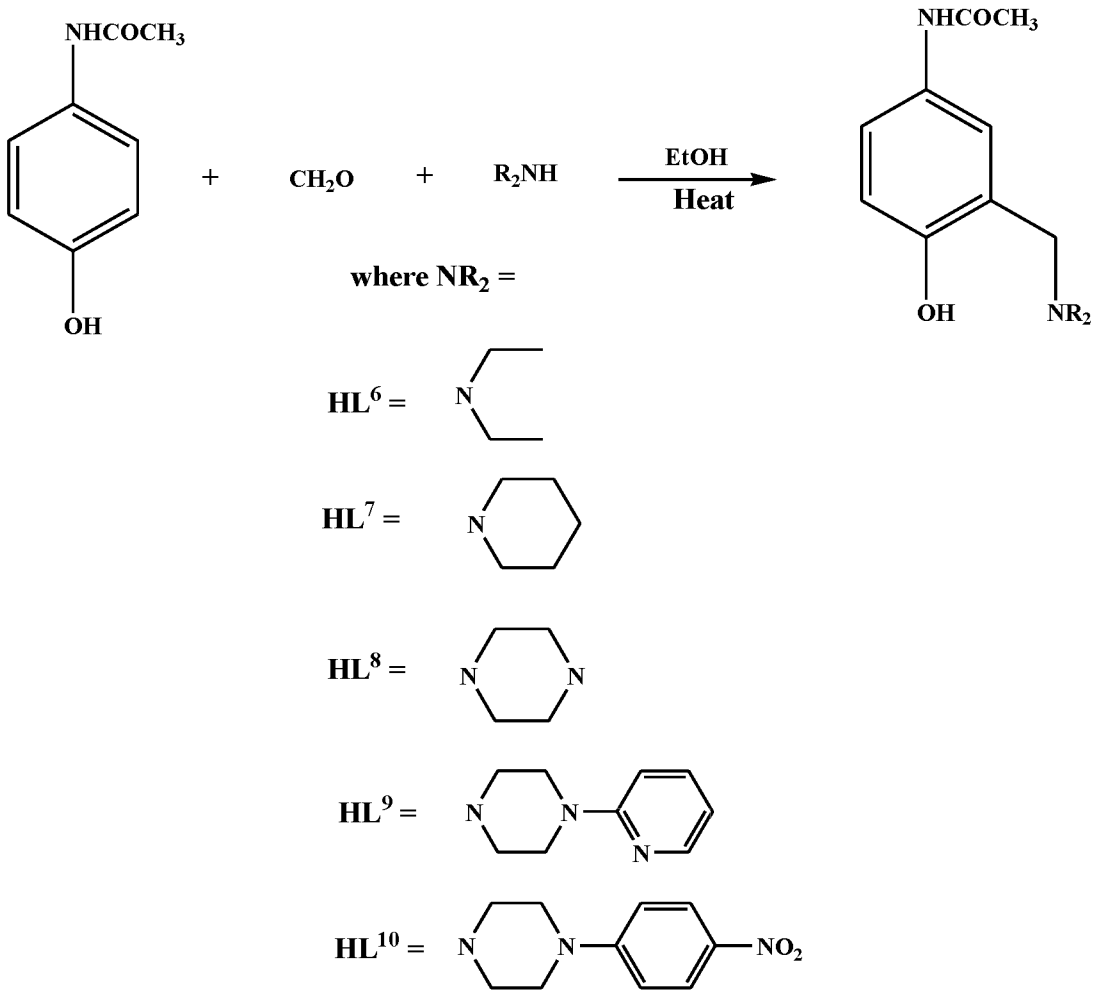

Scheme 2.2: Synthesis of Mannich bases of p-acetamidophenol (HL^{6-10}).

The synthesis of HL^3 and HL^8 involved aminomethylation using the two ends of the piperazine and the structures were confirmed by NMR spectroscopy and elemental analysis and the expected products are depicted in Figure 2.1.

2.4 Synthesis of the metal complexes

The idea was to make metal complexes in which the SCN^- can act as a bridging ligand, in addition to metal complexes without isothiocyanate or thiocyanate moieties.

2.4.1 Synthesis of the copper(II) complexes

1 mmol of copper(II) chloride dihydrate was dissolved in 3 mL of methanol and added drop wise to a vigorous stirring chloroform solution of the ligand. The resulting solution was stirred

at room temperature for 6 hrs until precipitates were obtained. The precipitate was filtered and washed thoroughly with chloroform:methanol mixture and then dried over silica gel in a desiccator. The elemental analysis results suggested complexes of the form ML and further characterisation were done through conductivity measurements as well as infrared and UV/visible spectroscopy.

The SCN^- containing copper complexes were synthesised by reacting equivalent amounts of ligand and metal salt with equivalent amount of potassium thiocyanate dissolved in minimal amount of methanol. The resulting solution was stirred at room temperature for 6 hrs until precipitates are obtained. The precipitates were treated as those above. The successful complexation of the SCN^- to the central metal ion was confirmed by infrared spectroscopy.

2.4.2 Synthesis of the iron(III) complexes

This was done by using the methods highlighted above for copper(II) complexes except that a few drops of triethylamine was used to deprotonate the ligand prior to complexation while iron(III) chloride hexahydrate was employed as the metal salt. Otherwise, the metal complexes could not be obtained.

References

1. APEX2, SADABS and SAINT, Bruker AXS Inc., Madison, Wisconsin, USA, **2010**.
2. G.M. Sheldrick, Acta Crystallogr., **A71**, 2015a, 3 – 8.
3. G.M. Sheldrick, Acta Crystallogr., **C71**, 2015b, 3 – 8.
4. C.B. Hubschle, G.M. Sheldrick, B. Dittrich, J. Appl. Cryst., **2011**, 44, 1281 – 1284.
5. A. Blade-Font, T. de Mas Rocabayera, JCS Perkin, **1982**, 1, 841 – 848.
6. K. S. Bharathi, S. Sreedaran, H. Priya, A. K. Rahiman, K. Rajesh, L. Jagadish, V. Kaviyarasan, V. Narayanan, J. Coord. Chem., **2009**, 62, 1356 – 1372.
7. S. Anbu, M. Kandaswamy, Polyhedron, **2011**, 30, 123 – 131.
8. D. Sriram, R. Vandana, D. M. Dinakaran, P. Yogeeswari, Med. Chem. Res., **2010,** 19, 524 – 532.
9. T. Latif, T. Javed, D.E. Lynch, R.J. Pryce, K.A. Byriel, Aust. J. Chem., **1999**, 52, 909 – 913.

CHAPTER THREE

RESULTS

This chapter consists of tables of the results of various spectroscopic and analytical techniques employed in the characterisation of the ligands and their Cu(II) and Fe(III) complexes.

Contained herein are the ^{1}H and ^{13}C NMR data of the ligands (Mannich bases) followed by the microanalysis (determination of % C, H, N and S content) of all the compounds reported in this work. The results from molar conductivity of 10^{-3} M DMSO solution of the metal complexes are also reported. The infrared data (4000 – 650 cm^{-1}) of the ligands were reported alongside their metal complexes. Lastly, the data from the electronic spectra of all the compounds are reported as determined in DMF and DMSO.

3.1.0 NMR data for the ligands

Table 3.1: ^{1}H-NMR chemical shifts δ (ppm) for the 4-methyphenol based ligands (HL^{1-5}).

Ligands	Ar-H	CH_3-Ar	Ar-CH_2	$(CH_2)_2N$	$(CH_2)_3$	CH_3CH_2N
HL^1	6.76 – 7.06 (m, 3H)	2.28 (s, 3H)	3.77 (s, 2H)	2.64 (q, 4H)	---	1.34 (t, 6H)
HL^2	6.71 – 6.97 (m, 3H)	2.24 (s, 3H)	3.62 (s, 2H)	2.50 (t, 4H)	1.55 (m, 6H)	---
HL^3	6.60 – 6.87 (m, 3H)	2.28 (s, 3H)	3.69 (s, 4H)	2.90 (s, 8H)	---	---
HL^4	6.65 – 8.21(m, 7H)	2.25 (s, 3H)	3.71 (s, 2H)	2.67 (t, 4H), 3.59 (t, 4H)	---	---
HL^5	6.75-8.14 (m, 7H)	2.28 (s, 3H)	3.75 (s, 2H)	2.73 (t, 4H), 3.48 (t, 4H)	--	---

All the ^{1}H NMR spectra were recorded in $CDCl_3$ and the assignment of individual protons is given in the appendix.

Table 3.2: ^{13}C-NMR chemical shifts δ (ppm) for the 4-methyphenol based ligands (HL^{1-5}).

Ligand	Ar-C	$\underline{C}H_3$-Ar	Ar-$\underline{C}H_2$	$(\underline{C}H_2)_2N$	$(\underline{C}H_2)_3$	$\underline{C}H_3CH_2N$
HL^1	128.2, 129.0, 129.3, 130.0, 155.6	20.5	57.0	46.3	---	11.2
HL^2	115. 9, 121.5, 128.0, 129.0, 129.1, 155.7	20.6	62.3	54.0	24.3 – 25.9	---
HL^3	115.8, 120.5, 124.4, 129.2, 129.3, 155.0	20.3	61.1	52.3	---	---
HL^4	107.1, 113.7, 115.5, 120.7, 128.4, 129.3, 137.4, 148.0, 155.2, 159.3	20.4	61.6	45.2, 52.4	---	---
HL^5	112.8, 115.8, 119.8, 125.6, 128.4, 129.3, 129.4, 138.8, 154.3, 154.7	20.2	60.6	46.7, 51.7	---	---

All the ^{13}C NMR spectra were recorded in $CDCl_3$ and the assignment of individual protons is given in the appendix.

Table 3.3: ^{1}H-NMR chemical shifts δ (ppm) data for the 4-acetamidophenol based ligands (HL^{6-10}).

Ligand	Ar-H	CH_3CONH	$Ar-CH_2$	$(CH_2)_2N$	$(CH_2)_3$	CH_3CH_2N
HL^6	7.35 – 8.01	2.42 (s, 3H)	4.58 (s, 2H)	3.48 (q, 4H)	---	1.65 (t, 6H)
HL^7	6.72 – 7.30	2.12 (s, 3H)	3.63 (s, 2H)	2.47 (t, 4H)	1.49 (m, 6H)	---
HL^8	7.06 – 7.71	2.38 (s, 3H)	3.97 (s, 4H)	2.90 (s, 8H)	---	---
HL^9	6.63 – 8.20	2.17 (s, 3H)	3.73 (s, 2H)	2.67 (t, 4H), 3.57 (t, 4H)	---	---
HL^{10}	6.65 – 9.70	1.97 (s, 3H)	3.58 (s, 2H)	2.08 (t, 4H), 2.57 (t, 4H)	---	---

All the ^{1}H NMR spectra were recorded in $CDCl_3$ except HL^6, HL^8 and HL^{10} that were recorded in DMSO-d_6 and the assignment of individual protons is given in the appendix.

Table 3.4: ^{13}C-NMR chemical shifts δ (ppm) for the 4-acetamidophenol based ligands (HL^{6-10}).

Ligand	Ar-C	$\underline{C}H_3CONH$	Ar-$\underline{C}H_2$	$(\underline{C}H_2)_2N$	$\underline{C}H_3CH_2N$	$(\underline{C}H_2)_3$
HL^6	115.7, 116.1, 122.7, 123.9, 131.3, 152.4, 167.9	23.8	49.6	46.1	8.4	---
HL^7	116.5, 121.2, 121.7, 122.3, 129.7, 155.5, 168.5	24.7	62.4	54.3	---	24.3, 26.2
HL^8	115.3, 119.9, 121.1, 130.9, 152.6, 168.2	23.7	58.3	52.0	---	---
HL^9	107.8, 113.8, 116.3,121.2,121.5,129.7, 137.7,147.9, 154.5, 159.3, 168.2	24.6	61.4	45.0, 52.3	---	---
HL^{10}	112.0, 114.2, 120.0, 125.0, 130.2, 130.3, 136.2, 151.3, 152.4, 153.9, 166.9	23.0	51.1	30.0, 45.5	---	---

All the ^{13}C NMR spectra were recorded in $CDCl_3$ except HL^8 and HL^{10} that were recorded in DMSO-d_6 and the assignment of individual protons is given in the appendix.

3.2.0 Physical and analytical data for the ligands and metal complexes.

Table 3.5: Physical and analytical data for the p-methylphenol based Mannich ligands (HL^{1-5}).

Ligand	Colour	%Yield	M.P (°C)	Molar Mass	Molecular Formula	%Found (Calculated) C	H	N
HL^1	Orange	46	Oil	193.28	$C_{12}H_{19}NO$	74.70 (74.57)	9.75 (9.90)	7.35 (7.25)
HL^2	White	53	47-48	205.29	$C_{13}H_{19}NO$	75.64 (76.05)	9.44 (9.32)	6.80 (6.82)
HL^3	White	70	210-212	326.42	$C_{20}H_{26}N_2O_2$	73.55 (73.59)	8.44 (8.03)	8.70 (8.58)
HL^4	Cream	62	126-128	283.36	$C_{17}H_{21}N_3O$	71.64 (72.05)	7.65 (7.47)	15.45 (14.82)
HL^5	Yellow	52	138-140	338.88	$C_{18}H_{21}N_3O_3.{}^1/_4C_2H_5OH$	64.64 (64.68)	6.52 (6.44)	12.04 (12.40)

Table 3.6: Physical and analytical data for the p-acetamidophenol based Mannich ligands (HL^{6-10}).

Ligand	Colour	% Yield	M.P (°C)	Molar Mass	Molecular Formula	%Found (Calculated) C	H	N
HL^6	White	65	191-192	236.30	$C_{13}H_{20}N_2O_2$	66.05 (66.07)	9.03 (8.54)	12.09 (11.86)
HL^7	Cream	71	153-155	248.31	$C_{14}H_{20}N_2O_2$	67.66 (67.71)	8.68 (8.11)	11.15 (11.28)
HL^8	White	74	240-242	412.46	$C_{22}H_{28}N_4O_4$	63.59 (64.06)	7.16 (6.84)	13.20 (13.58)
HL^9	Cream	64	178-180	326.38	$C_{18}H_{22}N_4O_2$	66.10 (66.23)	6.94 (6.79)	17.40 (17.17)
HL^{10}	Yellow	48	180-181	370.39	$C_{19}H_{22}N_4O_4$	61.34 (61.61)	5.62 (5.98)	15.25 (15.13)

Table 3.7: Physical and analytical data for 2-((diethylamino)methyl)-4-methylphenol (HL^1) complexes.

Complex	M.P(°C)	Molar mass	Molecular Formula	Colour	% Found (Calculated)				$\Lambda_M(\Omega^{-1}.cm^2.mol^{-1})$
					C	H	N	S	
1	162 - 164	309.28	$[Cu(L^1)ClH_2O]$	Light brown	46.28(46.58)	6.51(6.52)	4.75(4.53)	---	18.88
2	204 - 206	422.42	$[Cu(HL^1)(NCS)(H_2O)_3]Cl.H_2O$	Light brown	37.20(36.96)	6.23(6.44)	9.80(6.66)	7.85(7.57)	119.22
3	180 - 182	382.65	$[Fe(HL^1)Cl_3].^3/_2H_2O$	Brown	37.70(37.66)	5.49(5.66)	3.98(3.66)	---	19.24
4	152*	414.78	$[Fe(L^1)(NCS)Cl].4H_2O$	Brown	37.31(37.64)	6.75(6.56)	6.83(6.75)	7.51(7.72)	48.24

* = decomposition

Table 3.8: Physical and analytical data for 4-methyl-2-((piperidin-1-yl)methyl)phenol (HL^2) complexes.

Complex	M.P (°C)	Molar Mass	Molecular Formula	Colour	% Found (Calculated)				$\Lambda_M(\Omega^{-1}.cm^2.mol^{-1})$
					C	H	N	S	
5	136 - 138	321.35	$[Cu(L^2)ClH_2O]$	Green	48.58(48.58)	6.96(6.59)	4.00(4.35)	---	4.38
6	182 - 184	362.29	$[Cu(HL^2)(NCS)Cl]$	Dark green	46.44(46.41)	5.65(5.88)	7.26(7.73)	8.95(8.83)	33.74
7	161 - 163	571.20	$[Fe(HL^2)Cl_3].CHCl_3$	Brown	25.17(25.23)	5.30(5.65)	2.60(2.45)	---	5.33
8	220 - 222	462.28	$[Fe(HL^2)(NCS)Cl_2].4H_2O$	Light brown	30.53(36.37)	5.58(5.88)	5.83(6.05)	6.52(6.92)	27.96

Table 3.9: Physical and analytical data for 2-((4-(2-hydroxy-4-methylbenzyl)piperazin-1-yl)methyl)-5-methylphenol (HL^3) complexes.

Complex	M.P (°C)	Molar Mass	Molecular Formula	Colour	% Found (Calculated)				$\Lambda_M(\Omega^{-1}.cm^2.mol^{-1})$
					C	H	N	S	
9	135 - 136	514.96	$[Cu(HL^3)Cl_2]3H_2O$	Dark green	46.93(46.64)	6.25(6.26)	5.71(5.44)	---	39.20
10	180 -181	776.96	$[Cu_2(HL^3)(NCS)_3Cl]3H_2O.{}^1/_2X$	Brown	35.65(35.90)	3.17(3.40)	9.32(9.10)	12.39(12.38)	88.80
11	230 -232	433.77	$[FeL^3Cl].H_2O$	Ash	54.92(55.37)	7.85(7.04)	6.40(6.45)	---	48.9
12	150 - 152	528.41	$[FeL^3(NCS)].5H_2O$	Dark brown	47.47(47.73)	6.75(6.49)	7.66(7.95)	5.71(6.06)	57.71

x = chloroform

Table 3.10: Physical and analytical data for 4-methyl-2-((4-(pyridin-2-yl)piperazin-1-yl)methyl)phenol (HL^4) complexes.

Complex	M.P (°C)	Molar mass	Molecular Formula	Colour	% Found (Calculated)				$\Lambda_M(\Omega^{-1}.cm^2.mol^{-1})$
					C	H	N	S	
13	146 - 147	417.86	$[Cu(HL^4)Cl_2]$	Green	49.50(48.96)	5.27(5.08)	11.16(10.80)	---	13.65
14	161 - 162	450.68	$[Cu(HL^4)(NCS)Cl].{}^1/_4CH_3CN$	Brown	49.75(49.31)	4.74(4.87)	13.30(13.21)	6.99(7.10)	22.84
15	120 - 122	443.24	$[FeL^4Cl_2].H_2O{}^1/_2CH_3OH$	Reddish brown	47.55(47.42)	5.95(5.68)	9.48(9.48)	---	35.54
16	80 -82	856.61	$[Fe_2(L^4)_2(NCS)_2)].2CH_3OH$	Dark brown	53.680(53.28)	5.79(5.64)	8.08(8.17)	7.07(7.47)	31.65

Table 3. 11: Physical and analytical data for 4-methyl-2-((4-(4-nitrophenyl)piperazin-1-yl)methyl)phenol (HL^5) complexes.

Complex	M.P (°C)	Molar mass	Molecular Formula	Colour	% Found (Calculated)				$\Lambda_M(\Omega^{-1}.cm^2.mol^{-1})$
					C	H	N	S	
17	151- 153	501.64	$[CuHL^5Cl_2].^1/_3CHCl_3$	Brown	43.87(43.89)	3.74(4.05)	8.59(8.38)	---	8.15
18	138 - 140	712.53	$[Cu_2(HL^5)(NCS)_2]Cl_2$	Light brown	33.68(33.71)	2.63(2.83)	9.89(9.83)	8.33(8.88)	51.65
19	140-141	495.69	$[Fe(HL^5)Cl_3].H_2O$	Dark green	40.87(41.19)	4.36(4.68)	8.01(8.47)	---	41.32
20	139 - 142	793.00	$[Fe_2(HL^5)Cl_2(SCN)_2(H_2O)_2]Cl_2.^1/_2X$	Dark brown	31.30(31.05)	2.87(2.86)	9.23(8.83)	8.04(8.07)	116.10

x = chloroform

Table 3. 12: Physical and analytical data for N-(3-((diethylamino)methyl)-4-hydroxyphenyl)acetamide (HL^6) complexes.

Complex	M.P (°C)	Molar mass	Molecular Formula	Colour	% Found (Calculated)				$\Lambda_M(\Omega^{-1}.cm^2.mol^{-1})$
					C	H	N	S	
21	180 - 181	684.87	$[Cu(HL^6)_2Cl_2].H_2O.^1/_2CHCl_3$	Reddish brown	46.38(46.47)	6.02(6.25)	7.93(8.17)	---	6.24
22	168 - 170	759.29	$[Cu(HL^6)_2(NCS)_2].2H_2O$	Reddish brown	44.12(44.20)	5.63(5.96)	11.18(11.05)	8.70(8.44)	12.77
23	160 - 161	395.19	$[Fe(L^6)Cl]ClCH_3OH$	Brown	42.86(42.54)	6.25(6.58)	7.53(7.09)	---	51.65
24	160-162	706.99	$[Fe(HL^6)_2(NCS)_2Cl].^3/_2H_2O$	Brown	47.67(47.57)	5.705(6.13)	11.48(11.89)	9.28(9.05)	44.82

Table 3.13: Physical and analytical data for N-(4-hydroxy-3-((piperidin-1-yl)methyl)phenyl)acetamide (HL^7) complexes.

Complex	M.P (°C)	Molar mass	Molecular Formula	Colour	% Found (Calculated) C	H	N	S	$\Lambda_M(\Omega^1.cm^2.mol^{-1})$
25	153-155	430.70	$[Cu(HL^7)Cl_2].H_2O.{}^1/_4CHCl_3$	Light brown	39.32(39.73)	4.96(5.20)	6.59(6.50)	---	29.96
26	151 - 153	459.43	$[Cu(HL^7)(SCN)H_2O]Cl.2H_2O$	Brown	39.02(39.21)	5.37(5.70)	8.78(9.14)	7.10(6.98)	50.61
27	204 - 206	731.02	$[Fe(HL^7)_2ClH_2O]Cl3H_2O$	Brown	46.18(46.00)	6.88(6.62)	7.43(7.66)	---	59.52
28	168 - 169	477.27	$[Fe(HL^7)(NCS)ClH_2O]Cl.{}^3/_2H_2O$	Dark brown	37.34(37.67)	4.62(5.06)	8.51(8.80)	6.69(6.70)	82.54

Table 3. 14: Physical and analytical data for 2-((4-(2-hydroxy-4-acetamidobenzyl)piperazin-1-yl)methyl)-5-phenylacetamide (HL^8) complexes.

Complex	M.P (°C)	Molar mass	Molecular Formula	Colour	% Found (Calculated) C	H	N	S	$\Lambda_M(\Omega^{-1}.cm^2.mol^{-1})$
29	160 - 162	644.45	$[Cu_2L^8Cl_2].2H_2O$	Reddish brown	40.81(40.99)	4.59(4.37)	8.79(8.69)	---	31.65
30	>250	798.66	$[Cu_2(HL^8)(NCS)_2(H_2O)_2]Cl_2H_2O$	ash	36.32(36.09)	3.60(4.52)	10.54(10.52)	8.38(8.01)	60.65
31	190 - 192	628.85	$[Fe(HL^8)Cl_3].3H_2O$	Brown	41.61(42.01)	5.69(5.45)	8.79(8.90)	---	37.24
32	180 -182	913.76	$[Fe_2(HL^8)(NCS)_2Cl_4].4H_2OX/_2$	Dark brown	31.98(32.22)	3.73(4.02)	9.23(9.13)	7.14(7.02)	129.83

x = chloroform

Table 3. 15: Physical and analytical data for N-(4-hydroxy-3-((4-(pyridin-2-yl)piperazin-1-yl)methyl)phenyl)acetamide (HL^9) complexes.

Complex	M.P (°C)	Molar mass	Molecular Formula	Colour	% Found (Calculated) C	H	N	S	$\Lambda_M(\Omega^{-1}.cm^2.mol^{-1})$
33	168 - 170	532.94	$[Cu(HL^9)Cl_2].4H_2O$	Brown	40.95(40.56)	5.86(5.67)	10.59(10.51)	---	17.88
34	>250	712.63	$[Cu_2(HL^9)(NCS)_2 2H_2O]Cl_2 2H_2O$	Light brown	33.80(33.70)	4.42(4.24)	11.71(11.79)	11.61(8.98)	78.56
35	122 - 124	576.80	$[Fe(HL^9)Cl_3].6H_2O$	Dark brown	35.90(36.22)	6.32(5.74)	9.02(9.38)	---	44.16
36	181-183	840.33	$[Fe_2(HL^9)(NCS)_2(H_2O)_2Cl_2]Cl_2 6H_2O$	Brown	27.44(27.45)	4.19(3.92)	9.44(9.60)	7.28(7.62)	83.30

Table 3. 16: Physical and analytical data for N-(4-hydroxy-3-((4-(4-nitrophenyl)piperazin-1-yl)methyl)phenyl)acetamide (HL^{10}) complexes.

Complex	M.P (°C)	Molar mass	Molecular Formula		% Found (Calculated) C	H	N	S	$\Lambda_M(\Omega^{-1}.cm^2.mol^{-1})$
37	130-132	504.88	$[Cu(HL^{10})Cl_2]$	Dark brown	45.66(45.20)	4.61(4.39)	10.81(11.10)	---	37.06
38	170 - 172	800.46	$[Cu_2[HL^{10})_2(NCS)Cl_2 2H_2O].4H_2OCl_2 4X$	Reddish brown	34.92(34.51)	3.90(4.28)	8.37(8.74)	2.22(2.45)	161.77
39	189 - 191	564.76	$[Fe(HL^{10})Cl_3].CH_3OH$	Dark brown	42.61(42.53)	4.92(4.64)	9.83(9.92)	---	44.16
40	>250	764.89	$[Fe(HL^{10})(NCS)Cl]Cl 6H_2O$	brown	31.36(31.40)	4.56(4.48)	8.60(8.75)	4.10(4.12)	57.80

x = methanol

3.3.0 Mid-infrared data for the ligands and complexes

Table 3.17: Mid-infrared data for 2-((diethylamino)methyl)-4-methylphenol (HL^1) and metal complexes (cm^{-1}).

Compound	vOH	vCN	vC-O	vCNC	vCS
HL^1	3336	---	1256	1168	---
1	3350	---	1264	1158	---
2	3348	2119sp	1267	1157	757
3	3251	---	1268	1154	---
4	3229	2049s, br	1268	1156	828

sp = split, s = strong, br = broad

Table 3.18: Mid-infrared data for 4-methyl-2-((piperidin-1-yl)methyl)phenol (HL^2) and metal complexes (cm^{-1}).

Compound	vOH	vCN	vC-O	vCNC	vCS
HL^2	3014	---	1252	1115	---
5	3398	---	1260	1136	---
6	---	2076s, sh	1256	1135	783
7	3272	---	1266	1154	---
8	3349	2042s, br	1258	1153	824

sh = sharp, s = strong, br = broad

Table 3.19: Mid-infrared data for 2-((4-(2-hydroxy-5-methylbenzyl)piperazin-1-yl)methyl)-4-methylphenol (HL^3) and metal complexes (cm^{-1}).

Compound	vOH	vCN	vC-O	vCNC	vCS
HL^3	3023	---	1242	1150	---
9	3363	---	1206	1128	---
10	3387	2173w, 2086sp	1223	1132	758
11	3365	---	1258	1206	---
12	3362	2025br	1256	1207	739

sp = split, br = broad, w = weak

Table 3.20: Mid-infrared data for 4-methyl-2-((4-(pyridin-2-yl)piperazin-1-yl)methyl)phenol (HL^4) and metal complexes (cm^{-1}).

Compound	vOH	vCN	vC-O	vCNC	vCS
HL^4	3056	---	1256	1247,1143	---
13	3352	---	1240	1243, 1126	---
14	3382	2118s,sp	1268	1243,1126	874
15	3372	---	1266	1238, 1183	---
16	3368	2051s,br	1267	1236,1129	774

sp = split, s = strong, br = broad

Table 3.21: Mid-infrared data for 4-methyl-2-((4-(4-nitrophenyl)piperazin-1-yl)methyl)phenol ligand (HL^5) and its metal complexes (cm^{-1})

Compound	vOH	vCN	vC-O	vCNC	vCS
HL^5	3091	---	1316	1245, 1115	---
17	3437	---	1313	1244, 1108	---
18	3432	2173w, 2090w	1313	1228, 1105	755
19	3184	---	1299	1245, 1108	---
20	3184	2022br	1319	1246, 1105	714

w = weak, br = broad

Table 3.22: Mid-infrared data for N-(3-((diethylamino)methyl)-4-hydroxyphenyl)acetamide (HL^6) and its metal complexes.

Compound	vOH	vCN	vC-O	vCNC	vCS
HL^6	3259	---	1252sh	1205	---
21	3314	---	1247	1217	---
22	3282	2101s,sh	1253	1221	705
23	3372	---	1259	1209	---
24	3308br	2054s,br	1252br	1195	691

sh = sharp, br = broad, s = strong

Table 3.23: Mid-infrared data for N-(4-hydroxy-3-((piperidin-1-yl)methyl)phenyl)acetamide (HL^7) and its metal complexes (cm^{-1}).

Compound	vOH	vCN	vC-O	vCNC	vCS
HL^7	3276	---	1253	1149	---
25	3339	---	1254	1033	760
26	3337	2106sp,s	1255	1025	---
27	3364	---	1261	1117	---
28	3276	2035s,br	1257	1116	827

sp = split, s = strong, br = broad

Table 3.24: Mid-infrared data for 2-((4-(2-hydroxy-4-acetamidobenzyl)piperazin-1-yl)methyl)-5-phenylacetamide (HL^8) and its metal complexes.

Compound	vOH	vCN	vC-O	vCNC	vCS
HL^8	3250	---	1297	1141	---
29	3274	---	1259	1119	---
30	3290	2172s, 2108sd	1260	1070	749
31	3299	---	1255	1116	---
32	3253br	2035br	1260	1118	798

sd = shoulder, s = strong, br = broad

Table 3.25: Mid-infrared data for N-(4-hydroxy-3-((4-(acetamid-2-yl)acetamido-1-yl)methyl)phenyl)acetamide (HL^9) and its metal complexes (cm^{-1}).

Compound	vOH	vCN	vC-O	vCNC	vCS
HL^9	3534	---	1249sh	1213, 1142	---
33	3337	---	1248br	1162, 1120	---
34	3299	2173s, 2156sd	1244br	1180, 1062	868
35	3369	---	1265br	1162, 1112	---
36	3260	2051s, br	1251br	1161, 1129	737

sd = shoulder, s = strong, br = broad, sh = sharp

Table 3.26: Mid-infrared data for N-(4-hydroxy-3-((4-(4-nitrophenyl)piperazin-1-yl)methyl)phenyl)acetamide (HL^{10}) and its metal complexes (cm^{-1}).

Compound	vOH	vCN	vC-O	vCNC	vCS
HL^{10}	3264	---	1365	1238, 1113	---
37	3356br	---	1321	1255, 1110	---
38	3408br	2172s, 2088w,br	1320	1256, 1111	753
39	3351br	---	1316	1231, 1112	---
40	3337	2049br	1318	1236, 1112	730

w = weak, s = strong, br = broad

3.4.0 UV/Visible data for the ligands and complexes

Table 3.27: UV/Visible data for the HL^1 and its metal complexes (nm).

Compound	Solvent	Observed transitions			
		π –π*	n- π*	CT	d-d
HL^1	DMF	282	---	---	---
	DMSO	271	303	---	---
1	DMF	282	296	460	717
	DMSO	290	392	474	758
2	DMF	271	287	---	713
	DMSO	270	304	471	758
3	DMF	---	291	348	497
	DMSO	262	298	349	---
4	DMF	---	289	---	447
	DMSO	264	290	349	---

Table 3.28: UV/Visible data for the HL^2 and its metal complexes (nm).

Compound	Solvent	Observed transitions			
		π –π*	n- π*	CT	d-d
HL^2	DMF	285	---	---	---
	DMSO	289	---	---	---
5	DMF	288	---	---	692
	DMSO	270	313	454	733
6	DMF	288	---	434	722
	DMSO	265	290	345	457
7	DMF	292	---	369	513
	DMSO	287	---	370	---
8	DMF	---	290	413	---
	DMSO	262	291	350	456

Table 3.29: UV/Visible data for HL^3 and its metal complexes (nm).

Compound	Solvent	Observed transitions			
		π –π*	n- π*	CT	d-d
HL^3	DMF	285	290	---	---
	DMSO	276	292	---	---
9	DMF	285	---	426	751
	DMSO	272	297	417	831
10	DMF	284	323	407	591
	DMSO	271	299	408	692
11	DMF	289	---	363	---
	DMSO	278	297	364	---
12	DMF	293	321	363	---
	DMSO	269	298	345	---

Table 3.30: UV/Visible data for HL^4 and its metal complexes (nm).

Compound	Solvent	Observed transitions			
		π –π*	n- π*	CT	d-d
HL^4	DMF	---	292	---	---
	DMSO	275	309	---	---
13	DMF	272	295	422	738
	DMSO	---	315	373	768
14	DMF	272	294	---	720
	DMSO	274	316	471	749
15	DMF	--	298	377	---
	DMSO	272	301	371	---
16	DMF	---	310	346	502
	DMSO	274	305	---	470

Table 3.31: UV/Visible data for HL^5 and its metal complexes (nm).

Compound	Solvent	Observed transitions			
		π –π*	n- π*	CT	d-d
HL^5	DMF	287	371	429	---
	DMSO	270	366	433	---
17	DMF	287	381	410	730
	DMSO	298	364	448	761
18	DMF	290	381	400	603
	DMSO	315	364	446	891
19	DMF	290	369	427	---
	DMSO	318	361	431	---
20	DMF	295	364	424	---
	DMSO	313	374	439	---

Table 3.32: UV/Visible data for HL^6 and its metal complexes (nm).

Compound	Solvent	Observed transitions			
		π –π*	n- π*	CT	d-d
HL^6	DMF	272	300	---	---
	DMSO	264	298	---	---
21	DMF	307	372	529	839
	DMSO	320	344,	503	814
22	DMF	268	361	489	510
	DMSO	268	361	406	542
23	DMF	273	303	368	---
	DMSO	272	307	348	496
24	DMF	272	300	406	---
	DMSO	267	303	---	980

Table 3.33: UV/Visible data for HL^7 and its metal complexes (nm).

Compound	Solvent	Observed transitions			
		π –π*	n- π*	CT	d-d
HL^7	DMF	---	297	---	---
	DMSO	263	299	---	---
25	DMF	279	310	439	887
	DMSO	314	329	510	860
26	DMF	269	331	---	621
	DMSO	291	---	---	773
27	DMF	276	300	361	---
	DMSO	---	309	354, 395	504
28	DMF	270	299	370	---
	DMSO	---	306	338(sh)	---

Table 3.34: UV/Visible data for HL^8 and its metal complexes (nm).

Compound	Solvent	Observed transitions			
		π –π*	n- π*	CT	d-d
HL^8	DMF	270	297	---	---
	DMSO	---	299	---	---
29	DMF	272	303	466	---
	DMSO	311	349	478	856
30	DMF	269	331	---	621
	DMSO	306	---	439	668
31	DMF	---	305	363	532
	DMSO	282	348(sh)	---	---
32	DMF	---	312	366, 394	462
	DMSO	---	312	353	468

sh = shoulder

Table 3.35: UV/Visible data for HL^9 and its metal complexes (nm).

Compound	Solvent	Observed transitions			
		π –π*	n- π*	CT	d-d
HL^9	DMF	270	299	---	---
	DMSO	289	---	---	---
33	DMF	278	307	---	741
	DMSO	---	313	454	733
34	DMF	260	319	427	687
	DMSO	269	324(sh)	---	775
35	DMF	269	304	---	496
	DMSO	287	---	370	---
36	DMF	272	302	---	472
	DMSO	---	291	350	---

sh = shoulder

Table 3.36: UV/Visible data for HL^{10} and its metal complexes (nm).

Compound	Solvent	Observed transitions			
		π –π*	n- π*	CT	d-d
HL^{10}	DMF	303	373	443	---
	DMSO	275	331	---	---
37	DMF	271	366	408	942
	DMSO	305	363	427	---
38	DMF	271	378	403	1000
	DMSO	289	375	436	---
39	DMF	273	378	402(sh)	---
	DMSO	270	308	361	436
40	DMF	275	377	396	---
	DMSO	255	307	369	439

sh = shoulder

CHAPTER FOUR

DISCUSSION

The synthesised Mannich bases studied in this work were grouped into two categories depending on the type of substituted phenol used for the synthesis. Secondary amines including diethylamine hydrochloride, piperidine, piperazine, 1-(2-pyridyl)piperazine and 1-(4-nitrophenyl)piperazine were condensed respectively with p-methylphenol and p-acetamidophenol in the presence of formaldehyde/paraformaldehyde using protic solvents (ethanol or isopropanol). The synthesis (sometimes aided with a small amount of L-proline which is a proven catalyst in Mannich reaction) and the isolation of desired products (monobases) were successfully carried out as confirmed by various analytical and spectro-chemical techniques though the reaction is also likely to lead to di-substituted products as side products.

All the Mannich bases were obtained in high purity and in moderate yields with the single crystals of some of them isolated, the ligands are quite stable in air and with moderately high melting points ranging between (48 – 242) ^{o}C. The analytical and physicochemical data of the ligands are presented in Tables 3.5 and 3.6. The Cu(II) and Fe(III) complexes were prepared using a 1:1 metal salt to potassium thiocyanate ratio and obtained in moderately high yield (35 – 67 %) as this allows the inclusion of at least one coordination site occupied by a good leaving group (SCN- or halogen donor) [1]. Also, the synthesis is aimed at achieving bridged metal centres via the thiocyanate and this was reported in only a few cases in this study.

4.1 Molecular structure of the ligands

Four crystal structures and packing arrangements of isolated ligands are herein reported. The selected crystallographic data are contained in Table 4.1 in addition to a similar crystal of HL6 already reported. Figure 4.1 is a diagram of the torsional angles of interest. The synthesis and

crystal data of HL^6 has previously been reported in the literature [2], as a free base and as a salt albeit by a different methods of synthesis to the one reported in this work, a reference is made to the crystal data and structure refinement parameters.

Previous studies have indicated, that the most sensitive structural parameters upon intramolecular hydrogen bond formation are the O–H, C–O, C1–C2 and C2–C7 bond lengths [3, 4]. Changes in O–H and C–O bonds are direct consequences of the formation of hydrogen bonds, whereas C1–C2 and C2–C7 distance changes can be more related to intramolecular rearrangement and to steric and electronic interactions [3, 4]. The favourable geometry of these *ortho*- Mannich bases leads to the formation of stable intramolecular hydrogen bonds. The hydrogen bond is nonlinear in the intramolecularly hydrogen bonded systems, and for steric reasons the ring formed by the hydrogen bridge cannot be planar. Therefore, a careful analysis of the geometry of these compounds is necessary [5].

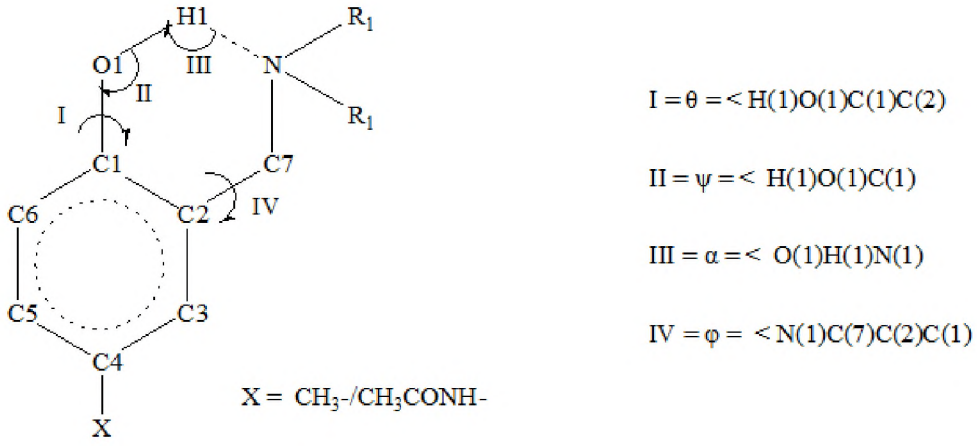

Fig. 4.1: Atom numbering and angles definitions in ortho-Mannich bases.

Table 4.1: Crystal data and structure refinement parameters for isolated ligands.

	HL^5-I This work	HL^5-II This work	$HL^6.HCl.H_2O$ This work	$HL^6.HCl.H_2O$ Latif et al.[2]	HL^7 This work
Empirical Formula	$C_{18}H_{21}N_3O_3$	$C_{18}H_{21}N_3O_3$	$C_{13}H_{21}N_2O_2,Cl,H_2O$	$C_{13}H_{23}ClN_2O_3$	$C_{14}H_{20}N_2O_2$
Formula weight	327.78	327.78	290.78	290.80	248.32
Crystal size (mm)	0.34 x 0.44 x 0.53	0.44 x 0.47 x 0.60	0.22 x 0.40 x 0.43	NA	0.08 x 0.59 x 0.64
Crystal System	Orthorhombic	Monoclinic	Monoclinic	Monoclinic	Monoclinic
Space group	P21 21 21	P21/c	P21/n	P21/n	Cc
a/Å	10.3038(4)	14.1804(7)	9.2145(4)	9.250(3)	8.8235(8)
b/Å	10.8285(5)	9.9963(5)	16.9337(8)	17.018(1)	18.4653(19)
c/Å	15.4149(5)	12.8548(7)	9.9058(5)	9.946(4)	9.0809(9)
α / °	--	90	90	NA	90
β / °	--	112.568(2)	96.476(2)	96.61(2)	114.903(4)
γ / °	--	90	90	NA	90
V / $Å^3$	1719.91(12)	1682.65(15)	1535.80 (13)	1555.3(624)	1342.00(2)
Z	4	4	4	NA	4
λ (MoKα)(Å)	0.71073	0.71073	0.71073	NA	0.71073
T(K)	200	200	200	298(2)	200

Table 4.1: (continued)

	HL^5-I This work	HL^5-II This work	$HL^6.HCl.H_2O$ This work	$HL^6.HCl.H_2O$ Latif et al.,[2]	HL^7 This work
D_{calc} / g/cm^3	1.264	1.292	1.258	1.242	1.229
μ/ mm^{-1}	0.0088	0.089	0.255	0.252	0.083
F (000)	696	696	624	624	536
Refl. Collected/unique	16381/4242	25983/4183	56116/3822	na	9221/2972
Data/parameters	3540/219	2960/219	3464/192	na	2672/168
θmin/max	2.3, 28.3	1.6, 28.3	2.4, 28.3	na	2.2/28.3
Final R indices [I > 2σ(I)]	R1 = 0.0360, wR2 = 0.0905	R1 = 0.0414, wR2 = 0.1183	R1 = 0.0298, wR2 = 0.0860	na	R1 = 0.0323, wR2 = 0.0821
GOOF	1.03	1.03	1.04	na	1.05
Max/min., Δρ	0.14/-0.18	0.20/-0.16	0.35/-0.19	na	0.20/-0.17

na = not available

As a parameter for non-planarity, the torsional angle around the C_{aryl}-C_{alkyl} bond (IV in Figure 4.1) was used. Values ranging from 38.0 – 45.8 degrees have previously been reported [6]. Some of the selected results of x-ray analysis including the selected distances (angstrom) and torsional angles (degrees) are given in Table 4.2 and the Table of bond lengths and angles can be found in the appendix.

Table 4.2: Selected distances (Å), and torsion angles (°) for ortho-Mannich bases in the solid state.

	HL^5-I	HL^5-II	HL^6	HL^7
R(N···O)	2.674(2)	2.678(16)	----	2.676(2)
R(O-H)	0.840	0.950	0.840	0.840
R(N···H)	1.920	1.940	0.853 (15)	1.930
R(C-O)	1.391(2)	1.391(2)	1.361(3)	1.362(2)
I	8.00(3)	3.90(2)	1.65(15)	2.10(3)
II	109.00	109.00	109.00	109.00
III	109.00	109.00	109.00	147.00
IV	38.60(2)	44.02(17)	97.85(11)	40.20(3)

4.1.1 4-methyl-2-((4-(4-nitrophenyl)piperazin-1-yl)methyl)phenol (HL^5)

After the synthesis, isolation and purification of the ligand, the two crystals denoted as I and II were grown and isolated using two different combinations of solvents. Crystal I was obtained from a dilute solution containing mixture of chloroform and ethanol (1:3) while II was from a 1:3 mixture of chloroform and toluene. The interest for this is the comparison with the work of Li *et al.* on polymorphism of the antitubercular isoxyl [7]. The mixtures were slowly evaporated in the dark with the crystals obtained after about five days. These were then collected, washed with ethanol and air-dried.

This was obtained in two crystal systems denoted as I and II with some significant differences in values of their selected distances and torsional angles. The molecular structure of the polymorphs I and II with atom labelling, displacement ellipsoids are drawn at the 50% probability level and a view along the b axis of the crystal packing are presented in Figures 4.2 and 4.3.

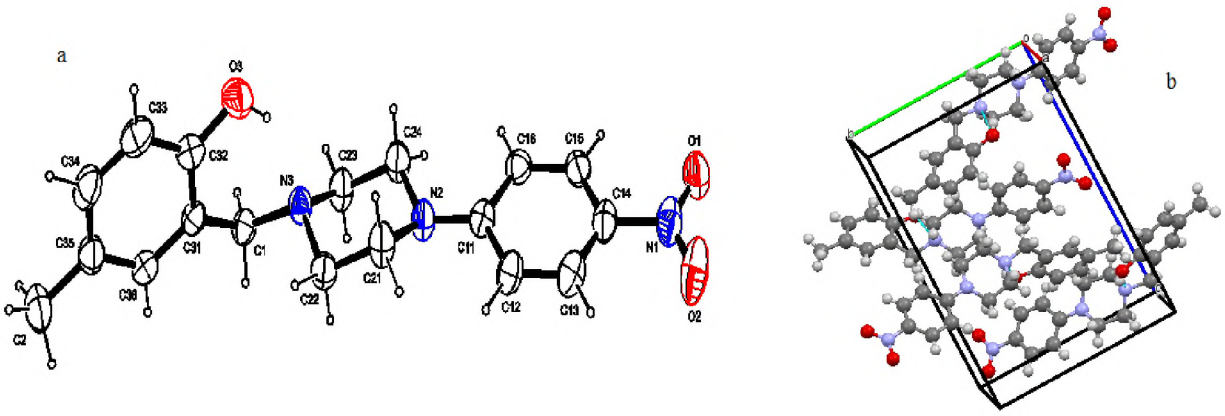

Fig. 4.2: (a) Molecular structure of polymorph I with atom labelling. Displacement ellipsoids are drawn at the 50% probability level. (b) A view along the b axis of the crystal packing of polymorph I.

Based on the foundation that these two crystal systems were obtained from the same building block, the slight differences in bond distances and torsional angles can be attributed to the packing arrangement in the crystal lattice. The values of the bond distances and torsional angles are listed in table 4.1. In the packing arrangement for II, no intermolecular hydrogen bonding are observed.

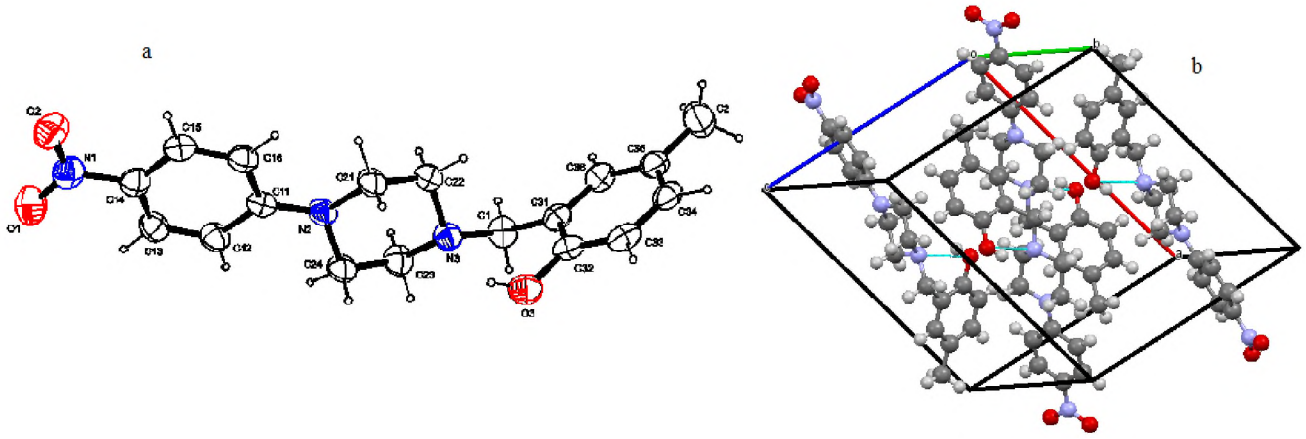

Fig. 4.3: (a) Molecular structure of polymorph II with atom labelling. Displacement ellipsoids are drawn at the 50% probability level. (b) A view along the b axis of the crystal packing of polymorph II.

In the following text, the quantities in square brackets refer to crystal system II. Parameters after which no brackets follow are the same for both the title compounds. Within the H-bond configuration; r(N···O) = 2.674(2) Å [2.6780(16) Å], r(O-H) = 0.8400 Å [0.9500 Å], r(N···H) = 1.920 Å [1.940 Å], r(C-O) = 1.940 Å. Even though there are differences in the values of the O-H bond distances, the r(C-O) remains the same implying that the difference in the H-bonding is not significant.

The selected torsional angles in the compounds are observed to be significantly different in terms of θ = H(3)O(3)C(32)C(31) is 8.0(3)°[3.9(2)°] and as φ = N(3)C(1)C(31)C(32) is 38.6(2)°[44.02(17)°]. This crystallographic data indicate the non-planarity of the chelate ring of the two polymorphic forms of HL[5]. Similar conclusion has been made by Filarowski *et al.*,[8] on 4,5-dimethyl- and 3,5,6-trimethyl-2-(N,N-dimethylaminomethyl) phenols in which similar torsional angles were reported at 31.1(3°) and 41.5(3°) respectively in both compounds. This observation led to the conclusion of the varying degree of H-bonding in the two polymorphs.

4.1.2 N-(3-((diethylamino)methyl)-4-hydroxyphenyl)acetamide (HL^6·HCl)

Even though this compound has been synthesized and its crystal structure reported by Latif *et al.* [2], the synthetic method used in this research is different and the focus herein in terms of the bond distances and torsional (bond) angles are different from those earlier reported [2].

The molecular structure of HL^6 hydrogen chloride salt with atom labelling, displacement ellipsoids are drawn at the 50% probability level and the view along the b axis of the crystal packing of the title compound are presented in Figure 4.4.

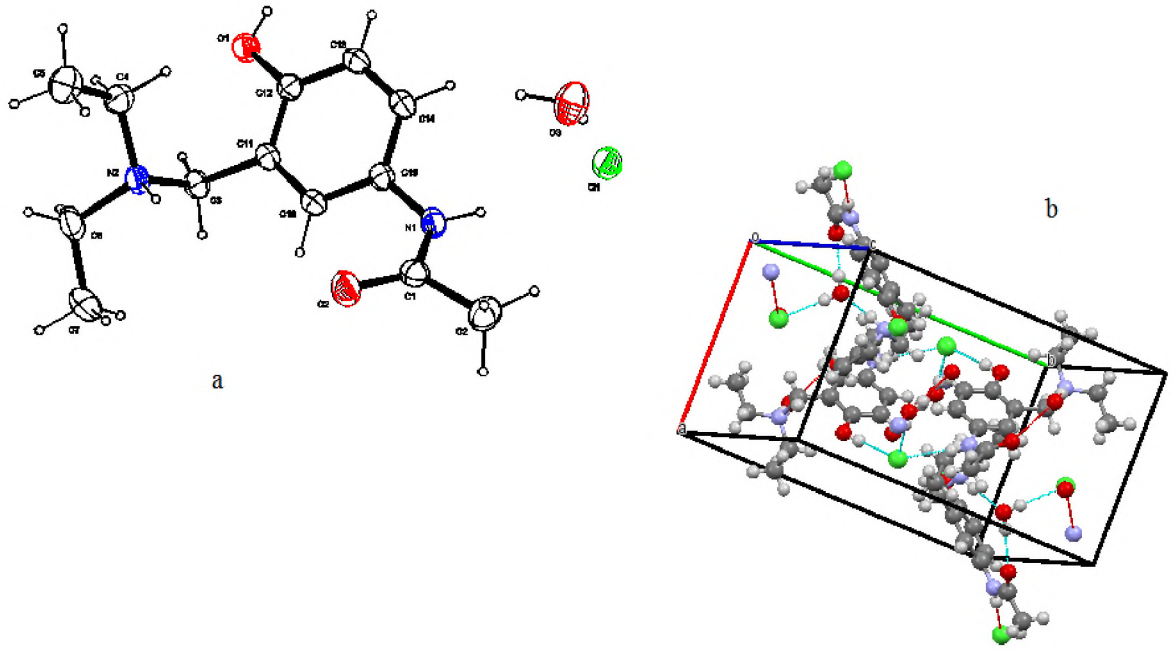

Fig. 4.4: (a) Molecular structure of HL^6 hydrogen chloride salt with atom labelling. Displacement ellipsoids are drawn at the 50% probability level. (b) A view along the b axis of the crystal packing of the title compound.

This crystal structure consists of molecules that are protonated at the diethylaminomethyl nitrogen, involved in a complex hydrogen-bonded network with free chlorine ions and free water molecules. The protonation however causes significant conformational difference and also disrupt the intramolecular hydrogen bonding interaction from the hydroxyl group.

The r(N…H) of 0.853 (15) Å are lower than commonly observed value of about 1.92 Å and this implies a strong hydrogen bonding. Also the φ = < N(2)C(3)C(11)C(12) torsional angle is 97.85(11)°. The results show that the diethylamine and 4-acetamidophenol molecules linked to form the Mannich base are not planar [9].

4.1.3 N-(4-hydroxy-3-((piperidin-1-yl)methyl)phenyl)acetamide (HL^7)

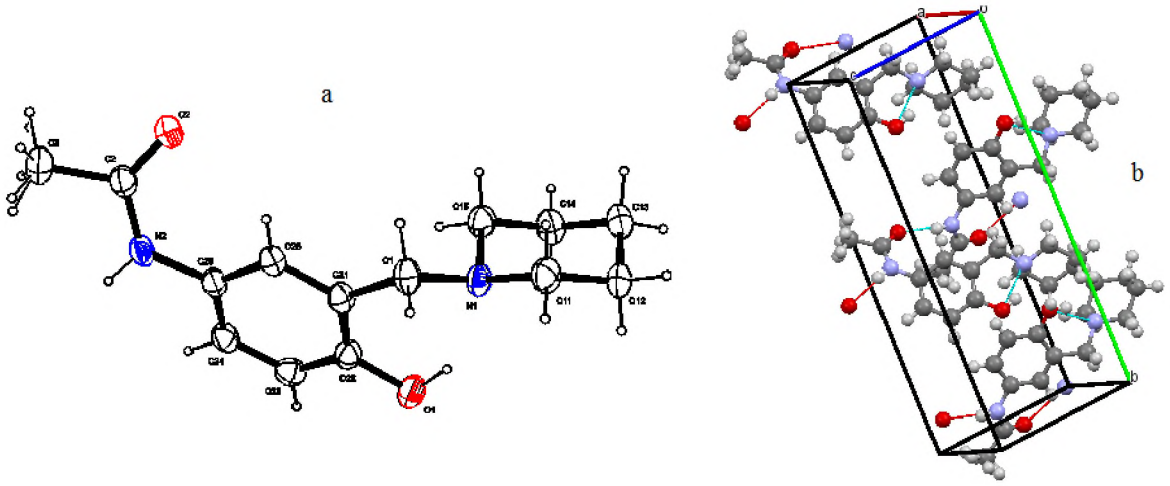

Fig. 4.5: (a) Molecular structure of HL^7 with atom labelling. Displacement ellipsoids are drawn at the 50% probability level. (b) A view along the b axis of the crystal packing of the title compound.

Figures 4.5a and b show the molecular structure of compound HL^7 and its packing arrangements in unit cells. The summary of the crystal data, experimental details and structure refinement for compound HL^7 are listed in Table 4.1. The crystal structure of the ligand comprises molecules that are involved in both intra- and inter-molecular hydrogen-bonding interactions resulting in the formation of dimeric species.

It is observed that the methyl group of the acetamido shows rotational disorder. Intramolecular hydrogen-bonding interactions occur from the phenyl hydroxyl group to the adjacent piperidylaminomethyl nitrogen [O-H---N, 2.676 (2) Å, < 147.00°]. The value of the C-O bond

distance is similar to the literature value of C_{ar}-O (1.362 Å) [10]. The torsional angle IV= φ = N(1)C(1)C(21)C(22) is 40.20 (3)^{o} and that indicates the non-planarity of the amine and phenolic components linked by an intramolecular hydrogen bonding.

4.1.4 Polymorphism in HL[5]

The focus herein is to discuss some of the peculiar differences in the two polymorphic forms of the new Mannich base [4-methyl-2-((4-(4-nitrophenyl)piperazin-1-yl)methyl)phenol]. The isolation, identification and characterization of different crystal forms (polymorphs, solvates, salts and co-crystals) of the same molecule or of aggregates of the same molecule with other molecules represents one of the most active areas of modern solid state chemistry [11].

The importance of polymorphism lies in the fact that physical properties (melting point, colour, solubility, refractive index, hardness, conductivity, etc.) of a given compound vary between the polymorphic forms [12]. Of great significance as far as the application is concerned are the polymorphic forms of pharmaceutically active substances. Since the solubility and dissolution rates are different the bioavailability is affected [13].

The analytical strategy in approaching a polymorphism study will be dictated by the availability of instrumentation, time and material [14]. Searching through the literature revealed some of the methods employable in elucidating some of the distinguishing features of polymorphs and popular among such are infrared spectroscopy, differential scanning calorimetry (DSC) and powdered x-ray diffraction (PXRD) amongst others [15]. Results from these techniques are outlined below:

4.1.4.1 Infrared spectroscopy (MIR)

FTIR spectra for form I and form II using ATR-FTIR with the investigation focused on O-H stretching bands in the spectral range 2800 - 2900 cm^{-1} and the (C-N-C) stretching bands of the piperazine moiety in the spectral range 1110 – 1260 cm^{-1} are presented in Figures 4.6 and 4.7.

The O-H bands are broad and occur at lower frequencies indicating the presence of hydrogen bonding, also the values of the stretching frequencies and shapes are distinguishing features between the polymorphs. The same rationale can be applied to the (C-N-C) stretching frequency.

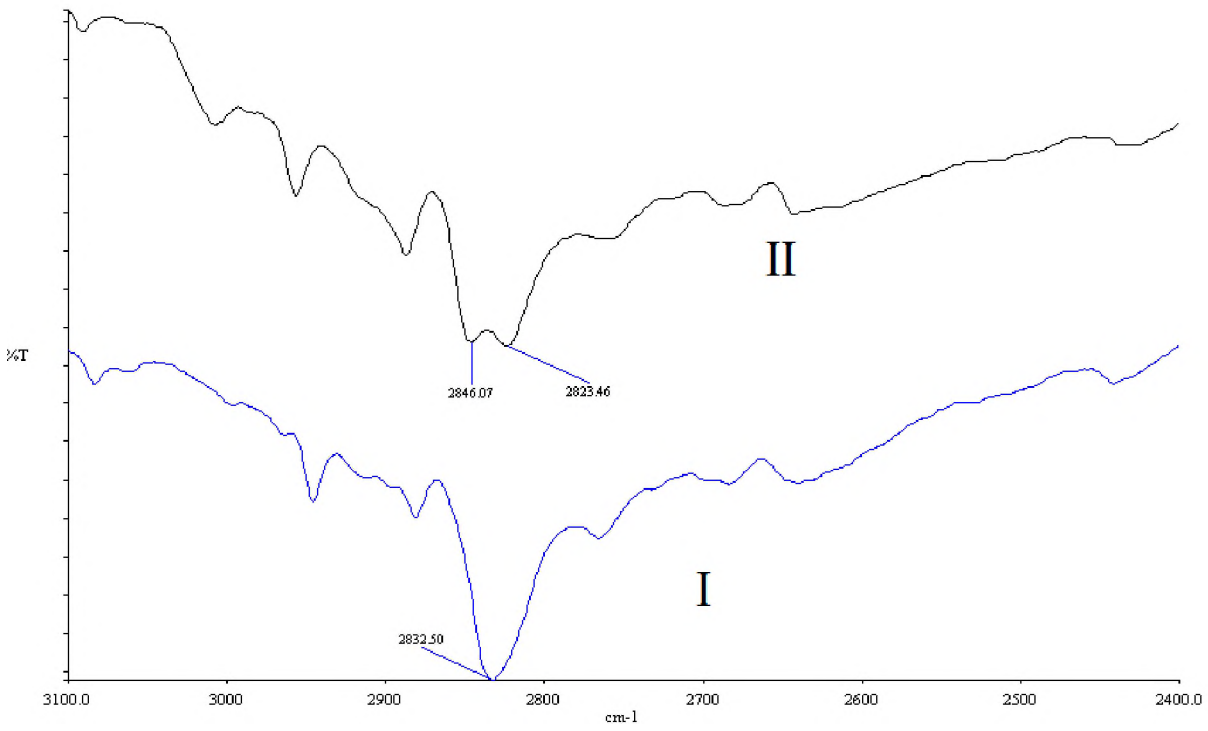

Fig. 4.6: ATR-IR spectra for forms I and II in the O-H stretching region.

The stretching frequency of the phenolic hydroxyl group of the ligand is observed as broad bands at 2832 cm^{-1} and 2846 cm^{-1} in forms I and II respectively. These low values of νCN is due to hydrogen bonding within the crystal packing [16]. The νCN of unsymmetrically substituted piperazine has been reported to respond to changes in conformation (boat – chair conformation) while two stretching frequencies are mostly recorded [17, 18]. The stretching frequencies are observed as broad bands at 1254/1115 cm^{-1} and 1245/1114 cm^{-1} in forms I and II respectively. The end of the piperazine with the nitrogen atom involved in H-bonding has a higher wavenumber than the other. These values of stretching frequencies are not significantly different and so the extent of hydrogen bonding is a little different between the two polymorphs.

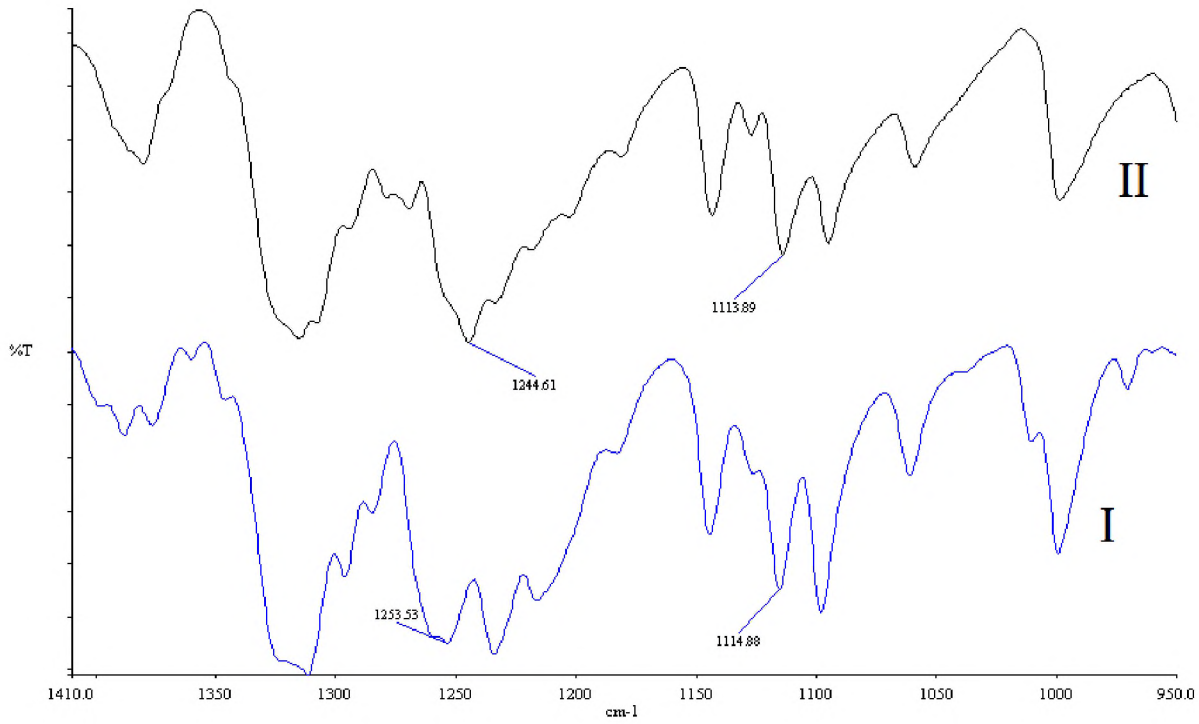

Fig. 4.7: ATR-IR spectra for forms I and II in the piperazine (C-N-C) stretching region.

4.1.4.2 Thermodynamic stability analysis

The DSC results for the two polymorphs are shown in Figure 4.8 below. The DSC trace for form I exhibited two endotherms, labelled A and B. The first endotherm (A) is attributed to a phase change in Form I. The second endotherm (B) results from the melting of the resulting crystal modification. The DSC trace for Form II exhibited only one endotherm (B), which represents the melting of form II.

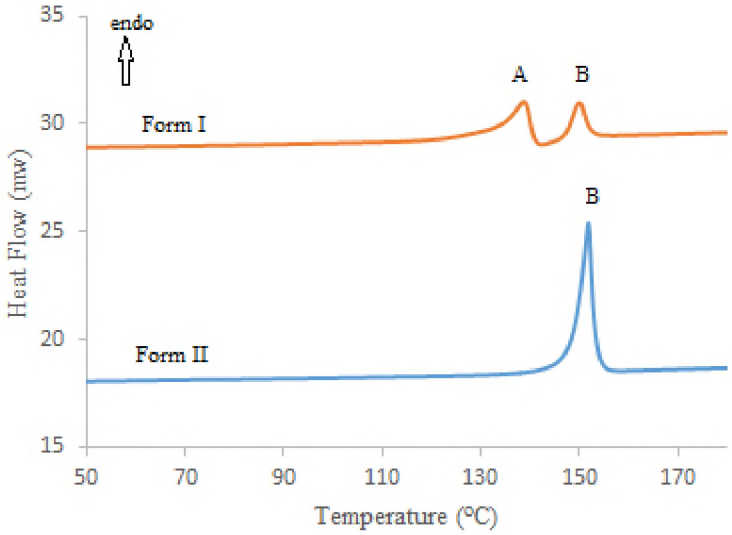

Fig. 4.8: DSC traces of form I and form II.

4.1.4.3 Powder X-ray diffraction (PXRD)

The PXRD patterns of form I and form II were subsequently recorded at room temperature and shown in Figure 4.9. Though variable temperature PXRD is a more ideal tool in differentiating polymorphs, runs at room temperature revealed different patterns for the two polymorphs.

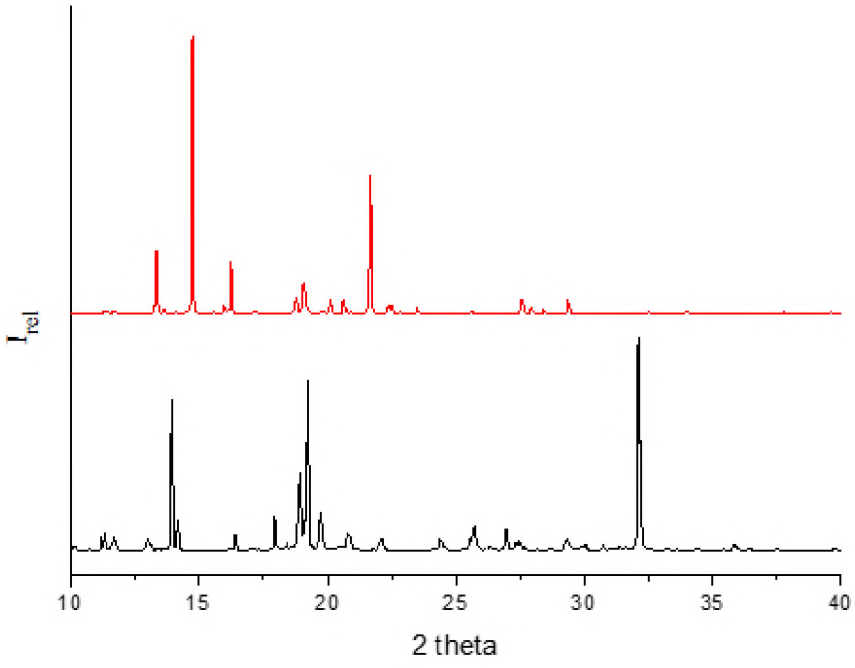

Fig. 4.9: Experimental PXRD patterns of form **I** (bottom) and form **II** (top).

Comparing our results with those found in the literature shows that polymorphs generally possess different PXRD patterns at room temperature with similar patterns only usually observed at the transition temperature [7].

4.2 ^{1}H and ^{13}C-NMR study of the ligands

The two ortho- positions on para-substituted phenols contain acidic protons that are available for Mannich reaction. Rigorous separation techniques including column chromatography are required in cases where mixture of products (mono- and di- bases) is encountered. NMR spectroscopic techniques are very useful in distinguishing mono- from di-Mannich bases by evaluating the integration of aminomethylated protons.

4.2.1 ^{1}H-NMR spectral data of p-cresol based ligands (HL^{1-5})

The ^{1}H-NMR spectral data of this series together with their assignments are presented in Table 3.1. The data obtained supports the structures depicted in Scheme 2.1 and are in agreement with proton NMR data typically observed for Mannich bases. In this group of compounds, focus is mainly on the methylene group joining the phenol and the secondary amine and piperazine protons.

The chemical shifts observed for the methylene protons ($ArCH_2N$) has been shown to be dependent on the substituents on the benzene ring and also on the electronic environment provided by the substituted amine component. The chemical shift values observed for ($ArCH_2N$) signal was found at δ 3.62 – 3.77 ppm and it appears as a singlet. This is similar to the values of δ 3.65 – 3.70 ppm reported in the literature for Mannich base from substituted phenols [19, 20]. The observation of this signal confirms the successful 3-part condensation of phenol and amine plus formaldehyde. HL^1 has been previously reported in the literature [21], the assignments in this work are in close agreement with those reported in the literature. HL^3 has also been reported in the literature but the method of synthesis reported herein is different

but with a lower yield - 70% compared to 87% reported by Ambu and Kandaswamy [20]. Ligands HL^2, HL^4 and HL^5 are new additions to the existing list of Mannich bases of p-cresols based on the literature search for this work.

The OH proton absorbed downfield at δ 6.92 -10.01 ppm. As these values are not extremely downfield as would be observed in the case of strong intramolecular H-bonding in solution, it is safe to assume that strong H-bonding in solution is only observed in the case of HL^5 with a δ-value of 10.01ppm. It is worth mentioning that the electronic environment provided by the amine component of the Mannich bases dictates the extent of the H-bonding which in turn affects the chemical shift of the Ar-OH signal. Strong intramolecular H-bonding in the ligand leads to a large downfield shift of the hydroxyl proton resonance. In the ligand HL^3 containing piperazine all the protons and carbons are isoelectronic at 2.90 and 52.3 ppm respectively revealing that the Mannich reaction took place at both ends of the piperazine whereas the piperazine units maintained its two different environments in HL^4 and HL^5 thus showing an unsymmetrical substitution [22]. A representative ^{1}H-NMR spectrum of p-cresol based ligand (HL^4) is presented in Figure 4.10 below while the ^{1}H-NMR spectra for all the other ligands can be found in the appendix.

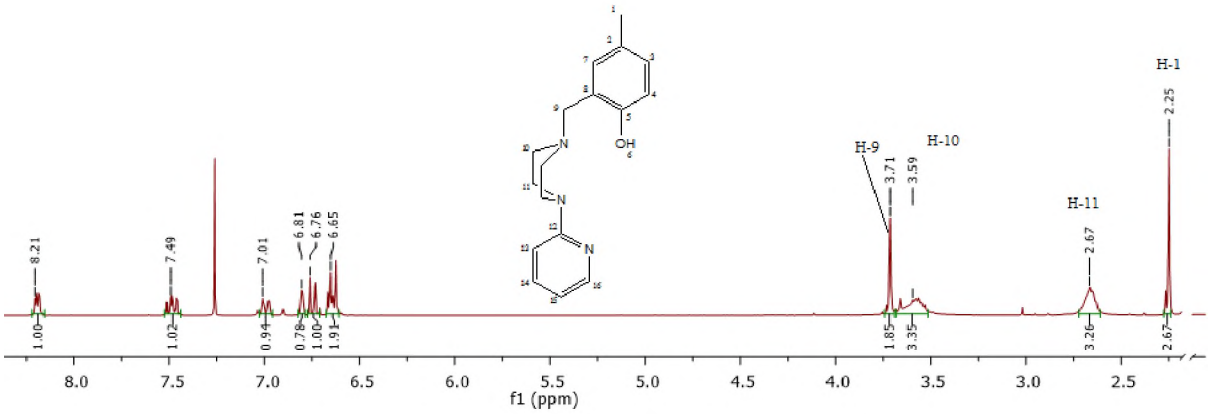

Fig. 4.10: ^{1}H-NMR spectrum of ligand HL^4 showing the methylene protons at 3.75 ppm.

The methyl groups on the phenol of the ligands are observed upfield as a sharp intense singlet signal between δ 2.20 – 2.30 ppm. Also, the chemical shifts due to the aromatic ring protons of both the phenolic moiety and the phenyl ring on the secondary amine are observed downfield as multiplets in the region δ 6.60 – 8.30 ppm for all the ligands. The expanded aromatic region (6.60 – 8.30 ppm) of $HL^4$is shown in Figure 4.11. All the protons and multiplicities are well accounted for.

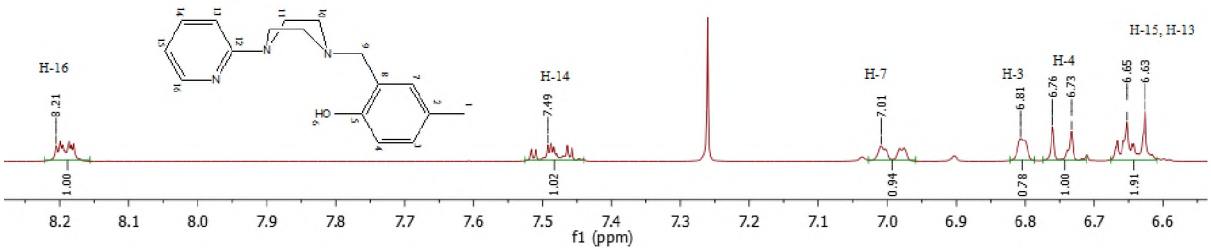

Fig. 4.11: ^{1}H-NMR spectrum of ligand HL^4 showing only the aromatic protons.

4.2.2 ^{13}C-NMR spectral data of p-cresol based ligands (HL^{1-5})

The ^{13}C-NMR data obtained and the corresponding assignments are listed in Table 3.2 for the p-cresol Mannich bases and the spectra accounts perfectly for all the carbon atoms of the Mannich bases in their various electronic environments. The signals for the $ArCH_2N$ in the various Mannich bases are observed in the region δ 56.0 – 63.0 ppm. Aromatic carbons are observed in the region of δ 107.0 – 160.0 ppm and in good agreement with those reported in the literature [20]. The ^{13}C-NMR data are in good agreement with their ^{1}H-NMR ones.

A typical ^{13}C NMR spectrum for HL^4 is provided in Figure 4.12 below. The ^{1}H and ^{13}C NMR spectra for all the p-cresol based Mannich ligands and their assignments can be found in the appendix.

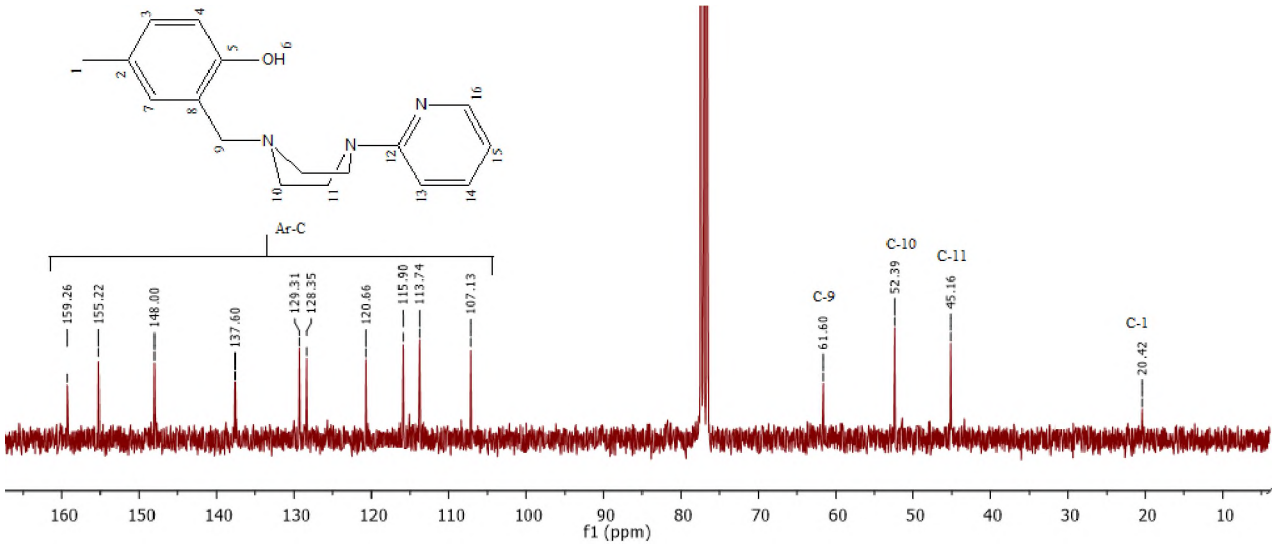

Fig. 4.12: ^{13}C-NMR spectrum of ligand HL^{4} showing the aminomethylated and other carbon atoms.

4.2.3 ^{1}H-NMR spectral data of p-acetamidophenol based ligands (HL$^{6\text{-}10}$)

The NMR spectral data is similar to those observed for the p-cresol Mannich bases especially in the aromatic region. The ^{1}H-NMR spectral data for the ligands together with the relevant assignments are provided in Table 3.3. Full ^{1}H and ^{13}C NMR spectra with their complete assignments can be found in the appendix.

The $ArCH_2N$ signal which serves as an indication of the successful condensation of the substituted phenols and amines are observed upfield as sharp, medium intense signals in the region of δ 3.56 – 4.15 ppm. These values are in close agreement with those reported in some of the studies conducted by Blade-Font and de Mas Rocabryca [23]. A representative ^{1}H NMR spectrum of HL^{7} is given in Figure 4.13 below to illustrate the spectral pattern.

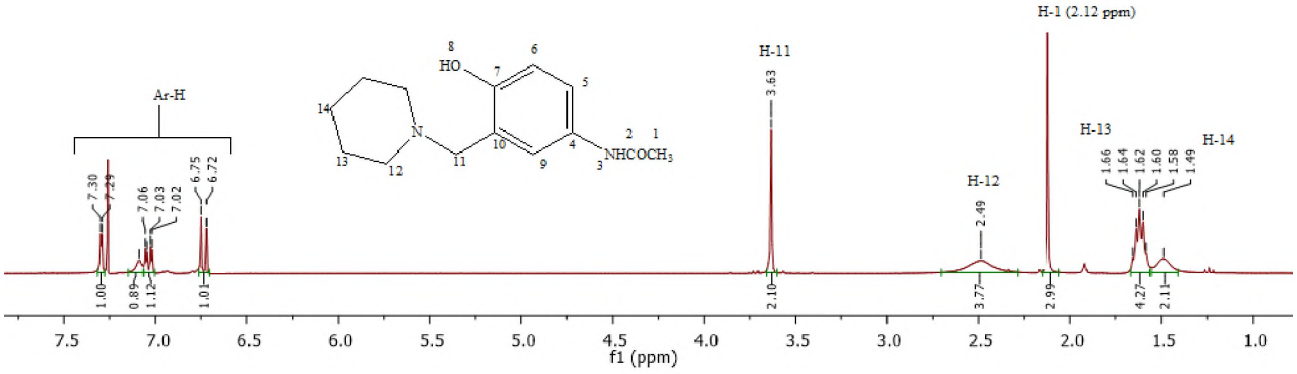

Fig. 4.13: ^{1}H-NMR spectrum of ligand HL^{7} showing the methylene and aromatic protons.

The aromatic region between 6.80 and 7.50 ppm of ligand HL^{7} is presented in Figure 4.14 with the three protons well assigned.

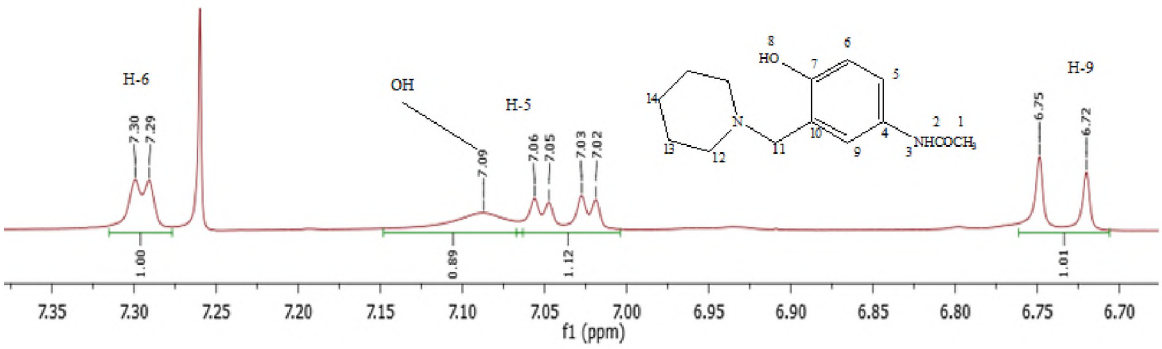

Fig. 4.14: ^{1}H-NMR spectrum of ligand HL^{4} showing only the aromatic protons and OH at 7.09 ppm.

The aromatic protons for the acetamidophenol and the aromatic rings attached to the amine are observed downfield in the range δ 6.60 – 8.20 ppm. The NMR features observed confirm monoaminomethylation on the ortho-position to the hydroxyl group. Even though there is a possibility of N-Mannich bases to be formed by acetamidophenols [24], this possibility is ruled out because there were no isoelectronic protons observed in the aromatic region. The peak for the hydroxyl proton was recorded at 10.61, 7.09 and 9.24 ppm in HL^{6}, HL^{8} and HL^{10} respectively.

To the best of the knowledge of the literature available, only HL^6 has been reported in the literature-synthesis, NMR and crystal data [2] with the NMR data in agreement with the ones reported in this work. In addition, the synthetic route has been highlighted in the course of other reactions [25]. All the other acetamidophenol ligands here are newly synthesised, characterised and reported. Asymmetric nature of the protons and carbon atoms of the piperazine in HL^9 and HL^{10} by the observation of two different signals in the ^1H and ^{13}C spectra for the piperazine unit. This observation is supported by the work of Al-Abdullah *et al.* [26]. It was observed that the ^1H chemical shift of HOD (deuterated water) in DMSO-d_6 at 3.30 ppm appear as a broad band near the peak of the aminomethylated hydrogens in HL^8 and HL^{10} and required careful attention in its interpretation.

4.2.4 ^{13}C-NMR spectral data of p-acetamidophenol based ligands

The ^{13}C-NMR data obtained and the corresponding assignments are listed in Table 3.4 for the p-acetamidophenol ligands. The signal for the $ArCH_2N$ is observed in the region δ 56.0 – 63.0 ppm. Aromatic carbons are observed in the region of δ 107.0 – 160.0 ppm. The ^{13}C-NMR spectra data are in good agreement with their ^1H-NMR ones.

In the ligand HL^8 containing piperazine, all the protons and carbons are isoelectronic at 3.55 and 52.0 ppm respectively revealing that the Mannich reaction took place at both ends of the piperazine whereas the piperazine units of the maintained its two different environments in HL^9 and HL^{10} thus showing an asymmetrical substitution. ^{13}C NMR spectrum of HL^7 showing all the carbon atoms is presented Figure 4.15 as a representative for this group.

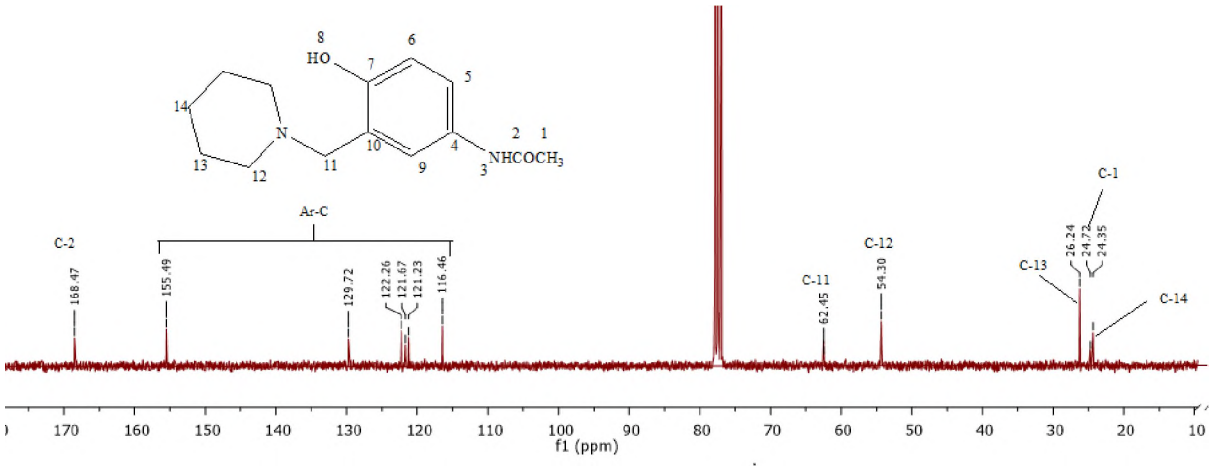

Fig. 4.15: ^{13}C NMR spectrum of HL^7 showing all the carbon atoms (the aminomethylated carbon (C11) is at 62.45 ppm.

4.3 Molar conductivities of ligands and their metal complexes

Molar conductivity measurements carried out in DMSO with 10^{-3} mol/dm^3 solution of the compounds revealed the electrolytic and non-electrolytic nature of the compounds. The ligands have molar conductivity values within the range of 3.28 – 36.99 and are considered as non-electrolytes. The molar conductivity values (reported in Tables 3.7 – 3.16) for the complexes are within the range of 4.38 – 161.77 $\Omega^{-1}.cm^2.mol^{-1}$. Conductivity measurements have frequently been used in structural characterisation of metal chelates (mode of coordination) within the limits of their solubility. Ali *et al.* [27] has reported that DMSO solutions with molar conductance less than 50 are non-electrolytes while those with molar conductance greater than 50 are electrolytes [27]. Also, 1:1 electrolytes have molar conductivity values in the range of 50 – 90 $\Omega^{-1}.cm^2.mol^{-1}$ while 1:2 electrolytes have molar conductivity values in the range 90 – 195 $\Omega^{-1}.cm^2.mol^{-1}$. All the metal complexes studied in this work are discussed based on this predicted values.

This technique provides a method of testing the degree of ionization of the complexes, the molecular ions that a complex liberates in solution in the case of anions present outside the

coordination sphere. The more anions present outside the coordination sphere, the higher will be its molar conductivity and vice versa [5] as in the case of 1:2 compared to 1:1 electrolyte. Table 4.3 presents the three groups of compounds involved in this study based on their electrolytic nature.

Table 4.3: Classification of compounds as electrolytes and non-electrolytes.

Non-electrolytes	**1:1 electrolytes**	**1:2 electrolytes**
HL^1, HL^2, HL^3, HL^4, HL^5, HL^6, HL^7, HL^8, HL^9, HL^{10},1, 3, 4,5,6,7,8,9,11, 13,14,15,16,17,19,21,22, 24, 25, 29, 31, 33, 35, 37, 39	10,12,18,23, 26, 27, 28,30, 34, 36, 40	2, 20, 32, 38

It is clear from the conductivity data, that some of the metal complexes are electrolytes. Also the molar conductance values indicate that the anions may be present outside or absent or inside the coordination sphere. Carrying out conductivity measurements in DMSO suffer some attendant challenges like high viscosity and strong donor capacity and therefore not much information are obtainable like those carried out in solvents like acetonitrile or methanol [28, 29]. Metal complexes with molar conductance in the range 35 – 161.77 $\Omega^{-1}.cm^2.mol^{-1}$ suggest 1:1 and 1:2 electrolytes in DMSO [30].

4.4 Mid-infrared study of the ligands and metal complexes

Here, a brief introduction is presented into the discussion of the infrared data of each ligand followed by its Cu(II) and Fe(III) complexes thus laying a foundation of what to expect within each group. The discussion of each group is concluded by the features of the thiocyanate containing metal complexes.

The prominent-diagnostic infrared data for all the Mannich bases and their metal complexes are presented in Tables 3.17 – 3.26. The most important diagnostic features are observed in the

stretching frequencies of the hydroxyl group (νOH) in the ligand or presence of coordinated water, the νC-O of the phenolic ligand and the (νCNC) in the amine component of the Mannich bases [5, 31]. The frequency of these bands are important in reporting H-bonding or complexation in metal complexes of Mannich bases.

H-bonding (particularly intramolecular type) is observed to influence greatly the lowering of the values of stretching frequencies of these bonds. Values in the range of 3400 – 3000 cm^{-1} are observed for the νOH. As shown by previous X-ray diffraction studies, the intramolecular hydrogen bond in Mannich base can be considered as strong, with the O···N distance of about 2.58 Å [32] and is close to the value of 2.67 Å reported for $HL^{5,6,7}$ in this study. As a distinction to intermolecular hydrogen bonds, the intramolecular H···N bond in a Mannich base with strong H-bond is not linear [32]. As previously noted in the solid state, the νOH band is usually broad; its frequency shift depends on the nature of the amine component and can be as large as 1000 cm^{-1} compared to a free OH group [6]. ^1H NMR spectroscopy run in deuterated $CDCl_3$ did not support the presence of strong H-bonded Mannich base in solution (evidenced by the OH appearance below 10 ppm) in contrast to the literature [16].

In this work, the νOH ranged from 3336 –3014 cm^{-1} and 3387-3250 cm^{-1} in p-cresol and p-acetamidophenol based ligands respectively. This observation leads to the conclusion that H-bonding are more pronounced in the p-cresol based ligands than the p-acetamidophenol based ligands and this can be attributed to the inductive effect provided differently by the substituents ortho to the phenolic hydroxyl group. Several other groups of compounds have shown considerable decrease in the stretching frequency of the phenolic OH which has been attributed to H-bonding. In particular, infrared spectroscopic studies conducted on Schiff bases by Freedman [33] showed the vibrational mode for the phenolic OH to extend over the range 3300 – 2300 cm^{-1} due to strong intramolecular hydrogen bonding of O-H to C=N [33].

The stretching frequencies ν(CNC) of the amine component of the ligand are observed in the range of 1240 – 1140 cm^{-1} and generally give medium intense bands. It was observed that ligands containing unsymmetrical piperazine moiety display two distinct stretching frequencies as reported in the literature [17, 34, 35]. Both the νOH and ν(CNC) are observed to shift significantly (upward or downward) averagely by 50 – 250 cm^{-1} and 5 – 80 cm^{-1} upon complexation respectively.

Asymmetrically substituted piperazine (e.g. 1-acetylpiperazine) has been reported to display two bands assigned to the CN vibration at about ν1 = 1254 cm^{-1} and ν2 at 1143 cm^{-1}, a metal ion occupying the core of the piperazine ring leads to a boat conformation unlike the chair conformation in a free ligand with shifts in frequencies also experienced [17].

Application of infrared spectroscopy for the purpose of differentiating between the various bonding modes of the thiocyanate is based on the fact that the S- or N-coordinated thiocyanate ligand gives significantly different shifts of absorption bands not only in relation to each other, but in comparison with non-coordinated thiocyanate anion as well [36]. Also stretching frequencies observed in the range 2180 – 2030 cm^{-1} are assigned to νCN of the thiocyanate and are observed in all the metal complexes indicating that the (SCN^-) is co-ordinately bound to the metal complexes. The absorption frequency, splitting and intensity are vital to assigning the nature of bonding as S-bonded, N-bonded, bridged etc. Also, the νCS is observed at 670 – 830 cm^{-1} [36] and this compliments the efforts to determine the nature of the bonding of the thiocyanate moiety.

Summarily from the literature, N-coordinated metal complexes display νCN as strong, broad bands between 2100 – 2050 cm^{-1} and νCS as weak band between 870 – 820 cm^{-1} [37] while S-coordinated metal complexes display νCN at lower value compared to N-coordinate forms [38] as strong, split bands between 2130 – 2085 cm^{-1} and νCS as a weak band between

760 – 700 cm^{-1}. In the case of bridged thiocyanate groups, νCN is observed between 2165 – 2065 cm^{-1} [39] and νCS between 800 – 750 cm^{-1}. The mid-infrared data for the p-cresol and p-acetamidophenol based ligands and their metal complexes are discussed below.

4.4.1 Mid-infrared data for the p-methylphenol based ligands and metal complexes

The full infrared spectra of the ligand along with its metal complexes can be found in the appendix.

4.4.1.1 Mid-infrared data for ligand (HL^1) and metal complexes 1 - 4

The infrared data for 2-((diethylamino)methyl)-4-methylphenol (HL^1) with its copper(II) and iron(III) complexes are reported in Table 3.19. Metal to ligand ratio in the complexes is (1:1) as confirmed from elemental analysis. All the metal complexes are non-electrolytes except **2** which is a 1:2 electrolyte in solution. Prominent diagnostic features adequate for the elucidation of the structure of the metal complexes include νOH, νC-O and νCNC. Only complexes **1** and **4** contain the ligand in its deprotonated form.

The νOH of the ligand is centred at 3336 cm^{-1} as a medium-intense, broad band but shifts upward by 12 and 14 cm^{-1} respectively to higher wavenumbers in complexes **1** and **2** indicating a relaxation in the H-bonding to give less intense bands and the broadness is reduced indicating complexation. Complexation with the ligand to give iron complexes **3** and **4** leads to the observation of broader OH band at lower frequencies 3251 and 3229 cm^{-1} respectively, this may also indicate the presence of coordinated water molecules. Shifts in the OH band are noted to coincide with upward shifts in the νC-O stretching bands of the phenol, thus indicating that the deprotonation of the ligand before complexation in **1** and **4** and the impact of the thiocyanate on hydroxyl group is after coordination in **2** [40]. νC-O frequencies have been reported to shift downward upon complexation with Cu(II) despite deprotonation of Schiff bases of 2-Hydroxy-1-naphthyaldehyde [41].

The νCNC frequencies are reduced upon complexation from 1168 cm^{-1} in the ligand to the range of 1158 – 1154 cm^{-1} in the metal complexes with the intensities fairly reduced. This is indicative of the involvement of the N-atom of the Mannich base in the complexation [42].

In the thiocyanate complexes **2** and **4**, the stretching vibration νCN is observed at 2119 cm^{-1} (broad, split) in the copper(II) complex **2** and 2049 cm^{-1} (broad) in the iron(III) complex **4**. It can be inferred that S-bonding and N-bonding are observed in the copper and iron complexes respectively. The assertion is supported by the observation of νCS at 757 cm^{-1} and 828 cm^{-1} for **2** and **4** respectively [36, 43].

4.4.1.2 Mid-infrared data for ligand (HL^2) and metal complexes 5 – 8

The infrared data for 4-methyl-2-((piperidin-1-yl)methyl)phenol (HL^2) with its copper(II) and iron(III) complexes are reported in table 3.18. All the metal complexes have a 1:1 (metal to ligand) ratio as determined from the elemental analysis and have molar conductivity values below 35 $\Omega^{-1}cm^2.mol^{-1}$ thus revealing them as non-electrolytes in solution. The Cu(II) ion in **5** is bonded to the deprotonated form of the ligand.

The νOH of the ligand is centred at 3014 cm^{-1} as moderate-intense, broad band, a feature in support of strong intramolecular hydrogen bonding but shifts upward to 3298 – 3372 cm^{-1} in the metal complexes. The band is not observed in the thiocyanate copper(II) complex of the ligand indicating deprotonation of the hydroxyl group of the ligand prior to complexation and the absence of coordinated water molecules. In the iron(III) complexes, the broad nature of the absorption band of the hydroxyl group νOH may be indicative of the presence of coordinated water molecules [44].

The stretching mode of νCNC showed a positive shift ~ 20 – 40 cm^{-1} in the metal complexes compared to the free ligands with the intensities also reduced. This is indicative of the involvement of the N-atom of the Mannich base in the complexation [45].

The stretching vibration νCN in the thiocyanato complexes is observed at 2076 cm^{-1} (strong, sharp) in the copper complex and 2049 cm^{-1} (broad) in the iron complex. In both metal complexes, N-bonding can be inferred because of the nature of the νCN absorption band. The assertion is supported by the observation of the νCS in the range of 783 cm^{-1} and 824 cm^{-1} for the copper and iron complexes respectively [37, 46].

4.4.1.3 Mid-infrared data for ligand (HL^3) and metal complexes 9 - 12

The infrared data for 2-((4-(2-hydroxy-5-methylbenzyl)piperazin-1-yl)methyl)-4-methylphenol (HL^3) with its copper(II) and iron(III) complexes are reported in Table 3.19. Elemental analysis supports (1:1) metal to ligand ratio (mononuclear) for all the metal complexes except **10** (dinuclear) in ratio (2:1) and deprotonated ligand is only encountered in complexes **10** and **12**. The thiocyanate complexes have molar conductivity values between 55 and 90 $\Omega^1.cm^2.mol^{-1}$ and so are 1:1 electrolytes while **9** and **10** are non-electrolytes.

Very strong intramolecular bonding in the metal complexes are expected because of the ligand's ability to form a six membered ring through hydrogen bonding and this is indicated by the νOH value of 3023 cm^{-1}. This value shifts to higher frequency in the range 3362 – 3387 cm^{-1} with the intensity increased; this is indicative of the hydroxyl groups of the phenol participating in the complexation and/or the presence of water molecule. The νC-O of the ligand observed at 1242 cm^{-1} shifts by 19 – 36 cm^{-1} to lower frequencies in **9** and **10** while an upward shift to higher wavenumbers was observed in **11** and **12**. This suggests the involvement of hydroxyl group of the ligand in complexation with subsequent loss of H-bonding in the copper(II) complexes (**9** and **10**) and deprotonation in the iron complexes (**11** and **12**) leading to a direct phenolate bond [47].

The stretching mode of νCNC is observed at a single frequency and showed a very interesting pattern. A single frequency is assigned to this ring vibration at 1150 cm^{-1} in the ligand and

downward shift ~ 18 – 22 cm^{-1} are observed in **9** and **10** and upward shift ~ 56 – 57 cm^{-1} are observed in **11** and **12** with the intensities remain unchanged. This is indicative of the involvement of the N-atoms of the Mannich base in the complexation in all cases with the direction of the shifts dictated by the boat-chair conformations of piperazine [18, 45].

In thiocyanate containing complexes **10** and **12**, the stretching vibration νCN is observed at 2086 cm^{-1} (strong, split) in the copper complex and 2025 cm^{-1} (broad) in the iron complex leads to the conclusion that S-bonding takes place in the copper(II) complexes and N-bonding in the iron(III) complexes as supported by the infrared data obtained. The assertion is supported by the observation of the νCS at 758 cm^{-1} and 739 cm^{-1} for the copper and iron complexes respectively [36, 43].

4.3.1.4 Mid-infrared data for ligand (HL^4) and metal complexes 13 - 16

Structural characterization data for the free ligand and its copper(II) complexes and iron(III) are provided in Table 3.20 while the spectra are provided in Figure 4.16 as a representative for this group of compounds. Complexes **13** – **15** are in 1:1 metal to ligand ratio (mononuclear) with the ligand deprotonated in **15** and **16** and only complex **16** is dinuclear within this group. In addition, all the metal complexes are non-electrolytes.

Very strong intramolecular H-bonding is responsible for the observation of the stretching frequency of the hydroxyl group of the ligand at 3056 cm^{-1} and this values shift to higher frequency in the range 3382 – 3368 cm^{-1} in the metal complexes indicating the loss of H-bonding upon complexation. The extent or nature of the involvement in complexation with metal ions can be supported by the νC-O of the phenolic ligand. The νC-O of the free ligand appeared as a sharp intense band at 1256 cm^{-1} but shifts to lower wavenumber 1240 cm^{-1} in **13** and averagely upward by ~ 19 cm-1 in **14** – **16**. The upward shift in **14** compared to **13** may be

due to the effect of the thiocyanate substitution while in **15** and **16**, this is a clear evidence of deprotonation of the hydroxyl group [40].

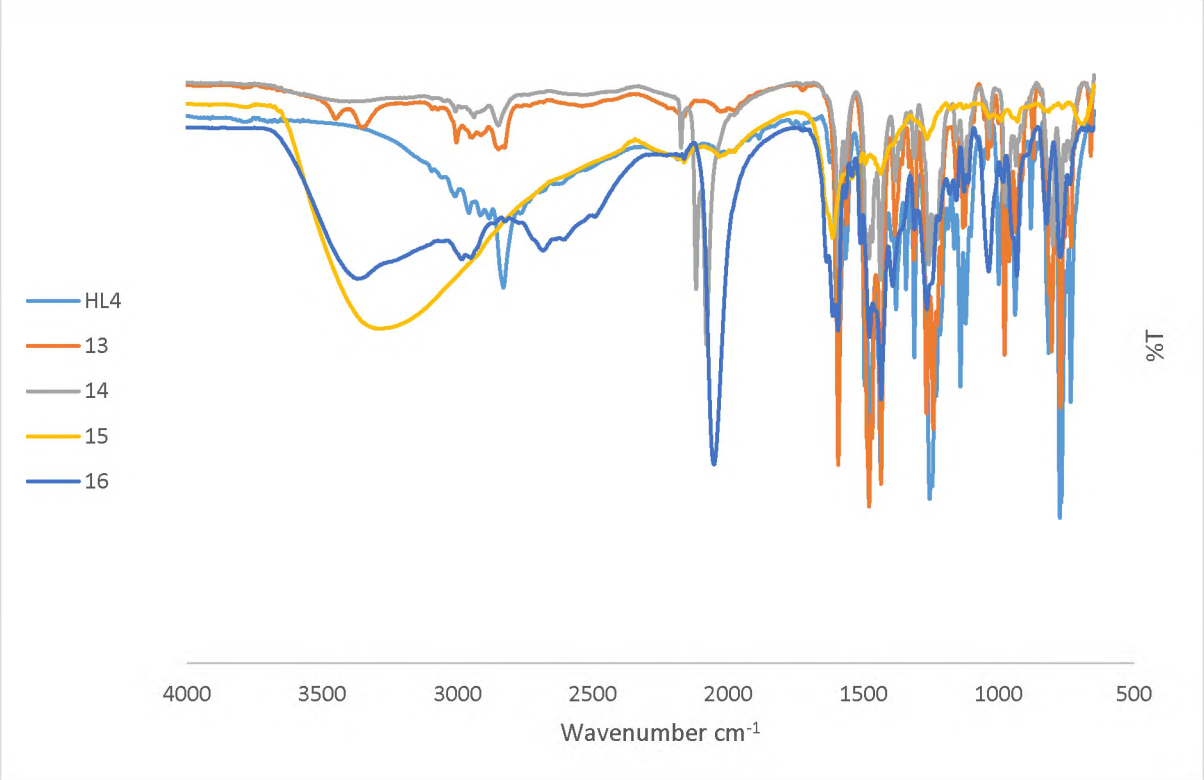

Fig 4.16: IR spectra of ligand HL^4 and its metal complexes **13 – 16**.

Two different stretching modes of νCNC ν1 = 1247 and ν2 = 1143 cm^{-1} are observed indicating the different electronic environments of the N-atoms of the piperazine moiety of the Mannich base. Negative shift ~ 4 – 17 cm^{-1} is observed in the copper and iron complexes with a reduction in their intensities. The exception is the case of complex **15** where an upward shift of 40 cm^{-1} is observed in ν2. This is indicative of the involvement of the both N-atoms of the piperazine in Mannich base in the complexation with the central metal ions and complexation followed by a change in the conformation of piperazine as is the case of **15** [18, 42].

For thiocyanate complexes **14** and **16**, the stretching vibration νCN is observed at 2118 cm^{-1} (strong, split) in the copper complex and 2051 cm^{-1} (broad) in the iron complex. S-bonding is therefore indicated for the copper(II) complex (**14**) and N-bonding in the iron(III) complex (**16**)

as observed from the infrared data obtained. The assignments are supported by the observation of the νCS at 874 cm^{-1} and 774 cm^{-1} for the copper and iron complexes respectively as observed in the literature [36, 48].

4.4.1.5 Mid-infrared data for ligand (HL^5) and metal complexes 17 – 20.

The infrared data for 4-methyl-2-((4-(4-nitrophenyl)piperazin-1-yl)methyl)phenol (HL^5) with its copper(II) and iron(III) complexes are reported in Table 3.21. The elemental analysis revealed that **17** and **19** are 1:1 (metal to ligand ratio) stoichiometry (mononuclear) while the stoichiometry of **18** and **20** which are thiocyanate containing metal complexes are in ratio 2:1 (metal to ligand ratio) i.e. dinuclear. The thiocyanate complexes **18** and **20** are 1:1 and 1:2 electrolytes respectively (Ali) while **17** and **19** are non-electrolytes.

The involvement of H-bonding is responsible for the observation of the stretching frequency νOH of the ligand at 3091 cm^{-1} and this values shift to higher frequency of 3432 cm-1 in the copper complexes (**17** and **18**) and 3184 cm^{-1} in the iron complexes **19** and **20**. This is indicative of complexation between the ligand and metal ion and the subsequent loss of hydrogen bonding. The presence of water molecules in the iron complexes only is also supported by the observation of broad (OH) bands [20].

The νC-O of the ligand centers at 1316 cm^{-1} but shifts downward in **17**, **18** and **19** by 3 – 17 cm^{-1} thus indicating complexation through the phenol of the ligand. An upward shift to higher wavenumbers is recorded in **20** by 3 cm^{-1} and is not attributed to deprotonation since **18** and **19** are isostructural with respect to the metal ion, the positive and negative shifts in stretching frequency from that of the ligand is considered as relating to the electronic properties of the central metal ions previously reported in the literature for the hydroxyl groups of salicylaldimines [49, 50].

Two different stretching modes of νCNC centred at 1245 cm^{-1} (ν1), 1115 cm^{-1} (ν2) as intense bands are observed indicating the different electronic environments of the N-atoms of the piperazine moiety of the Mannich base. The nature of the shifts of these bands indicate the involvement of the two nitrogen atoms of the piperazine unit in the ligand [18]. Changes were observed in the vibrational frequencies with ν2 more affected than ν1 as well as a reduction in intensity and increase in broadness. Vibrational mode (ν1) largely remained unchanged in frequency except in complex **18** where it shifts downward by 17 cm^{-1} emphasising its involvement in coordination. Vibrational mode (ν2) shifts downward by 7 cm^{-1} in **17** and **19** compared to 10 cm^{-1} in **18** and **20** suggests a greater involvement of the nitrogen atom in the thiocyanate complexes.

For thiocyanate complexes **18** and **20**, suggested bonding modes are S- and N- respectively because of the observation of the stretching vibration νCN at 2173 cm^{-1} (strong, split) and 2022 cm^{-1} (broad) in **18** and **20** respectively. The assignment is supported by the observation of the νCS at 755 cm^{-1} and 714 cm^{-1} for the copper and iron complexes respectively [37, 46].

4.4.2 Mid-infrared data for the p-acetamidophenol based ligands and metal complexes

Mannich bases of acetamidophenols have not received considerable attention compared to their cresol counterparts with only some few biological activities reported for their free ligands and that has even resulted in fewer reports on their metal complexes. The application of Mannich bases of acetamidophenol (acetaminophen or popularly paracetamol) and synthesis of its azo dyes have been reported [51, 52]. Sriram *et al.* carried out Mannich reaction involving p-acetamidophenol and some amines enroute to aromatic amino analogues of artemisinin though spectroscopic (including infrared) characterisation was not reported [25]. The full spectra can be found in the appendix.

4.4.2.1 Mid-infrared data for ligand (HL^6) and metal complexes 21 - 24

Structural characterization data from infrared spectroscopy for the free ligand with its copper(II) and iron(III) complexes are provided in Table 3.22. All the complexes are mononuclear with deprotonated ligand only encountered in **23** which happened to be only one with 1:1 metal to ligand ratio and the only 1:1 electrolyte in this group while the rest of the metal complexes are in 1:2 metal to ligand ratio.

The stretching frequency of the hydroxyl group of the phenol was observed at 3259 cm^{-1} as a sharp medium-intense band suggesting the occurrence of little or no H-bonding in the ligand. Positive shifts of ~ 23 – 65 cm^{-1} and ~ 49 – 113 cm^{-1} is observed in the spectra of the copper(II) and iron(III) complexes respectively compared to the ligand. The bands are sharper in **21** and **22** but became broad in **24** and suggest the presence of non-hydrogen bonded coordinated water molecules. Complementing this observation with those of νC-O (1252 cm^{-1}) in the ligand can give some understanding. Slight downward shifts were observed in the νC-O of the complexes (about 5 cm^{-1}) with the only upward shift recorded for **23** and is as evidence of deprotonation as is seen from its elemental analysis [44].

The symmetric stretching mode νCNC is observed at 1205 cm^{-1} in the ligand but shifts upward to higher wavenumber to 1217 cm^{-1} in **21** and 1221 cm^{-1} in **22**, this is taken as an indication of the involvement of the nitrogen atom in coordination [45]. The upward shift observed in **23** can be ascribed to the bonding of the iron to the deprotonated phenolic group and the lowering of νCNC, **24** is an indication of the involvement of N-atom in complexation [42].

The successful introduction of the thiocyanate into the coordination sphere of complexes **22** and **24** was confirmed by the observation of strongly-intense bands at 2101 cm^{-1}(split) in the copper(II) complex **22** and 2054 cm^{-1} (broad) in the iron complex **24**. These bands support the

following bonding modes: S-bonding and N-bonding in the copper and iron complexes respectively [37, 43].

4.4.2.2 Mid-infrared data for ligand (HL^7) and metal complexes 25 - 28

Successful synthesis of the metal complexes was achieved using the ligand (N-(4-hydroxy-3-((piperidin-1-yl)methyl)phenyl)acetamide) and the hydrated metal chloride salts. All the metal complexes were obtained in a metal: ligand ratio 1:1 and all are 1:1 electrolytes except **25** which is a non-electrolyte. The IR data are reported in Table 3.23 and Figure 4.17 as representative spectra for this class of compounds.

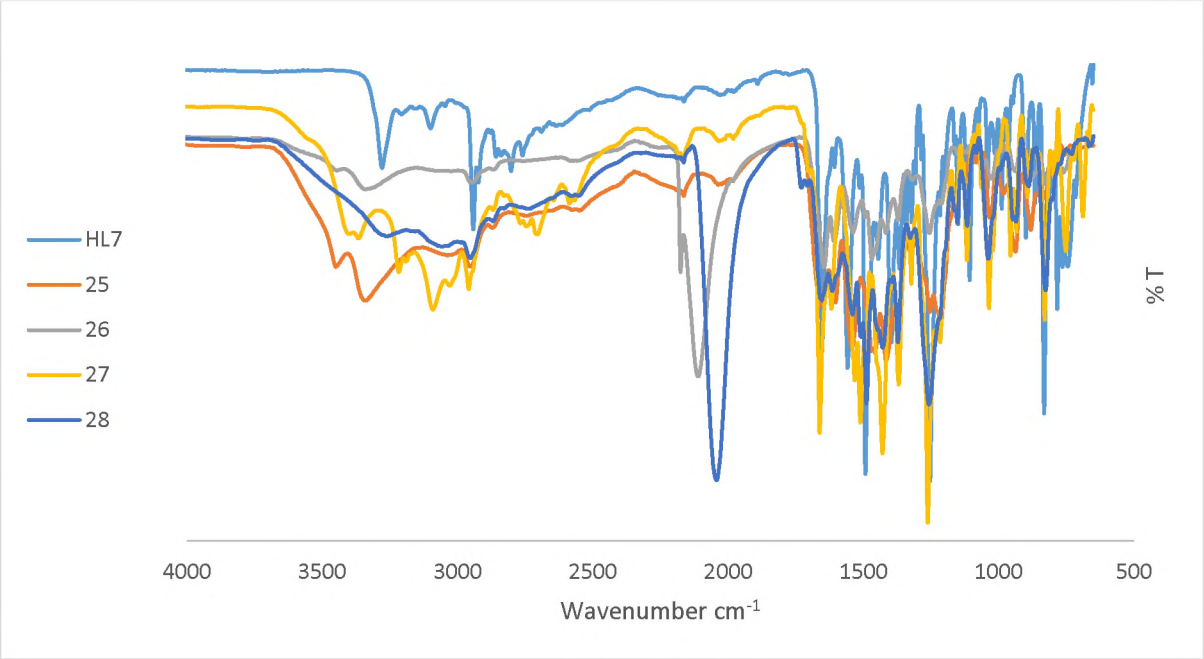

Fig. 4.17: Mid-infrared spectra of ligand HL^7 and its metal complexes.

The hydroxyl group of the ligand is observed as a sharp band at 3276 cm^{-1} (presence of hydrogen bonding is also observed in solution by NMR) but with complexation increased within the range of 3276 – 3364 cm^{-1} and became broader. This suggests coordination and possibly the presence of solvated water molecules particularly in the iron(III) complexes. Further upward shifts observed in the νC-O of the ligand at 1253 cm^{-1} to a range of 1254 –

1261 cm^{-1} is in support of the involvement of the phenolic hydroxyl group in complexation. Upward shifts in νC-O are usually observed in the case of a deprotonated hydroxyl group leading to the formation of a direct metal-oxygen bond. Increase in the νC-O without deprotonation has been reported by Mahmoud and El-Haty [49].

Evidence to support the involvement of the amine nitrogen atom on complexation is obtained by a downward shift of ~ 22 – 124 cm^{-1} in the stretching of the bond (CNC) in the Mannich base at 1149 cm^{-1}. This leads to the appearance of broad bands for νCNC in all the metal complexes and most noticeable in the case of **26**; this further suggests the involvement of the N–atom in bonding with the central metal atom [42, 53]. Complex **27** showed the greatest variation as reflected by the largest νC-O shift and least shift in the νCNC.

The bonding of the (SCN) to the central metal ion in the thiocyanate complexes is confirmed from the infrared spectra by the observation of νCN absorption bands at 2106 cm^{-1} and 2035 cm^{-1} in the copper(II) (**26**) and iron complex(III) (**28**) respectively. It can therefore be inferred that there is S-bonding in the copper(II) complex and N-bonding in the iron(III) complex. This is further supported by the presence of the band due to νCS at 760 and 827 cm^{-1} in the copper and iron complexes respectively [36, 46].

4.4.2.3 Mid-infrared data for ligand (HL^8) and metal complexes 29 - 32

The infrared data for (HL^8) with its copper(II) and iron(III) complexes are reported in Table 3.24. According to elemental analysis, only **29** is coordinated to the deprotonated ligand while **31** is the only mononuclear complex with 1:1 metal to ligand ratio while the rest are dinuclear in ratio 2:1 within this group. The thiocyanate complexes **30** and **32** behaved as 1:1 and 1:2 electrolytes respectively while the others are non-electrolytes in solution.

The stretching frequency of the phenolic OH was observed at 3250 cm^{-1} as a medium intense band suggesting the absence of strong intramolecular H-bonding. Positive shifts of ~ 3 – 49

cm^{-1} are observed in the spectra of the metal complexes respectively compared to the ligand. The bands observed at 3253 – 3299 cm^{-1} in the spectra of the metal complexes are broad and suggest the presence of solvated water molecules may overlap the bonded hydroxyl group [20].

It is possible to correlate the involvement of the hydroxyl groups of the ligand with the stretching frequencies of the νC-O. Decrease in the stretching frequency is expected upon complexation and that is true for all the complexes as observed by the reduction in the νC-O from 1297 cm^{-1} to about 1260 cm^{-1} in the metal complexes however, elemental analysis revealed **29** contains the ligand in its deprotonated form [46].

The coordination of the N-atom of the amine component of the Mannich base with the central metal ion is supported by the lowering of the stretching frequency of the νCNC of the ligand at 1141 cm^{-1} by ~ 22 – 71 cm^{-1} upon complexation with the greatest reduction observed in **30**. The bands also became broader upon complexation and this further lends support to the coordination mode [45].

For the thiocyanate complexes **30** and **32**, the observation of the stretching vibration νCN at 2106 cm^{-1} (strong, split) and 2035 cm^{-1} (broad) respectively suggests different bonding modes in **30** and **32**. The suggestion is supported by the observation of the νCS at 749 cm^{-1} and 798 cm^{-1} for the copper and iron complexes respectively. S-bonding and N- bonding is implied in **30** and **32** respectively as proposed by Kabesova and Gazo [36].

4.4.2.4 Mid-infrared data for ligand (HL^9) and metal complexes 33 - 36

Structural information obtained by infrared spectroscopy for the ligand and its metal complexes are reported in Table 3.25. Complexes **33** and **35** are mononuclear with metal to ligand ratio of 1:1 while the thiocyanate containing metal complexes **34** and **36** are dinuclear with metal to ligand ratio of 2:1. Only the thiocyanate containing ligands behaved as 1:1 electrolytes in solution for this group.

The Mannich base displayed a medium intense band at 3354 cm^{-1} attributed to the stretching mode of the hydroxyl group of the phenolic part of the ligand. Shifts to lower frequencies were observed in all the metal complexes indicating the coordination through the hydroxyl group [42] however the shifts were more pronounced in the thiocyanate complexes. The extent of shifts ranged from 165 – 197 cm^{-1} in **33** and **35** to 235 – 274 cm^{-1} in **34** and **36**. Support for the coordination of the hydroxyl group can be obtained by considering the νC-O (sharp intense band) as well which shifted from 1249 cm^{-1} by 4 cm^{-1} downward in **33** and upward in **35** by 6 cm^{-1} with all the bands appearing broader. Upward shifts have been previously reported upon complexation without deprotonation for some lanthanide complexes of Schiff bases of aniline [50].

Two bands assigned to the stretching modes of the two νCNC of the piperazine within the ligand are at ν1 = 1213 cm^{-1} and ν2 = 1142 cm^{-1}. Considerable lowering to 1180 - 1162 cm^{-1} and 1129 – 1062 cm^{-1} is observed for ν1 and ν2 respectively with the effect being most pronounced in complex **34**. This observation is evidence of both N-atoms of the piperazine moiety of the ligand being involved in the complexation [18, 42].

Bonding of the thiocyanate to the central metal ion was confirmed by the observation of strongly-intense bands at 2140 cm^{-1}(split) in the copper(II) complex and 2051 cm^{-1} (broad) in the iron(III) complex. These bands support the following bonding modes: S-bonding and N-bonding in the copper and iron complexes respectively. The bonding modes are supported by the νCS at 868 cm^{-1} and 737 cm^{-1} for the copper and iron complexes respectively as reported in the literature [37, 43].

4.4.2.5 Mid-infrared data for ligand (HL^{10}) and metal complexes 37 - 40

Infrared data of N-(4-hydroxy-3-((4-(4-nitrophenyl)piperazin-1-yl)methyl)phenyl)acetamide and its Cu(II) and Fe(III) complexes are presented in Table 3.26. All the metal complexes are

obtained in ratio 1:1 (mononuclear) with **38** reported as the only dinuclear complex. Complexes **38** and **40** behaved as 1:2 and 1:1 electrolytes in solution respectively.

Presence of H-bonding is observed in both the free ligand and the complexes due to the observation of lower frequency and broadness of the hydroxyl band in the free ligand at 3264 cm^{-1} and the band shifted to higher frequencies in the range 3406 – 3337 cm^{-1} as a result of complexation with the broadness maintained. This observation is complimented by the increase in the stretching frequency of νC-O in the ligand at 1315 cm^{-1} by 2 – 5 cm^{-1}. This is attributed to coordination to the phenolic hydroxyl group and not due to deprotonation before coordination as similar observations have been reported in the literature [49, 54].

Two different stretching modes of νCNC centred at ν1 = 1238, ν2 = 1113 cm^{-1} are observed indicating the different electronic environments of the N-atoms of the piperazine moiety of the Mannich base with only ν1 underwent changes in frequency upon complexation and is indicative of the involvement of only one of the N-atoms within the piperidine ring of the Mannich base in the complexation. Upward shifts in the range ~ 20 cm^{-1} observed in copper(II) complexes **37** and **38** while there are downward shifts of about 5 cm^{-1} in iron(III) complexes **39** and **40**. It can be inferred that complexation takes place followed by a boat-chair conformation change only in **37** and **38** [18, 45].

The stretching vibration νCN in the thiocyanate complexes is observed at 2172 cm^{-1} (strong, split) in the copper complex **38** leads to the suggestion of a bridging mode with the thiocyanate acting as a bidentate ligand. This observation is supported by the elemental analysis and conductivity measurements. While a broad band at 2049 cm^{-1} is recorded for the iron complex **40** suggesting N-bonding in the iron(III) complex. The assignment is supported by the observation of the νCS at 753 cm^{-1} and 730 cm^{-1} for complexes **38** and **40** respectively [36, 37].

4.5 Electronic transitions of the compounds

The UV spectra of the Mannich bases and their metal complexes were recorded in DMF and DMSO at 1000 – 250 nm and the data are presented in Tables 3. 27 to 3. 36. The expected intra-ligand transitions including (n → π* and π → π*) are all observed at about 250 – 350 nm with the n → π* at higher wavelengths than the π → π* transitions [55, 56]. The intraligand transition associated with nitro group was observed at 429 and 443 nm in DMF for HL^5 and HL^{10} respectively [57], a similar report exist for nitro-anilines at 367 nm as reported by S. Kumar; this band generally underwent a hypsochromic shift in the metal complexes [58]. As much as possible each transition is identified and well defined in this work.

Solvents can bring about shifts of the ligand bands (solvochromatism), the effect is more pronounced with polar solvents and may also cause other changes as a result of solvent coordination, or even dissociation of the complex. Solvochromatism is based on the assumption that ground state is less polar than the excited state for almost all molecules. Therefore, a polar solvent will tend to stabilize ions in the excited state by lone pairs of electron or hydrogen bonding [59].

Similarly, information on the possible electronic transitions of the metal centre is obtained from the visible region of the electromagnetic spectrum; the nature of these transitions indicates the probable geometry of the metal complexes; this information were closely compared to observation from elemental analysis and molar conductivity of the metal complexes in solution of DMSO. Sometimes, the expected charge transfer L→M band, below 400 nm is not observed and is possibly masked by the broad energy band of the solvent. This has been previously reported in the literature [60].

The UV/Visible spectral data for the copper(II) and iron(III) complexes of the isolated ligands were obtained in DMF and DMSO at 1000 – 250 nm with the solvent effect on spectra thus revealed. The spectral properties of the copper(II) and iron(III) complexes are discussed below.

4.5.1 UV-Visible spectral properties of copper(II) complexes

The UV data of all the compounds are recorded in Tables 3.27 to 3.36 and the spectra may be found in the appendix. Representative spectra will be shown in the discussion below. Minor shifts were observed in the intra-ligand transitions and particularly the n → π* transition to shorter or longer wavelengths in few cases upon coordination [61], not much information can be deduced from this except that there are changes in the electronic environment of the benzene rings and the hydroxyl groups of the ligands as a result of coordination with metal ions.

The focus herein will be on the observed transitions between 350 and 850 nm and these are attributed to charge-transfer bands and d-d transitions. The number and position of these transitions observed vary for the solvents used (i.e. DMF and DMSO), this is an indication of the possibility of coordination of the solvent to the copper ion, or reflect variation in stabilizing the excited state (solvochromatism). For example, Cu(II) complexes (whether mononuclear or dinuclear) have been reported to give three transitions: a weak broad band in the 640 – 700 nm region for the d–d transition, a moderately intense band in the 340 – 425 nm region for the phenolato-to-copper charge-transfer transition, and a more intense band at 220 – 250 nm for the intraligand π–π* charge-transfer transition [19, 62]. It can be suggested that n → π* transitions will be around 250 – 350 nm in the Mannich bases. The intense absorbance bands occurring in the range 363 – 378 nm, are assigned to $Cu^{II} \rightarrow O^{-}_{axial}$ and/or $O^{-}_{equatorial} \rightarrow Cu^{II}$ charge-transfer transitions [63, 64].

Studies on the electronic properties of pyridine, various monomethyl substituted pyridine and various di-substituted lutidine thiocyanate copper(II) compounds in the solid state revealed d-

d transitions in the range 763 – 583 nm and charge transfer bands resulting from the thiocyanate in the range 450 – 403 nm [65].

The position at which the phenolato-to-copper LMCT band is observed is sensitive to the electron density on the Cu(II) ion. An electron withdrawing group at the para position of the phenolic ring will increase the Lewis acidity of the copper center, thus shifting the phenolato to copper LMCT band to higher energy whereas an electron donating group at the para position of the phenolic ring, decreases the Lewis acidity of the copper center and hence shifts the LMCT band to the lower energy [66, 67]. An orderly discussion of the Cu(II) complexes for the ligands (HL^1 – HL^{10}) is discussed below followed by a general discussion of the Fe(III) complexes.

Copper complex **1** is non-electrolytic (a four coordinate system), based on the deprotonated form of HL^1 it showed an absorption band at 460 nm in DMF which is considered a ligand to metal (phenolato-Cu) charge transfer band while the band at 717 nm is at a higher wavelength than that characteristic of square planar geometry [68], the spectra is displayed in Figure 4.18. Coordination of solvent could have resulted in the observation of an octahedral geometry in solution. A similar situation is proposed to take place in DMSO with the $^2E_g \rightarrow {}^2T_{2g}$ which is characteristic of an octahedral geometry of Cu(II) in solution. The thiocyanate containing complex **2** (a conducting1:1 electrolyte) showed one d-d transition in DMF at 713 nm, this observed transition is in support of an octahedral geometry with the solvents binding and the charge transfer band masked while two transitions are observed at 471 and 758 nm in DMSO. The band at 471 nm clearly reflects the charge transfer band attributed to the thiocyanate with the transition at 758 nm is to a $^2E_g \rightarrow {}^2T_{2g}$ transition which is characteristic of an octahedral geometry of Cu(II) in solution [19].

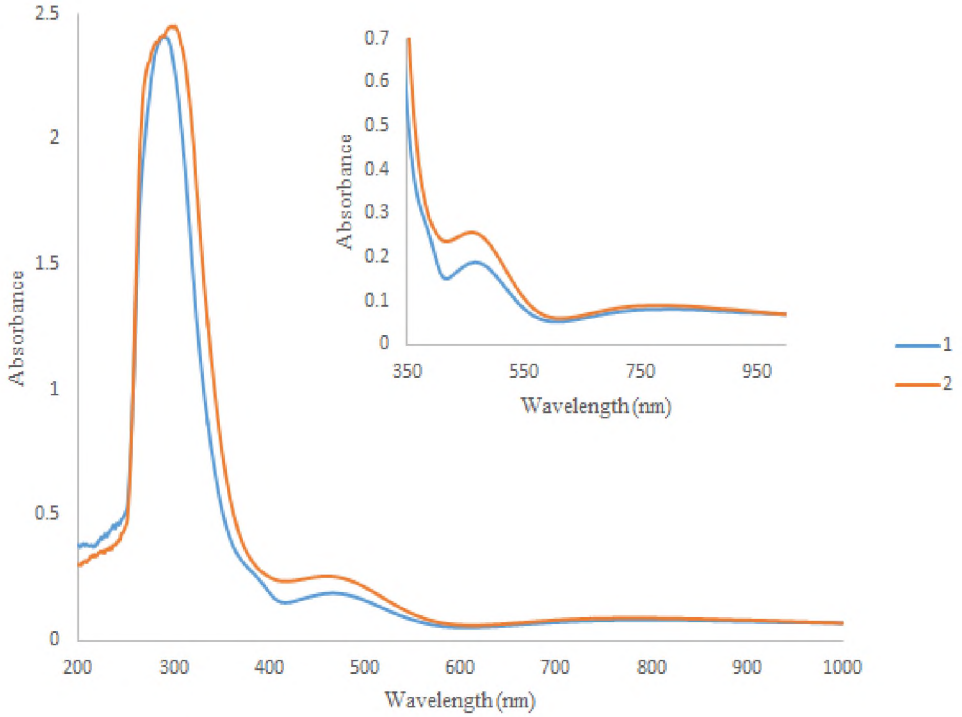

Fig. 4.18: UV spectra of complexes **1** and **2** in DMSO. (Inserted are spectra of CT/d-d transitions).

Spectral data of copper complexes of HL^2 are listed in table 3.28. Complex **5** has a molar conductivity of 4.38 $\Omega^{-1}.cm^2.mol^{-1}$, showed only one transition in DMF at 692 nm and may reflect a distorted square pyramidal [55]; the elemental analysis showed the Mannich base binding in its deprotonated form. The charge transfer band is masked by the intraligand transitions. However, in DMSO, the (phenolato-Cu) charge transfer band is observed at 454 nm in addition to a d-d transition at 733 nm leading to the conclusion on an octahedral geometry by the metal ion in DMSO. In complex **6** across the two solvents, two transitions are observed with the role played by the two solvents clearly evident. Thiocyanate complexes are well noted for their charge transfer transitions and that is observed at 434 and 345 nm in DMF and DMSO respectively. The wavelengths at which the transitions occur in solution leads to the suggestion that the complex is square planar in the solid state but assumes different geometries in solution.

Transitions assigned to $^2B_{1g} \rightarrow {}^2E_g$ have been observed for Cu(II) complexes of Mannich bases [55].

The molar conductivity values obtained for complexes **9** and **10** shows that the complexes are electrolytic (1:1) in nature. Bands observed include d-d transitions at 751 and 831 nm for complex **9** in DMF and DMSO respectively. These are attributed to the single transitions each expected in an octahedral environment corresponding to $^2E_g \rightarrow {}^2T_{2g}$, the proposed geometry is in line with the molecular formulae. Also charge transfer (metal to ligand) bands are observed at 426 and 417 nm in DMF and DMSO respectively for complex **9**. The spectra of complex **10** are quite similar to that complex **9** though the elemental analysis suggests a dinuclear complex and the transitions occur at higher energies. The values of the d-d transitions are typical of those of binuclear Cu(II) complexes in distorted square pyramidal geometry [64]. Other transitions in **10** at about 407 nm in both solvents are assigned to ligand to metal charge transfer bands typical of thiocyanates [65].

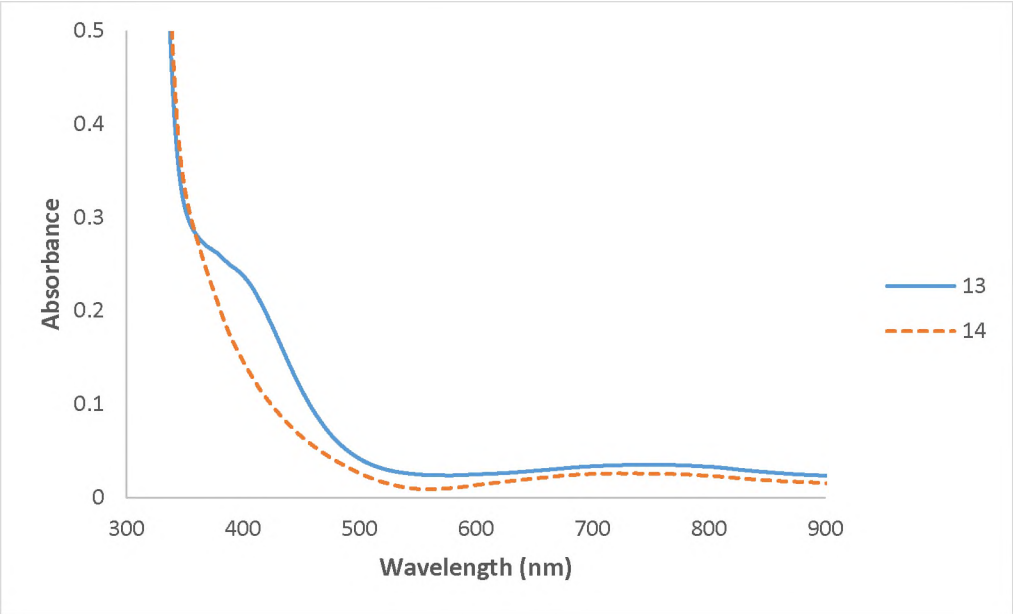

Fig. 4.19: Electronic spectra of complexes **13** and **14** recorded in DMF.

The low values obtained from the molar conductivity studies in DMSO showed the metal complexes **13** and **14** as non-electrolytes and this observation is in close agreement with results from the elemental analysis. Octahedral geometries are proposed for complexes **13** and **14** with only one d-d transition observed in the range 720 – 770 nm in both solvents here studied (Figure 4.19). The coordination of the solvents is identified since these compounds are 5 coordinate complexes from the proposed structure and the supposed presence of metal to ligand charge transfer bands is identified by the bands at 422 nm for **13** in DMF and at 471 nm **14** in DMSO.

The copper complexes **17** is a non-electrolyte while **18** behaved as a 1:1 electrolyte as observed from conductivity measurements [27], in addition **17** is mononuclear while **18** is binuclear. The d-d transition of complex **17** is observed as a single transition in DMF at 730 nm and in DMSO at 761 nm. These values are typical of Cu(II) ion in the octahedral geometry with the observed transition corresponding to $^2E_g \rightarrow {}^2T_{2g}$,the transitions at 410 and 448 nm in DMF and DMSO respectively correspond to ligand-metal charge transfer transitions. For the thiocyanate complex **18**, the d-d transition observed in DMF at 603 nm is typical of square planar geometry of binuclear complexes [19], however in DMSO the ΔE is reduced and therefore relate this to the presence of coordinating solvents resulting in an octahedral geometry. Transitions at 400 and 446 nm are typical of ligand to metal charge transfer bands typical of thiocyanate [65].

Both Cu(II) complexes of HL^6 which are **21** and **22** are obtained in metal to ligand ratio (1:2). **21** displayed one transition in DMF and DMSO at 839 and 814 nm respectively. This is characteristic of an octahedral geometry. Ligand to metal charge transfer bands in 21 are observed at 529 and 503 nm in DMF and DMSO respectively. The elemental analysis of **22** revealed a 6 – coordinate system with the d-d transitions poorly visible in the two solvents. These observations are in agreement with the low values of molar conductivity observed for the metal complexes in solution; the complexes are non-electrolytes. As commonly observed,

complex **22** displayed charge transfer (ligand to metal) transitions at 489 and 406 nm in DMF and DMSO respectively typical of thiocyanate complexes.

Copper(II) complexes of HL^7 are mononuclear with **26** a 1:1 electrolyte while **25** is a non-electrolyte and displayed one transition each in the range 510 – 890 nm across the two solvents in which they were studied. Elemental analysis suggests both complexes as 4–coordinate systems in the solid state but these assumed different coordination in solution. In **25**, the band at 439 nm (sh) observed in DMF is adjudged to be a ligand to metal charge transition and the d-d transition is recorded at 887 nm typical of an octahedral geometry while in DMSO the transition at 510 nm is assigned to $^2B_{1g} \rightarrow {}^2A_{1g}$ transition in a square planar geometry. In **26**, single transitions in DMF at 621 nm and 773 nm in DMSO are assigned to $^2B_{1g} \rightarrow {}^2A_{1g}$ and $^2E_g \rightarrow {}^2T_{2g}$ (d-d) transitions commonly observed in square planar and octahedral geometries of Cu(II) complexes of Mannich bases [19, 55].

Both Cu(II) complexes of HL^8 are dinuclear with only **30** being electrolytic while the ligand is deprotonated in **29** only. The band observed for complex **29** at 466 nm in DMF is attributed to d-d transition of a square planar geometry $^2B_{1g} \rightarrow {}^2E_g$ of a square planar geometry [55] with no charge transfer band observed (Figure 4.20). In DMSO the ligand to metal charge transfer band is observed at 478 nm while the d-d transition is observed at 856 nm (distorted octahedral geometry) with the solvent supposedly playing some role (Figure 4.20). Complex **30** showed similar but lower energies in DMSO compared to DMF in the range 620 – 670 nm with square planar geometry proposed. Ligand to metal charge transfer transition is expected for complex **30** being a thiocyanate complex and is only recorded at 439 nm in DMSO.

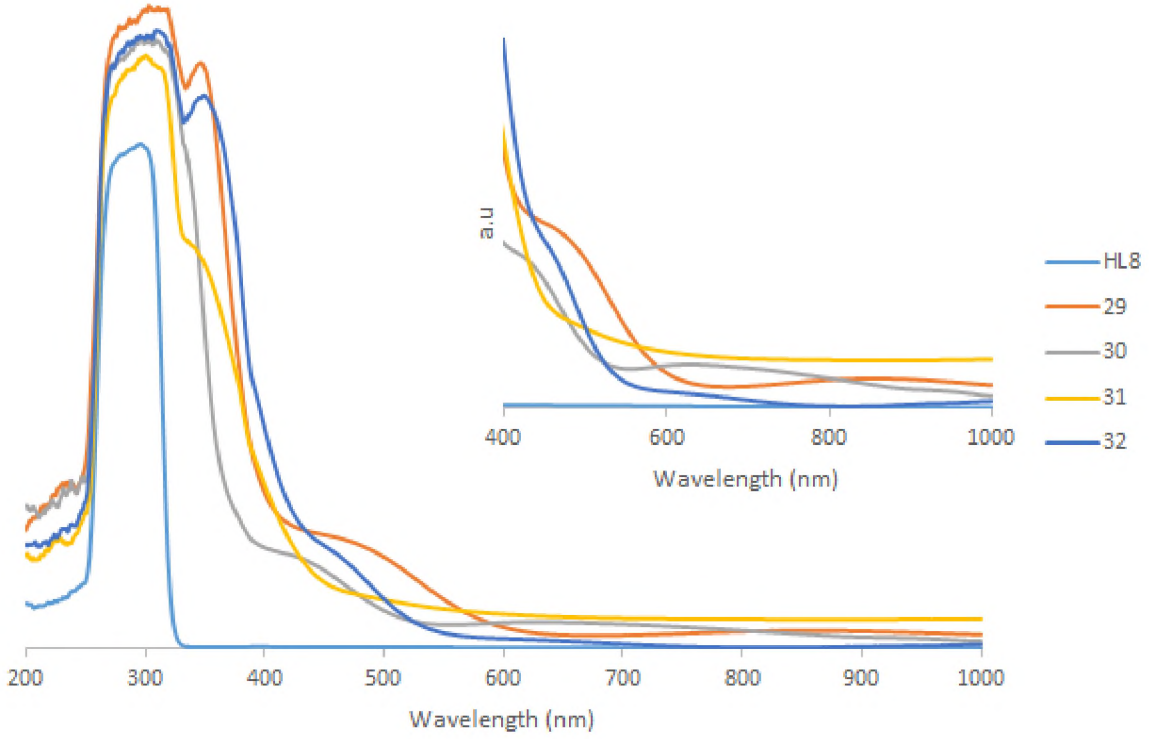

Fig. 4.20: UV spectra of HL^8 and its metal complexes in DMSO. Inserted are the C-T and d-d transitions.

The Cu(II) complex **33** is mononuclear and behaved as a non-electrolyte while **34** is dinuclear and behaved as a 1:1 electrolyte. Complex **33** only displays a single d-d transition at 741 nm in DMF typical of an octahedral geometry, a similar transition is observed an equally assigned in DMSO at 733 nm alongside a ligand to metal charge transfer transition at 454 nm. Complex **34** showed a single transition at 687 nm assigned to $^2E_g \rightarrow {}^2T_{2g}$ transition in a distorted octahedral geometry with a ligand to metal charge transfer transition typical of thiocyanates observed at 427 nm. In DMSO, the d-d transition observed for **34** at 775 nm is attributed to $^2E_g \rightarrow {}^2T_{2g}$ and also suggests an octahedral configuration.

Copper(II) complex **37** is mononuclear and non-electrolytic in nature while the elemental analysis and infrared data suggests that **38** is made up of two copper centres bridged by the thiocyanate. The d-d transitions are of low energies in two complexes and are only observable

in DMF, in addition low wavelengths of d-d transitions are sometimes reported for square planar configuration of Mannich base Cu(II) complexes at about 470 nm [55]. Summarily, lower energies for most transitions are observed in DMSO compared to DMF and this can be attributed to the protic nature of the different solvents observed in solution. Also, most of the thiocyanate copper(II) complexes give an intense charge transfer transition between 340 – 490 nm as expected. A peak or shoulder at 350 - 370 nm is due to phenolato to copper(II) charge transfer as reported in the literature [69].

4.5.1.1 Effect of para-substitution

In general, there is a somewhat profound effect of the substitution on the para-position involving either methyl (CH_3-) or acetamido (CH_3CONH-) groups on the energy of the d-d transition. Copper complexes of the methyl substituted Mannich bases have their d-d transition in the various geometries occur at higher wavelengths compared to the acetamido substituted ones.

The position of the phenolato-to-copper LMCT charge-transfer has been reported to be sensitive to the electron density on the copper centers [66, 67]. There is a slight increase in wavelength for the complexes when the electron donating substituent (CH_3), of the phenolic ring is replaced by a stronger electron donating (CH_3CONH). The CT bands were recorded at 345 – 475 nm and 345 – 490 nm in the Cu(II) complexes of p-methylphenol and p-acetamidophenol Mannich bases. Greater electron donating ability increases electron density at the phenolic oxygen, causing the red shift [19].

4.5.2 UV/Visible spectral properties of Fe(III) complexes

Here a general description is given for the spectral properties observed for iron(III) complexes. Several reports have indicated the non-diagnostic nature of the d-d transitions observed for the iron(III) complexes as no full structural conclusion can be drawn from them. The electronic

spectra of the complexes are dominated by $\pi \rightarrow \pi^*$ and $n \rightarrow \pi^*$ transitions of the ligands. Iron (III) complexes are generally octahedral in shape, and a very few are in tetrahedral geometry [70]. ESR measurements were carried out to further characterise the complexes based on the g values.

The electronic spectra of iron(III) complexes of N,N'-tetra(4-antipyryl-methyl)-1,2-diaminoethane (a Mannich base) were recorded in a freshly prepared solution of DMF, exhibited one band in the region 428 nm assignable to the spin allowed electronic $^5T_{2g}(F) \rightarrow {}^5E_g$ transition characteristic of the Fe(III) ion in octahedral configuration [71].

All the iron(III) complexes display a medium to intense band in the range 346 – 532 nm in DMF and 350 – 504 nm in DMSO. This transition is assigned to the charge transfer transition and/or d-d transition peculiar to a Fe^{3+} ion in an octahedral configuration. Palaniandavar and coworkers [72] have reported that the electronic spectra of all the iron(III) phenolate complexes they studied exhibit an intense band in the visible region (490-550 nm). This band is assigned to the phenolate $(\pi_1) \rightarrow Fe(III)(d\pi)$ charge transfer transition. Also, reports by Garg *et al.* [70], on substituted thiosemicarbazones of 2-acetylpyridine found out that there is no significant difference between the spectrum obtained in solution and solid state, so the structures are similar. Bands between 384 and 667 nm were assigned to $d \rightarrow n^*$ metal to ligand charge transfer as well as $S \rightarrow Fe$ ligand to metal charge transfer transitions. The bands below 667 nm are assigned to d-d transitions of the spin-paired d^5 iron(III) cations. A similar report has also been observed for non-heme Fe dimer complexes [73, 74]. Ray *et al.*, determined the UV spectra of Fe(III) complex of 2,6-Bis(N-phenyl-carbamoyl)pyridine in MeCN, DMF, and DMSO solution and observed an intense ligand-to-metal charge transfer (LMCT) band at ~440 nm [75]. They concluded that it is quite possible that the expected d-d transition is hidden under the charge-transfer band.

4.5.3 Rationale for the impact of thiocyanate on UV-Vis. Spectra

A factor that plays a key role in whether a transition metal complex is high- or low-spin is the nature of the ligands. The d- orbital energy splitting is influenced by how strongly the ligand interacts with the metal. Ligands that interact only weakly produce little change in the d orbital energy levels, whereas ligands that interact strongly produce a larger change in d orbital energy levels [76]. In the list of ligands (spectrochemical series) from weaker to stronger, generally $SCN^{--} < NCS^{--}$ and both are stronger than Cl.

Neighbouring metal ions can perturb the internal electronic transitions that have been adequately assigned to NCS^{-}. Also it has been argued that S-thiocyanate complexes have a strong characteristic band at (333 nm) and N-thiocyanato complexes at (263 nm). Barnes and Day in 1964 have however discussed the origin of this intense band which lies between 333 and 250 nm in many thiocyanate complexes, and the distinction is not so clear cut. Such bands are not observed with non-reducible ion [77] such as La^{3+}, Gd^{8+} or Zn^{2+} and it was concluded that these transitions were associated with a charge transfer to a reducible metal ion such as Cu(II)/Cu(I) and Fe(III)/Fe(II). They also reported that at the nitrogen end, a highly oxidized metal ion is proposed to hinder the transfer of charge from nitrogen to carbon, thereby raising the energy of the ligand transition while a metal ion at the sulphur end will have the opposite effect and stabilize the ligand excited state by withdrawing charges from the nitrogen [77].

The standard reduction potential for the following processes Cu(II)/Cu(I) and Fe(III)/Fe(II). are 0.153 and 0.771 Volts [78 – 80] and so the charge transfer bands of Fe(III) complexes are expected at lower wavelengths compared to those of Cu(II) complexes. Finally, the favourable formation of S-thiocyanate complexes in Cu(II) complexes and N-thiocyanate complexes is supported from the infrared study [36].

References

1. A. E. M. Ramadan, S. Y. Shaban, M. M. Ibrahim, J. Coord. Chem., **2011**, 64, 3376 – 3392.
2. T. Latif, T. Javed, D.E. Lynch, R.J. Pryce, K.A. Byriel, Aust. J. Chem., **1999**, 52, 909 – 913.
3. S.M. Melikova, A. Koll, A. Karpfen, P. Wolschann, J. Mol. Struct., **2000**, 523, 223 – 239.
4. A. Koll, S.M. Melikova, A. Karpfen, P. Wolschann, J. Mol. Struct. **2001**, 559, 127 – 145.
5. A. Koll, P. Wolschann, Monatshefte fur Chemie, **1996**, 127, 475 – 486.
6. W. Robien, H. Vollenkle, P. Wolschann, Z. Phys. Chem., **1982,** 130, 123 – 128.
7. J. Li, S. A. Bourne, M. M. de Villiers, A. M. Crider, M. R. Caira, Cryst. Growth Des. **2011**, 11, 4950 – 4957.
8. A. Filarowski, A. Szemik-Hojniak, T. Glowiak, A. Koll. J. Mol. Struct., **1997**, 404, 67 – 74.
9. J. Wan, P-C. Lui, N-N. Tian, H-L. Zhu, J. Chem. Sci., **2010**, 122, 597 – 606.
10. F. H. Allen, O. Kennard, D. G. Watson, L. Brammer, A. G. Orpen, R. Taylor. J. Chem. Soc. Perkin Trans. II, **1987**, 12, S1 - S19.
11. D. Braga, F. Grepioni, L. Maini, M. Polito, Struct. Bond, **2009**, 132, 25 – 50.
12. B. Perrenot, G. Widmann, Thermo. Acta, **1994**, 234, 31-39.
13. D. Giron, Acta Pharm. Jugosl., **1990**, 40, 95-157.
14. T. L. Threlfall, Analyst, **1995**, 120, 2435 – 2460.
15. F. El-Kabbanya, S. Taha, M. Hafez, Spectrochim. Acta Part A, **2011**, 78, 981 – 988.
16. P. E. Hansen, J. Spanget-Larsen, Molecules, **2017**, 22, 552 – 573.
17. N. Emir, M. Bilge, M. Tursun, G. Kesan, C. Parlak, Spectrochim. Acta Part A, **2014**, 127, 388–395.
18. C. Cretu, R. Tudose, L. Cseh, W. Linert, E. Halevas, A. Hatzidimitriou, O. Costisor, A. Salifoglou , Polyhedron, **2015**, 85, 48 – 59.
19. K. S. Bharathi, S. Sreedaran, H. Priya, A. K. Rahiman, K. Rajesh, L. Jagadish, V. Kaviyarasan, V. Narayanan, J. Coord. Chem., **2009**, 62, 1356 – 1372.
20. S. Anbu, M. Kandaswamy, Polyhedron, **2011**, 30, 123 – 131.
21. M. Umayal, G. Mugesh, Inorg. Chim. Acta, **2011**, 372, 353 – 361.

22. A. V. Bogdanov, A. M. Vazykhova, N. R. Khasiyatullina, D. B. Krivolapov, A. B. Dobrynin, A. D. Voloshina, V. F. Mironov, Chem. Het. Comp., **2016**, 52, 25 – 30.
23. A. Blade-Font, T. de Mas Rocabayera, JCS Perkin, **1982**, 1, 841 – 848.
24. G. Roman, Eur. J. Med. Chem., **2015**, 89, 743 – 816.
25. D. Sriram, R. V. Devakaram, M. Dinakaran, P. Yogeeswari, Med. Chem. Res., **2010**, 19, 524 – 532.
26. E. S. Al-Abdullah, H. M. Al-Tuwaijri, H. M. Hassan, M. E. Haiba, E. E. Habib, A. A. El-Emam, Int. J. Mol. Sci., **2014**, 15, 22995 – 23010.
27. I. Ali, W. A. Wani, K. Saleem, Synth. React. Inorg. Met-Org. Nano-Met. Chem., **2013**, 43, 1162 – 1170.
28. M Shakir, S. P. Varkey, P. S. Hammed, Polyhedron, **1994**, 13, 1355 - 1361.
29. N. Raman, J. Dhaveethu, A. Satthivel, J. Chem. Sci., 2007, 119, 303 – 310.
30. M. Tofazzal, H. Tarafder, M. A. Ali, D. J. Wee, K. Azahari, S. Silong, A. Crouse, Trans. Met. Chem., **2000**, 25, 456 – 460.
31. M.M. Habeeb, G.A. Gohar, A.N.I. Darwish, M.A. Kharaba, Spec. Lett., **1995**, 6, 861 – 877.
32. S. Sobczyk, L. Sobczyk, Bull. Acad. Pol. Sci., **1978,** 7, 549 – 555.
33. H. H. Freedman, J. Am. Chem. Soc., **1961**, 83, 2900 – 2905.
34. P. J. Hendra, D. B. Powell, Spectrochim. Acta, **1962**, 18, 299 - 306.
35. G. Kesan, C. Parlak, Spectrochim. Acta Part A, **2014**, 118, 1113 – 1120.
36. M. Kabesova, J. Gazo, Chem. Zvesti, **1980**, 34, 800 – 841.
37. R. J. H. Clark, C. S. Williams, Spectrochim. Acta, 1966, 22, 1081 – 1090.
38. P. C. H. Mitchell, R. J. P. Williams, J. Chem. Soc., 1960, 1912 – 1918.
39. R. Li, B. Moubaraki, K. S. Murray, S. Brooker, Eur. J. Inorg. Chem., **2009**, 2851– 2859.
40. R. C. Maurya, R. Verma, T. Singh, Synth. React. Inorg. Met-org. Chem., **2003**, 33, 309 – 325.
41. S. Ya-Li, L. Xue-Song, Transition Met. Chem., **2009**, 34, 931 – 936.
42. H. I. Harbatsevich, N. V. Loginova, T. V. Koval'chuk, N. P. Osipovich, A. T. Gres, I. I. Azarko, G. I. Polozova, J. Appl. Spect., **2015**, 713 – 718.
43. P. Bhowmik, S. Chattopadhyay, M. G.B. Drew, C. Diaz, A. Ghosh, Polyhedron, **2010**, 29, 2637 – 2642.
44. Y. Prashanthi, K. Kiranmai, N.J.P. Subhashini, Spectrochim. Acta Part A, **2008**, 70, 30 – 35.
45. I. Bhat, S. Tabassum, Spectrochim. Acta, A, **2009**, 72, 1026 – 1033.

46. Y. Zhong-Lu, Z. Lin, S. Da-Hua, W. Xiao-Ling, L. Xiao-Fang, M. Yu-Ping, Inorg. Chem. Comm., **2010**, 13, 996 – 998.
47. K. Pothiraj, T. Baskaran, N. Raman, J. Coord. Chem., **2012**, 65, 2110 – 2126.
48. N.T. Madhu, P.K. Radhakrishnan, M. Grunert, P. Weinberger, W. Linert, Thermo. Acta, **2003**, 407, 73 – 84.
49. M. R. Mahmoud, M. T. El-Haty, J. Inorg, Nucl, Chem, **1980**, 42, 349 – 353.
50. B. S. Kumari, G. Rijulal, K. Mohanan, Synth. React. Inorg. Met-Org. Nano-Met. Chem. **2009**, 39, 24 – 30.
51. W.H. Huang, H.F. Lee, A.R. Lee, J. Chinese Pharm. Sci., **2002**, 54, 485 – 490.
52. S.M. Abdallah, Arabian J. Chem., **2012**, 5, 251 – 256.
53. M. Sharma, M. Saleem, M.S. Pathania, H. N. Sheikh, B. L. Kalsotra, Chin. J. Chem., **2009**, 27, 311 – 316.
54. G.F. De Sa, E. Giesbrecht, L. C. Thompson, J. Inorg, Nucl. Chem., **1975**, 37, 109 – 112.
55. M. J. Al-Jeboori, A. J. Abdul-Ghani, A. J. Al-Karawi, Transition Met. Chem., **2008**, 33, 925–930.
56. A. Dumbrava, R. Olar, M. Badea, M. N. Grecu, F. Patrascu, L. Marutescu, N. Stanica, J. Therm. Anal Calorim., **2014**, 115 , 2447 – 2455.
57. B. Liu, X. Lin, H. Li, K. Li, H. Huang, L. Bai, H. Hu, Y. Liu, Z. Kang, Cryst. Growth Des., **2015**, 15, 4355 – 4362.
58. S. Kumar (2006), Spectroscopy of Organic Compounds. In Organic Chemistry; National Science Digital Library at NISCAIR: India, e-books, p 14 – 17.
59. M. A. Qazi, I. Qureshi, S. Memon, New J. Chem., **2010**, 34, 2579 – 2586.
60. A. I. Francisco, M. D. Vargas, T. P. Fragoso, J. W. de M. Carneiro, A. Casellato, F. de C. da Silva, V. F. Ferreira, J. P. Barbosa, C. Pessoa, L. V. Costa-Lotufo, J. D. B. M. Filho, M O. de Moraesd, A. S. Mangrich, J. Braz. Chem. Soc., **2010**, 21, 1293 - 1302.
61. H. Keypour, M. Shayesteh, R. Golbedaghi, A. G. Blackman, S. A. Cameron, Transition Met. Chem., **2013**, 38, 611 – 616.
62. R. Mahalakshmy, R. Venkatesan, P. S. Rao, Trans. Met. Chem., **2004**, 29, 623 – 629.
63. E. Bill, J. Muller, T. Weyhermuller, K. Wieghardt, Inorg. Chem., **1999**, 38, 5795 – 5802.
64. S. M. M. Romanowski, F. Tormena, V. A. dos Santos, M. de F. Hermann, A. S. Mangrich, J. Braz. Chem. Soc., **2004**, 15, 897 – 903.
65. M. Kabesova, J. Kohout, J. Gazo, Monatsh. Chem., **1976**, 107, 641.

66. E.W. Ainscough, A.G. Bingham, A.M. Brodie, J. Husbands, J.E.J. Plowman, J. Chem. Soc., Dalton Trans., **1981**, 1701 – 1707.
67. R.C. Holz, J.M. Brink, F.T. Gobena, C.J. O'Conner, Inorg. Chem., **1994**, 33, 6086 – 6092.
68. A. P. Neves, C. C. Barbosa, S. J. Greco, M. D. Vargas, L. C. Visentin, C. B. Pinheiro, A. S. Mangrich, J. P. Barbosae, G. L. da Costae, J. Braz. Chem. Soc., 2009, 20,712 - 727.
69. M. Thirumavalavan, P. Akilan, M. Kandaswamy, K. Chinnakali, G. S. Kumar, Inorg. Chem., **2003**, 42, 3308 – 3317.
70. B. S. Garg, M. R. P. Kurup, S. K. Jain, Tran. Met. Chem., **1988**, 13, 247 – 249.
71. A.B.P. Lever, Inorganic Electronic Spectroscopy, Elsevier Publishing Company, Amsterdam, **1968**, 318.
72. R. Viswanathan, M. Palaniandavar, T. Balasubramanian, T. P. Muthiah. Inorg. Chem., **1998**, 37, 2943 – 2951.
73. C.A. Brown, G.J. Remar, R.L. Musselman, E.I. Solomon, Inorg. Chem., **1995**, 34, 688 – 717.
74. L. Casella, M. Gullotti, A. Pintar, L. Messouri, A. Rockenbauer, M. Gyor, Inorg. Chem., **1987**, 26, 1031 - 1038.
75. M. Ray, D. Ghosh, Z. Shirin, R. Mukherjee, Inorg. Chem., **1997**, 36, 3568 – 3572.
76. G. Contreras, R Schmidt, J. Inorg. Nucl. Chem., **1970**, 127 – 136.
77. J. C. Barnes, P. Day, J. Chem. Soc., **1964**, 3886 – 3892.
78. G. Milazzo, S. Caroli, V. K. Sharma, (1978). Tables of Standard Electrode Potentials, Wiley, Chichester.
79. A. J. Bard, R. Parsons, J. Jordan, (1985). Standard Potentials in Aqueous Solutions, Marcel Dekker, New York.
80. S. G. Bratsch, J. Phys. Chem. Ref. Data, **1989**, 18, 1 – 21.

CHAPTER FIVE

CATECHOLASE ACTIVITY

Studies on catechol oxidation have received an increasingly great attention owing to the tremendous importance of this process. For example its role in higher plants to form quinones which are highly reactive compounds that can undergo auto-polymerization to produce melanin which may be responsible for protecting tissues from damage against pathogens and insects [1]. This protective process therefore also has great impact in food preservation. Catechol oxidase, which is also known as o-diphenol oxidase, catalyzes exclusively the oxidation of catechols (i.e., o-diphenols) to the corresponding o-quinones (called catecholase activity). The rate for catechol conversion in sweet potatoes has been measured to be 2.3 x 10^3 /s, corresponding to a rate-limiting free-energy barrier of around 13 kcal/mol [2 – 4].

Catalytic activities can be carried out either by isolation and analysis of the product by ^{1}H NMR spectroscopy (the conversion and recyclability can then be calculated) [5, 6] or using UV-Visible spectroscopy to monitor the λ_{max} of the product. The UV-Visible spectroscopic technique that was adopted in this research allows for the determination of the kinetic parameters of the first-order catalytic reaction [7, 8].

In the current study, all the complexes were subjected to catecholase-mimetic activities to find out their capability to act as catalysts for the oxidation of alcohols to quinones, like catechol oxidase. In most investigations involving the study of potential catecholase activity of coordination compounds, 3, 5-di-tert-butylatechol (3, 5-DTBC) is chosen as the model substrate. Its low redox potential makes it easy to oxidize and the bulky tert-butyl substituents prevent further over-oxidation reactions such as ring-opening [9 - 11].

The oxidation product 3, 5-di-tert-butylquinone (3, 5-DTBQ) is highly stable and shows maximum absorption at 400 nm in DMF. Solutions of complexes were treated with 100

equivalents of 3, 5-DTBC under aerobic conditions [12]. It was found that under anaerobic conditions little product was formed, so the solvent was saturated with O_2 before the kinetic experiments. Oxygen must participate directly in the catalytic cycle of the oxidation reaction acting as a thermodynamic driving force by reoxidizing any generated copper(I) species back to the active copper(II) species [13]. Similar redox processes have been reported for Fe(III)/Fe(II) processes [14, 15].

Immediately after the addition of substrate 3,5-DTBC to the solutions of the metal complexes various LMCT bands of the complexes disappeared and a new band corresponding to 3,5-DTBQ appeared at 390–410 nm, this observation has previously been observed by Zippel *et al.*[16] and Singh *et al.*, [17]. They suggested that this could only be due to the formation of Cu(I) and not due to the destruction of the complex because the chelating ligands used by them (and in these studies), are much stronger than the substrate, solvent or quinone.

In this work, a new band at about 383 nm is observed constantly in all the metal complexes studied upon the addition of the substrate in DMF, which remained throughout the entire time for which the kinetic study is carried out. This band can be interpreted as a charge transfer band from 3, 5-DTBC to the central metal ion and is an evidence of a likely form of bond existing between the metal ion and the substrate in solution [18]. The grating change of the instrument (which occurs near this wavelength) was kept away from the position of the maximum absorbance to avoid erroneous data.

5.1 Initial slope (or rate) method

This is the method adapted from Sanyal *et al.*,[19] and is based on the principle below; the mechanism involves the formation of a catalyst-substrate complex (CS) which subsequently breaks down in a second step to form free catalyst (C) and the product (P) as shown below.

$$C + S \underset{k_2}{\overset{k_1}{\rightleftharpoons}} CS \underset{k_4}{\overset{k_3}{\rightleftharpoons}} C + P$$

The above mechanism leads to application of the Michaelis-Menten equation [20]:

$$V = \frac{V_{max}[S]}{K_M + [S]}$$

Where,

V = initial rate

[S] = concentration of the substrate (3, 5-DTBC)

$K_M = (k_2 + k_3)/k_1$, Michaelis-Menten constant for the metal complex

V_{max} = maximum initial rate attained for a particular concentration of the metal complex in the presence of a large excess of 3, 5-DTBC

The Michaelis-Menten equation can be transformed algebraically into the well-known Lineweaver- Burk equation [21] as follows:

$$\frac{1}{V} = \frac{K_M}{V_{max}} \cdot \frac{1}{S} + \frac{1}{V_{max}}$$

The determination of V_{max} enables the evaluation of the catalytic turnover rate (k_{cat}).

5.1.1 Experimental procedure

5 sets of substrate concentrations (ranging from 20 to 100 equivalent of the metal ion concentration) were prepared in a solution of DMF. A definite amount of catalyst was added to all of them maintaining a catalyst: substrate stoichiometry around 1:100. The kinetic profile at the λ_{max} (nm) corresponding to that catalyst was recorded on a UV-Visible spectrophotometer in the range 300 – 550 nm at an interval of 5 mins over a period of 2 hours. The V_∞ is recorded at 2 hours.

The slopes of the linear fits were measured and the initial rate values calculated. These initial rate values were plotted against [substrate] to give the V vs S curve. After which the double-reciprocal plot (1/V vs 1/S) was plotted to get the Line-weaver Burk plot. The kinetic parameters (V_{max}, K_M and k_{cat}) using the relevant equations below were then calculated as follows and displayed in Tables 5.2 to 5.11.

The intercept of the Line-weaver Burk plot is equal to ($1/V_{max}$) and the V_{max} was calculated from the inverse.

K_{cat} was obtained by dividing the V_{max} by the concentration of metal solution which in this experiment is equal to 10^{-4} M and the unit is in sec^{-1}. This unit is then converted appropriately to per hour unit to give the catalytic turnover rate.

Also from the Line-weaver Burk plot, the slope is equal to K_M/V_{max} and the respective values of V_{max} earlier obtained are then imputed to obtain the K_M for the biomimetic activity of the metal complex.

Representative plots of the increase in absorbance around 400 nm, after the addition of 100 equivalents of 3, 5-DTBC to a 10^{-4} M solution of the selected metal complexes in DMF are also presented for each ligand series. The spectra of the solution were recorded every 5 min with replicate measurements carried out and the value of the standard deviation is included in brackets in Table 5.2 – 5.11.

5.2 Results and discussion

Thirty-nine out of the forty copper(II) and iron(III) complexes that were screened for their biomimetic abilities showed catecholase activity, i.e. were able to convert 3,5-di-tert butyl catechol (3,5-DBTC) to 3,5-di-tert butyl quinone (3,5-DBTQ) at the maintained ambient temperature for this study. Also comparably high turnover rates were observed to show that the various compounds were catalytically active. Due to the several factors that are involved in

the catecholase activity observed for the various complexes studied, the turnover rate (*k*cat) is adopted in ranking the metal complexes in order of their biomimetic strength, the higher the turnover rate, the better the catecholase activity displayed by the metal complex and vice versa. The results of catecholase activity are presented are presented in Tables 5.2 – 5.11 each followed by a brief discussion.

Table 5.1: Kinetic Parameters for the Oxidation of 3,5-DTBC to 3,5-DTBQ reported in the literature for some selected compounds.

	K_{cat} (h^{-1})	Solvent	References
$[Zn_2(L^1)_2X_2]$, $[ZnH(L^2)X_2]$ L^1 and L^2 = Mannich bases	3.312 – 23.18	DMF-Water	7
$Fe^{III}L(\mu\text{-}OAc)_2Fe^{II}](ClO_4)H_2O$ L = Mannich base	11.96 – 16.33	MeOH-Water	15
$[Cu_2(L^n)(OAc)](ClO_4)$ L^n = Mannich base	10.08 – 28.44	Methanol	22
$[Cu_2(L)(\mu\text{-}OH)(H_2O)(ClO_4)_2]$ L= Mannich base	76	DMSO	23
$[Cu_2(L^1)(OH)(H_2O)(NO_3)_2]$ L = Schiff base	26.9 – 246.8	DMSO	24
$[Cu_2(L^2)_2(Br)_2]$ L = Mannich base	78.48	MeCN	25

5.2.1 Catecholase activity of metal complexes of p-methylphenol Mannich bases

In each set of complexes discussed below the first pair are copper(II), the second are iron(III) complexes. Within this pairs alternate, the metal chloride and then the metal thiocyanate.

All the copper(II) and iron(III) complexes of 2-((diethylamino)methyl)-4-methylphenol (HL^1) are mononuclear with **1** and **4** containing the ligand in its deprotonated form. Complexes **2** – **4** are octahedral while **1** is square planar in geometrical configuration. These group of metal

complexes demonstrated a moderately high catalytic ability compare with values reported in the literature [7] on the employed substrate (3,5-DTBC) in this research. Catecholase activity plots and the overlay of the Line-weaver Burk plots for complexes **1- 4** are given in Figures 5.2 and 5.3 respectively while the change in spectra pattern of complex **1** is shown below in Figure 5.1 as a representative of this set.

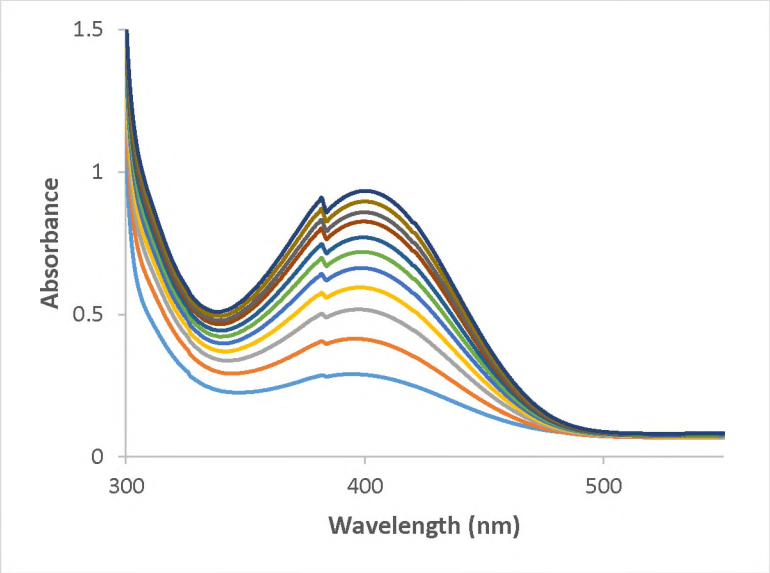

Fig. 5.1: Increase in absorbance around 400 nm, after addition of 100 equivalents of 3,5-DTBC to a 10^{-4} M DMF solution of **1**.

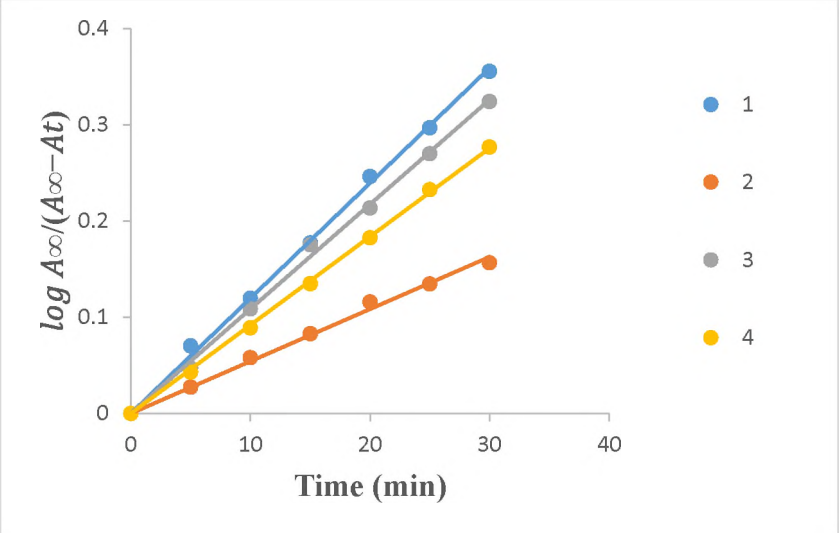

Fig. 5.2: Catecholase activity of complexes **1- 4.**

From the Line-weaver Burk plots, kinetic parameters including the maximum reaction velocity (V_{max}), Michaelis-Menten constant (K_M) and the catalytic turnover rate (k_{cat}) were then calculated and given in Table 5.2 below.

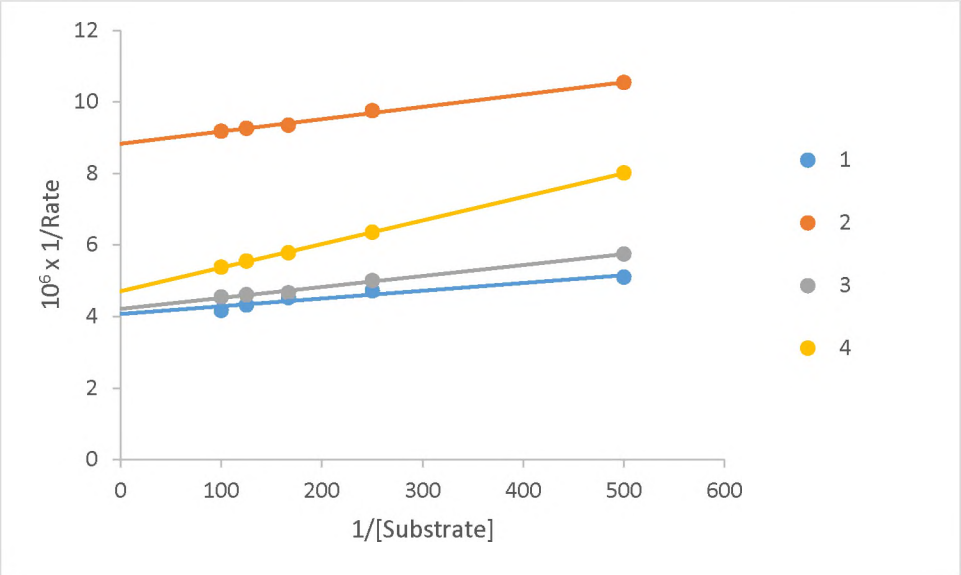

Fig. 5.3: Overlay of the Line-weaver Burk plots of complexes **1 – 4.**

Comparative evaluation of the various metal complexes can be made from values obtained for the catalytic turnover rate (k_{cat}) in the range of 4.07 – 8.75 h^{-1}. It can be immediately observed that complexes without thiocyanate group appear to be better catalysts than those containing it. Similar observation has been made by Kao *et al.* [26] on catecholase activity of Cu(II) complexes of Schiff bases from salicylaldehyde whereby those containing azide and thiocyanate showed less activity.

Table 5.2. Kinetic parameters for the oxidation of 3, 5-DTBC catalysed by metal complexes of HL^1 (solvent: DMF).

Complex	K_M(M)	V_{max}(Ms^{-1})	k_{cat} (h^{-1})
1	$(5.27 \pm 0.22) \times 10^{-4}$	$(2.43 \pm 0.13) \times 10^{-7}$	8.75 ± 0.46
2	$(3.91 \pm 0.21) \times 10^{-4}$	$(1.13 \pm 0.06) \times 10^{-7}$	4.07 ± 0.22
3	$(7.31 \pm 0.39) \times 10^{-4}$	$(2.38 \pm 0.13) \times 10^{-7}$	8.55 ± 0.40
4	$(1.41 \pm 0.08) \times 10^{-4}$	$(2.13 \pm 0.14) \times 10^{-7}$	7.67 ± 0.56

Similar catalytic ability investigation of the metal complexes (**5 – 8**) of 4-methyl-2-((piperidin-1-yl)methyl)phenol (HL^2) showed that all the metal complexes demonstrated catecholase activity. All complexes in this set are mononuclear with square planar and octahedral geometries reported for the Cu(II) and Fe(III) complexes respectively. Also only complex **5** contains the ligand in its deprotonated form. A representative example showing the increase in the absorbance around 400 nm can be seen for complex **6** in Figure 5.4 below.

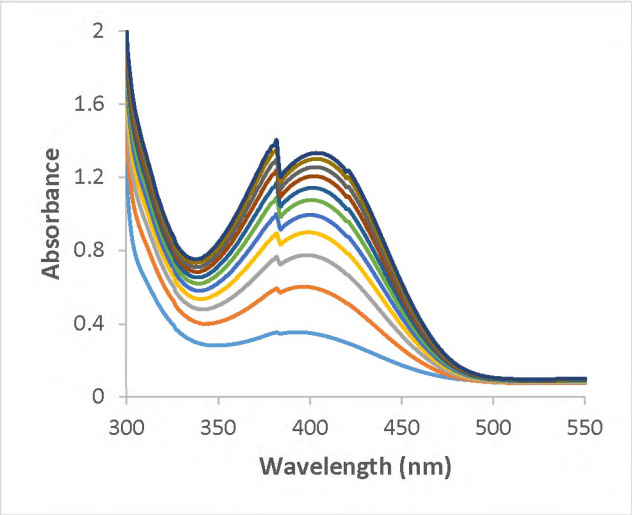

Fig. 5.4: Increase in absorbance around 400 nm, after addition of 100 equivalents of 3,5-DTBC to a 10^{-4} M DMF solution of **6**.

The catecholase activity plots and the overlay of the Line-weaver Burk plots for complexes **5 - 8** are given in Figures 5.5 and 5.6 below.

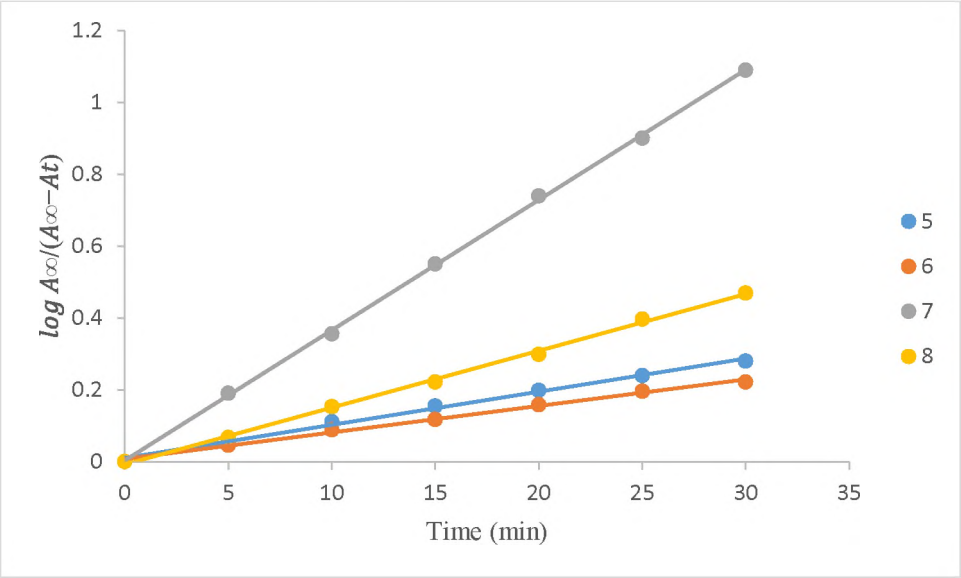

Fig. 5.5: Catecholase activity of complexes **5- 8.**

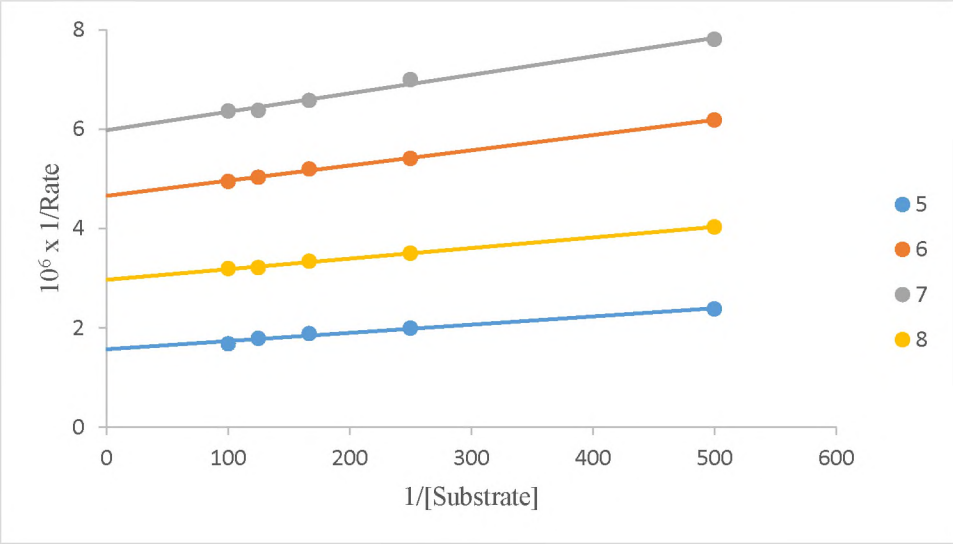

Fig. 5.6: Overlay of the Line-weaver Burk plots of complexes **5 – 8.**

Summary of results obtained from the Line-Weaver Burk plot are displayed in Table 5.3

Excellent turnover rates [15] of 22.72 and 12.00 h^{-1} were recorded for complex **5** and **8** respectively, also noted is the presence of thiocyanate in complex **6** reduces its catalytic ability.

Table 5.3. Kinetics parameters for the oxidation of 3, 5-DTBC catalysed by metal complexes of HL^2 (solvent: DMF).

Complex	K_M(M)	V_{max}(Ms^{-1})	k_{cat} (h^{-1})
5	$(1.04 \pm 0.06) \times 10^{-3}$	$(6.31 \pm 0.33) \times 10^{-7}$	22.72 ± 1.01
6	$(6.32 \pm 0.41) \times 10^{-4}$	$(2.06 \pm 0.04) \times 10^{-7}$	7.42 ± 0.50
7	$(6.22 \pm 0.41) \times 10^{-4}$	$(1.67 \pm 0.09) \times 10^{-7}$	6.02 ± 0.41
8	$(7.08 \pm 0.43) \times 10^{-4}$	$(3.33 \pm 0.17) \times 10^{-7}$	12.00 ± 0.78

Similarly, investigation of catalytic abilities of metal complexes **9** – **12** of 2-((4-(2-hydroxy-4-methylbenzyl)piperazin-1-yl)methyl)-5-methylphenol (HL^3) showed that only complexes **10** – **12** are active. The proposed geometry for complexes **10**, **11** and **12** in this set is octahedral with distorted square planar geometry proposed for **10**. Anbu and Kandaswamy [27] have previously carried out a preliminary study on the ability of a mononuclear complex similar to **9** (but in which the ligand was deprotonated and the complex was in square planar geometry) to oxidise 3, 5-DBTC in acetonitrile [27] unlike the study here which was conducted in DMF, the compound showed catalytic ability based on their method of initial rate, though detailed kinetic studies were not carried out by them. It can be concluded that the geometry, polarity and coordinating abilities of the various solvents may be responsible for the lack of catalytic ability observed in DMF by complex **9**. The tendency of solvent polarity (use of coordinating solvent) to reduce catecholase activity has been noted by Das *et al.*[28]. There are reports that highlighted the role played by geometry (octahedral, trigonal bipyramidal and square planar) [29, 30] in catecholase activity. The change in spectral pattern for complex **12** is displayed in Figure 5.7 as a representative of this set of metal complexes. The catecholase activity plots and the overlay of the Lineweaver Burk plots for complexes **10 - 12** are given in Figures 5.8 and 5.9 below.

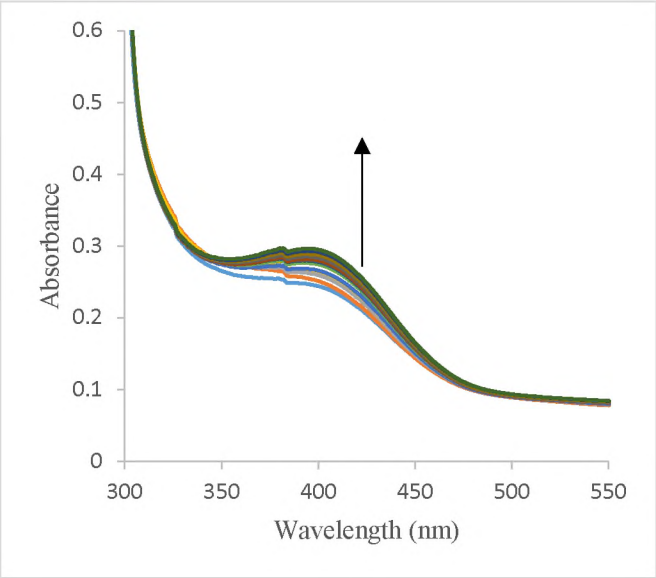

Fig. 5.7: Increase in absorbance around 400 nm, after addition of 100 equivalents of 3,5-DTBC to a 10^{-4} M DMF solution of **12**.

Results (given in Table 5.4) from the double reciprocal plots give the various kinetic parameters and comparison on the influence of the central metal ion and the presence of thiocyanate can be made.

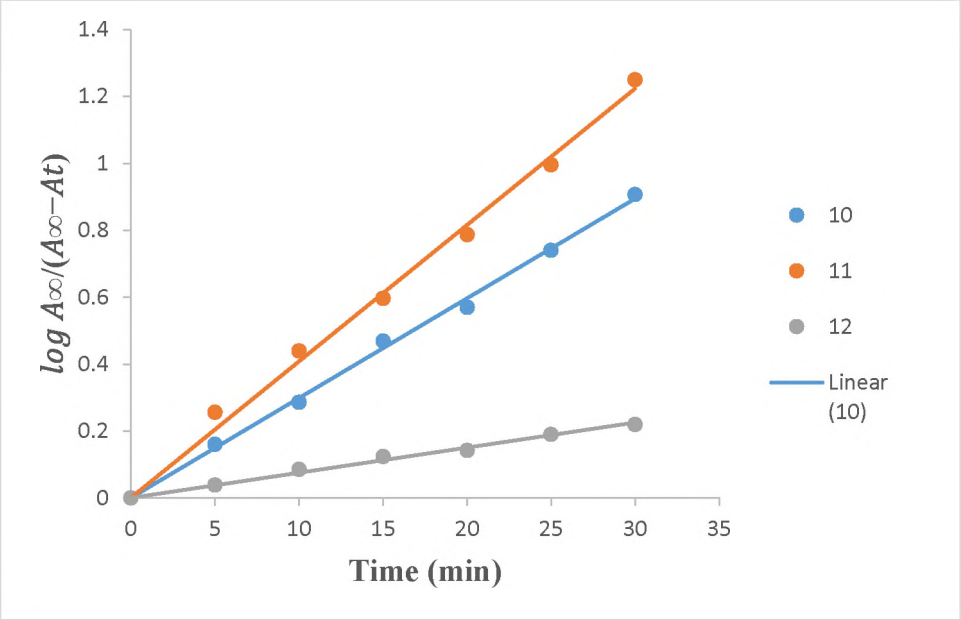

Fig. 5.8: Catecholase activity of complexes **10 - 12**

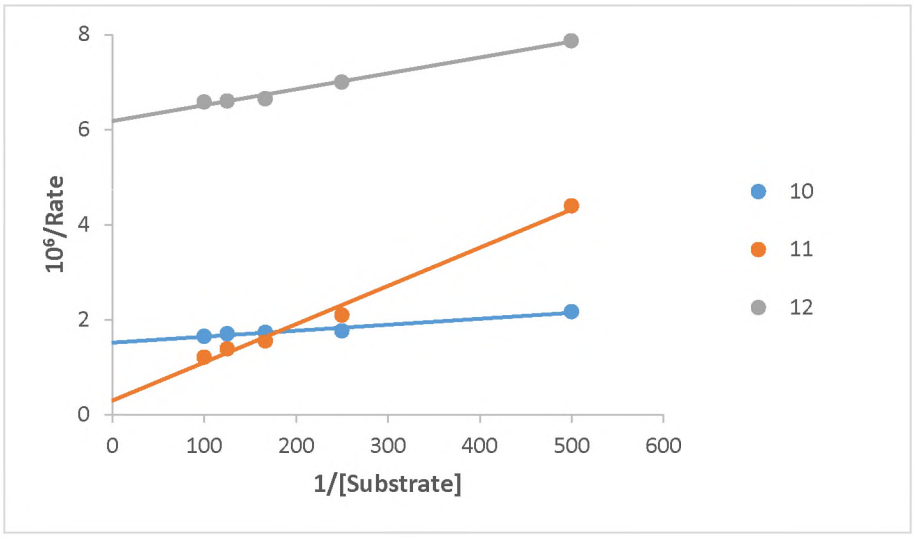

Fig. 5.9: Overlay of the Line-weaver Burk plots of complexes **10 – 12.**

The iron(III) complex **11** has the highest turnover rate in this series and so is the best amongst those of this ligand. Turnover rate of 112.32 h^{-1} is comparable to what previous authors have identified as excellent catalytic ability in the range of 45 – 440 h^{-1} [31].

Table 5.4. Kinetics parameters for the oxidation of 3, 5-DTBC catalysed by metal complexes of HL^3 (solvent: DMF).

Complex	**K_M(M)**	**V_{max}(Ms^{-1})**	**k_{cat} (h^{-1})**
9	I	I	I
10	$(8.40 \pm 0.33) \times 10^{-4}$	$(6.67 \pm 0.37) \times 10^{-7}$	24.01 ± 0.91
11	$(2.51 \pm 0.15) \times 10^{-2}$	$(3.12 \pm 0.20) \times 10^{-6}$	112.32 ± 3.72
12	$(5.40 \pm 0.31) \times 10^{-4}$	$(1.61 \pm 0.09) \times 10^{-7}$	5.80 ± 0.41

I = inactive

Detailed kinetic investigation of catecholase activity for metal complexes of the new ligand 4-methyl-2-((4-(pyridin-2-yl)piperazin-1-yl)methyl)phenol (HL^4) resulted in the observation of activity for all the metal complexes **13 – 16**. The course of the reaction followed by UV spectroscopy for the complex copper thiocyanate **14** is presented in Figure 5.10 below. The

plots of catalytic activity of the various metal complexes with 100 equivalent of the substrate are given in Figure 5.11 while the overlay of the Lineweaver Burk plot is given in Figure 5.12 as a representative for these set of complexes. The catalytic abilities of metal complexes of this ligand are yet to be reported in the literature.

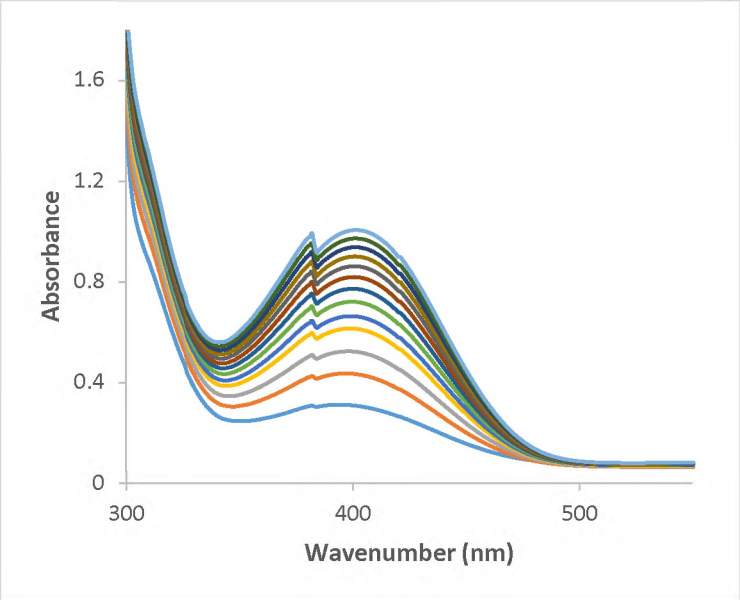

Fig. 5.10: Increase in absorbance around 400 nm, after addition of 100 equivalents of 3,5-DTBC to a 10^{-4} M DMF solution of **14**.

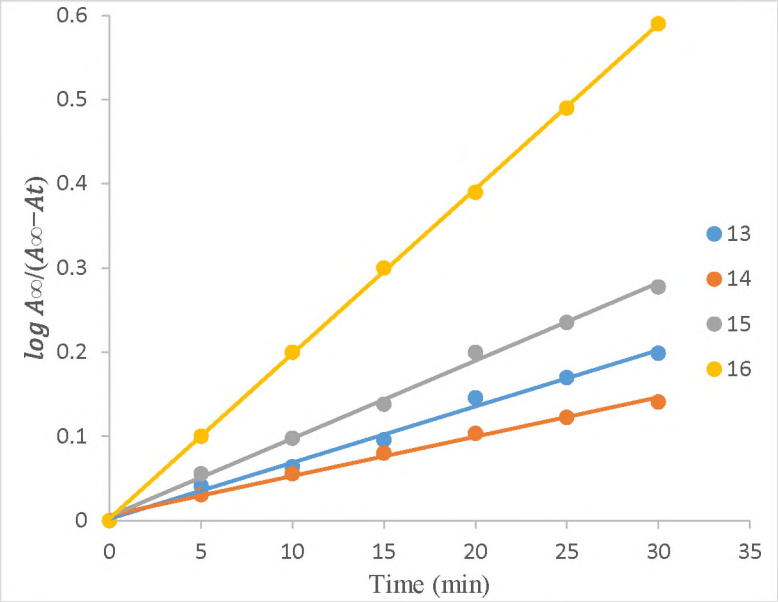

Fig. 5.11: Catecholase activity of complexes **13 – 16.**

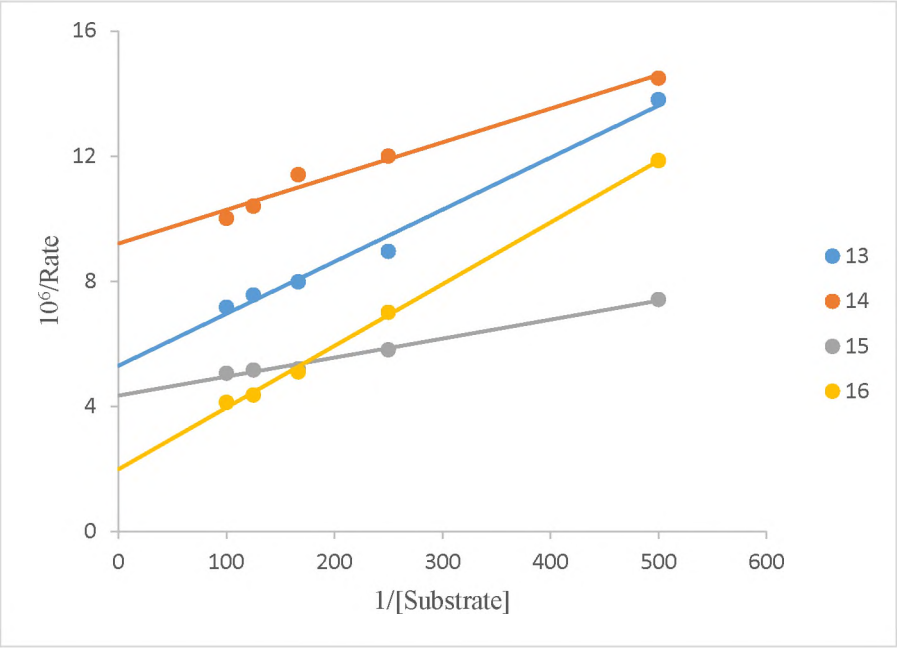

Fig. 5.12: Overlay of the Line-weaver Burk plots of complexes **13– 16.**

Kinetic parameters including V_{max}, K_M and k_{cat} were evaluated from the Lineweaver Burk plots and the results are presented in Table 5.4. All the complexes generally display moderate catalytic abilities judging from their turnover rates (3.81 – 17.93 h^{-1}), this may be attributed to the presence of the bulky pyridine ring in the ligand and the geometry of the metal ion as square planar complexes are generally known for their excellent catalytic abilities compared to other (five coordinate) geometries which unfortunately are prevalent here [32, 33].

A less electron-donating group such as pyrazine or pyridine enhanced the catalytic activity of the complex, probably favouring the reduction of Cu(II) into Cu(I) that occurs in the beginning of the catalytic cycle according to reports. Secondly, the presence of a bulkier coordinating group in the ligand e.g pyridine may decrease the kinetic rate, preventing the approach of catechol to the metal centre [34]. This has also been reported in series of amino acids [35].

Table 5.5. Kinetics parameters for the oxidation of 3, 5-DTBC catalysed by metal complexes of HL^4 (solvent: DMF).

Complex	K_M(M)	V_{max}(Ms^{-1})	k_{cat} (h^{-1})
13	$(3.11 \pm 0.15) \times 10^{-3}$	$(1.87 \pm 0.08) \times 10^{-7}$	6.73 ± 0.33
14	$(1.14 \pm 0.06) \times 10^{-3}$	$(1.06 \pm 0.06) \times 10^{-7}$	3.81 ± 0.14
15	$(1.31 \pm 0.07) \times 10^{-3}$	$(2.16 \pm 0.11) \times 10^{-7}$	7.78 ± 0.40
16	$(9.67 \pm 0.39) \times 10^{-3}$	$(4.98 \pm 0.30) \times 10^{-7}$	17.93 ± 1.10

The metal complexes of a new ligand 4-methyl-2-((4-(4-nitrophenyl)piperazin-1-yl)methyl)phenol are herein described. Complexes **17** and **19** are mononuclear while **18** and **20** that contain thiocyanates are dinuclear. Metal complexes **17 - 20** of the new ligand HL^5 displayed a very interesting pattern in their catecholase efficiency; the observation is that the thiocyanate complexes exhibited higher catalytic abilities than the metal complexes without it. It must be noted however that the complexes **18** and **20** which contain thiocyanate are dinuclear while **17** and **19** are mononuclear. Literature search has turned out reports that dinuclear complexes have better catecholase abilities than their mononuclear ones as the reduction of oxygen generally requires two metal centres [34, 35].

As a representative of this set the change in spectral pattern of complex **17** in DMF with the addition of the solution 3,5-DTBC, after observing the reaction for 1 h is displayed in figure 5.13 below. The catecholase plots followed by the overlay of the Line-Weaver Burk plots are displayed in Figures 5.14 and 5.15 respectively.

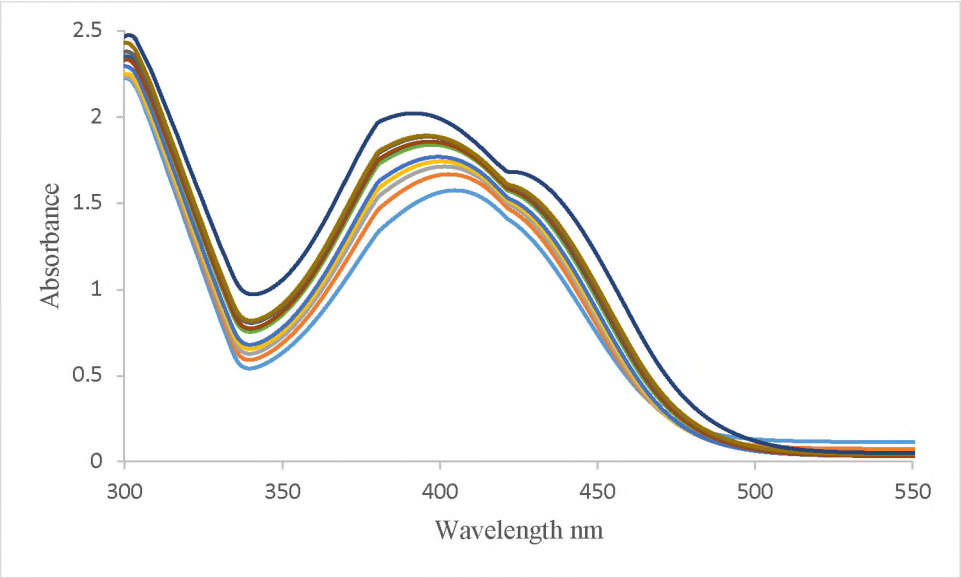

Fig. 5.13: Increase in absorbance around 400 nm, after addition of 100 equivalents of 3,5-DTBC to a 10^{-4} M DMF solution of **17**.

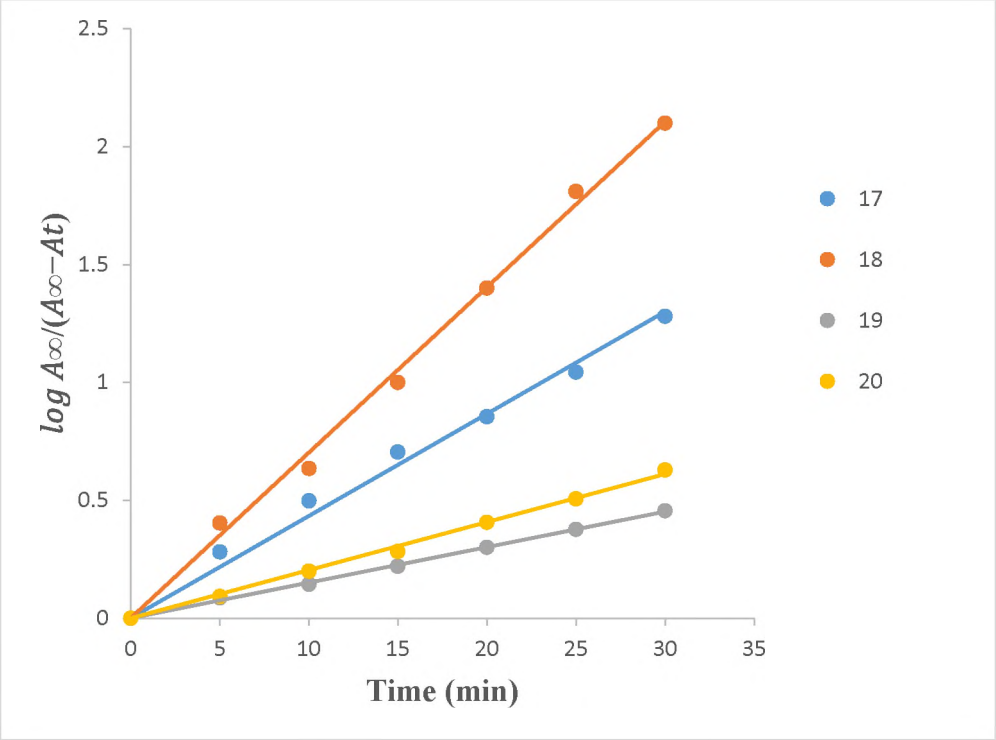

Fig. 5.14: Catecholase activity of complexes **17 – 20.**

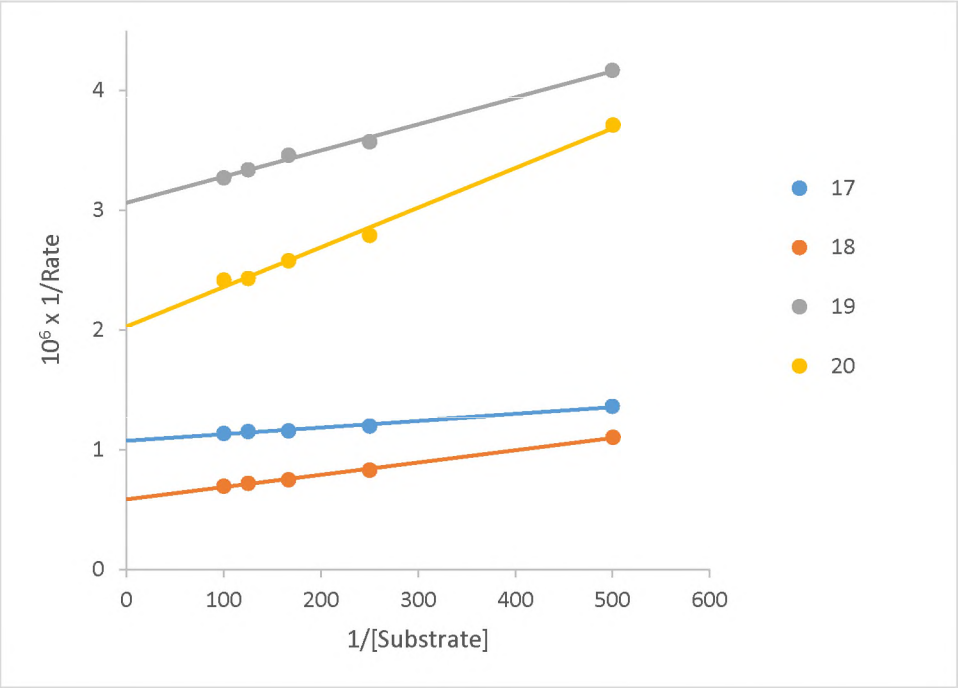

Fig. 5.15: Overlay of the Line-weaver Burk plots of complexes **17– 20.**

Results from the Line-weaver Burk plots led to the calculation of the kinetic parameters V_{max}, K_M and k_{cat} which are presented in Table 5.6 below. Values in the range of 11.70 – 60.84 h^{-1} are observed for the turnover rate of the metal complexes. Nitro-groups are also known to greatly influence by their electronic effect the redox properties of metal ion centres [36]. Nitro (NO_2) is an electron withdrawing group mostly due to resonance effect rather than inductive effect, its presence may further aid Cu(II)/Cu(I) reduction process which is important to catecholase activity. However, its distance from the metal ion centre may make the effect less profound.

Table 5.6. Kinetics parameters for the oxidation of 3, 5-DTBC catalysed by metal complexes of HL^5 (solvent: DMF).

Complex	K_M(M)	V_{max}(Ms^{-1})	k_{cat} (h^{-1}
17	$(5.19 \pm 0.27) \times 10^{-4}$	$(9.39 \pm 0.44) \times 10^{-7}$	33.81 ± 1.65
18	$(1.73 \pm 0.08) \times 10^{-3}$	$(1.69 \pm 0.09) \times 10^{-6}$	60.84 ± 3.40
19	$(7.08 \pm 0.34) \times 10^{-4}$	$(3.25 \pm 0.17) \times 10^{-7}$	11.70 ± 0.52
20	$(1.61 \pm 0.08) \times 10^{-3}$	$(4.87 \pm 0.25) \times 10^{-7}$	17.53 ± 0.91

5.2.2 Catecholase activity of metal complexes of p-acetamidophenol Mannich bases

The change of the substituent to one having more powerful positive inductive effect at the para position of the phenolic ring is observed to have noticeable effect on the catalytic abilities of the various metal centres. These trends are highlighted and discussed below for the metal complexes of each of the ligands. Again, in each set of complexes the first pair are copper(II), the second are iron(III), within these pairs the metal chloride is alternated with the metal thiocyanate.

Complexes **21**, **22** and **24** of HL^6 were obtained in metal to ligand ratio (1:2) and are non-electrolytes with only complex **23** in ratio 1:1 (metal to ligand), a 1:1 electrolyte and contains the ligand in its deprotonated form. The catalytic abilities of complexes **21 – 24** (octahedral geometry) of HL^6 on 20 – 100 equivalents of the substrate were recorded in DMF and the results indicated that all the metal complexes displayed moderately low activity except **21** (with a turnover rate of 56.12 h^{-1}) that has considerably high catalytic activity. Figure 5.16 displays the increase in absorbance around 399 nm, after the addition of 100 equivalents of 3, 5-DTBC to a 10^{-4} M DMF solution of **23** as a representative for this series of complexes. The spectra were recorded every 5 mins.

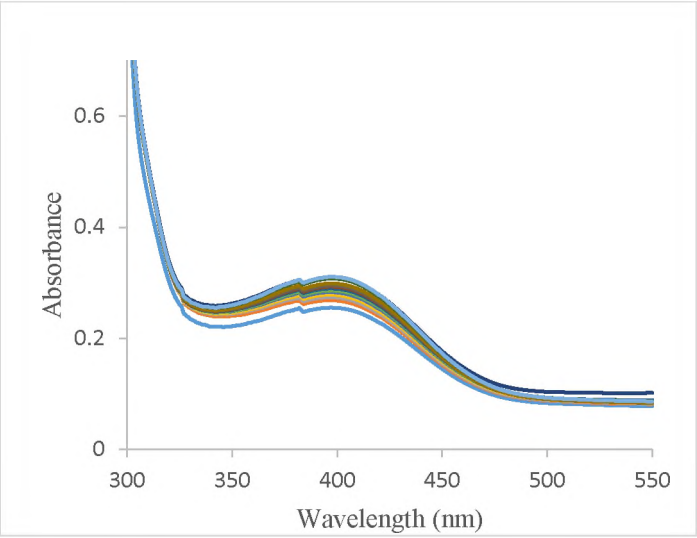

Fig. 5.16: A plot of change in absorbance vs. time to evaluate the initial rate of the catalytic oxidation of 3,5-DTBC by **23** in DMF.

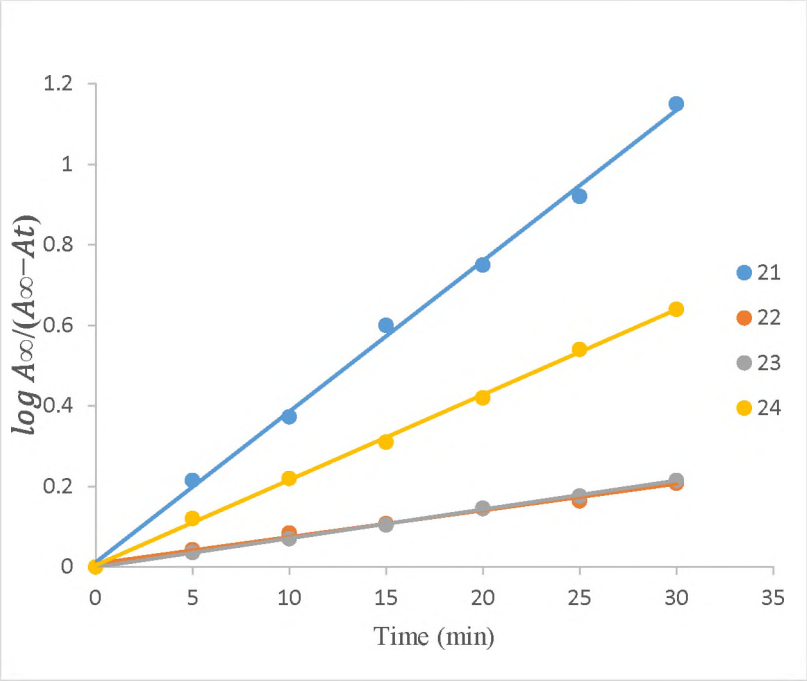

Fig. 5.17: Catecholase activity of complexes **21 – 24.**

The plot of $log\ A\infty/(A\infty - At)$ vs. time to evaluate the initial rate of the catalytic oxidation of 3,5-DTBC by the various metal complexes in DMF is given in Figure 5.17 above. Detailed kinetic studies yielded the Lineweaver Burk plots for all the active compounds and are displayed in Figure 5.18.

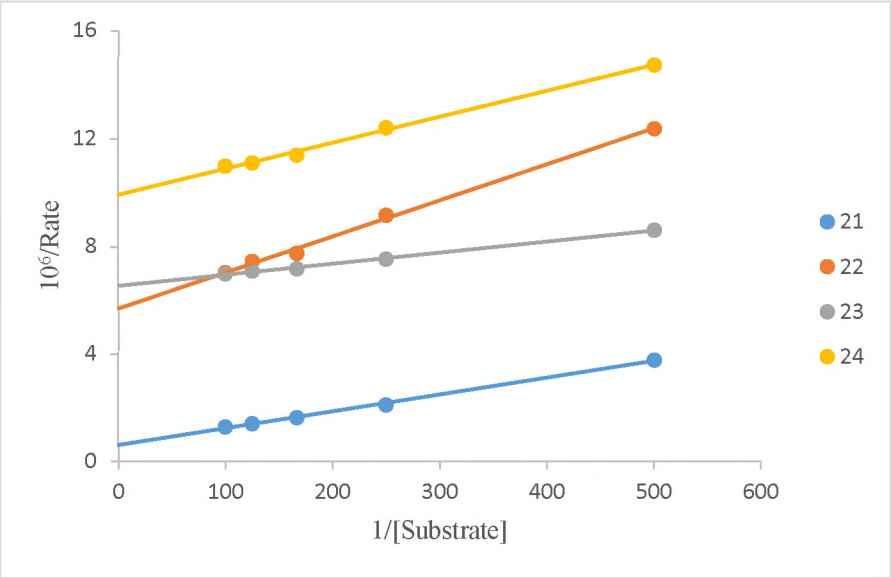

Fig. 5.18: Overlay of the Line-weaver Burk plots of complexes **21– 24.**

Details of the kinetic studies including values of the k_{cat} (turnover rates) are presented in Table 5.7. Complex **21** displayed the highest activity within this series with a turnover rate of 56.52 h^{-1} and this is in close agreement with the observation that geometry consideration (particularly square planar and octahedral) favours catecholase activity owing to steric effects and ease of the incoming group. The presence of the two chlorides that are excellent leaving groups may be responsible for the excellent catecholase activity. The thiocyanate metal complexes displayed lower catecholase activity.

Table 5.7. Kinetics parameters for the oxidation of 3, 5-DTBC catalysed by metal complexes of HL^6 (solvent: DMF).

Complex	**K_M(M)**	**V_{max}(Ms^{-1})**	**k_{cat} (h^{-1})**
21	$(9.75 \pm 0.60) \times 10^{-3}$	$(1.57 \pm 0.13) \times 10^{-6}$	56.52 ± 0.62
22	$(2.30 \pm 0.13) \times 10^{-3}$	$(1.72 \pm 0.12) \times 10^{-7}$	6.19 ± 0.41
23	$(6.31 \pm 0.35) \times 10^{-4}$	$(1.54 \pm 0.11) \times 10^{-7}$	5.54 ± 0.25
24	$(9.70 \pm 0.55) \times 10^{-4}$	$(1.01 \pm 0.06) \times 10^{-7}$	3.60 ± 0.20

Below are described the catecholase activity of the metal complexes of a new Mannich base N-(4-hydroxy-3-((piperidin-1-yl)methyl)phenyl)acetamide (HL^7). All the metal complexes in this series were obtained in 1:1 metal to ligand ration except **27** (1:2), also, only complex **25** is a non-electrolyte while the rest are (1:1) electrolytes. The iron(III) complexes of HL^7 are more catalytically active than their copper(II) counterparts. Though compound **25** is structurally similar to its counterpart **5**, electronic properties of substituents are known to greatly influence their behaviour in solution and also stability of the metal substrate adduct in solution is of great consideration here. The wavelength scan for the catecholase activity of complex **26** in DMF recorded for 1 h at an interval of 5 min is given in Figure 5.19 below as a representative for this series. The catecholase activity plots involving 100 equivalent of substrate is presented in Figure 5.20 and the overlay of Lineweaver-Burk Plots is presented in Figure 5.21.

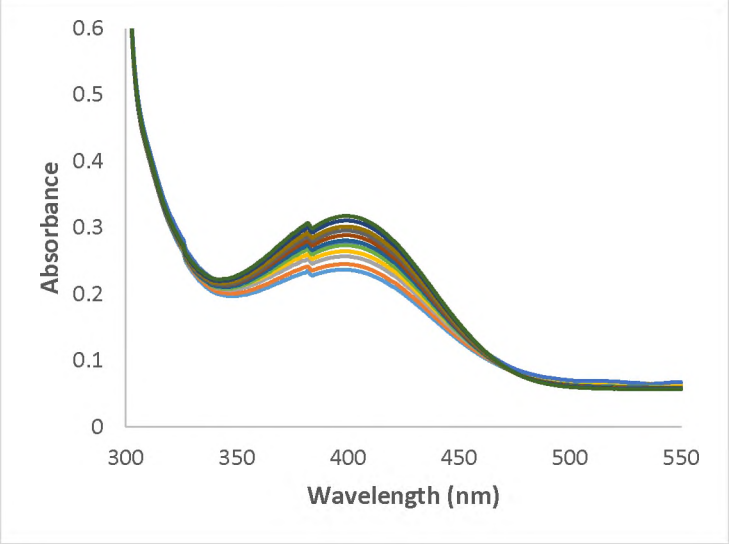

Fig. 5.19: A plot of change in absorbance vs. time to evaluate the initial rate of the catalytic oxidation of 3,5-DTBC by **26** in DMF.

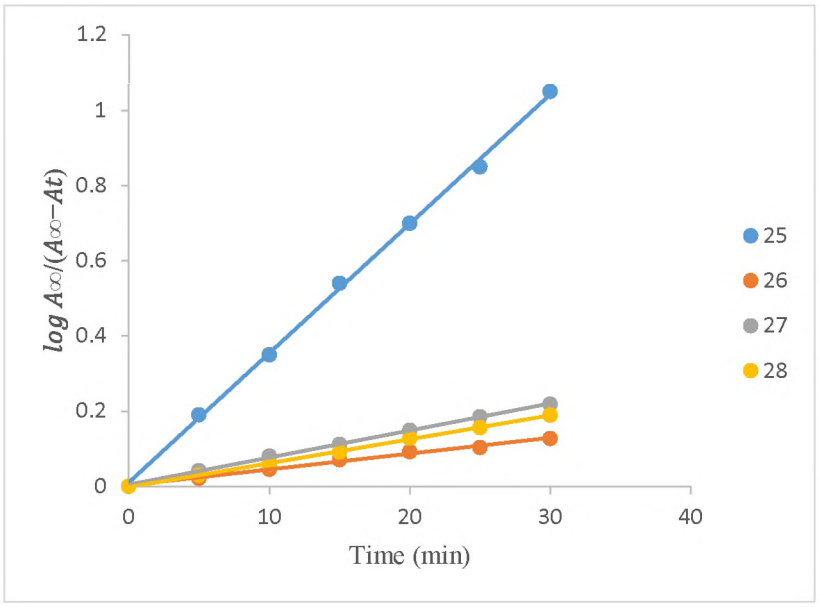

Fig. 5.20: Catecholase activity of complexes **25 – 28.**

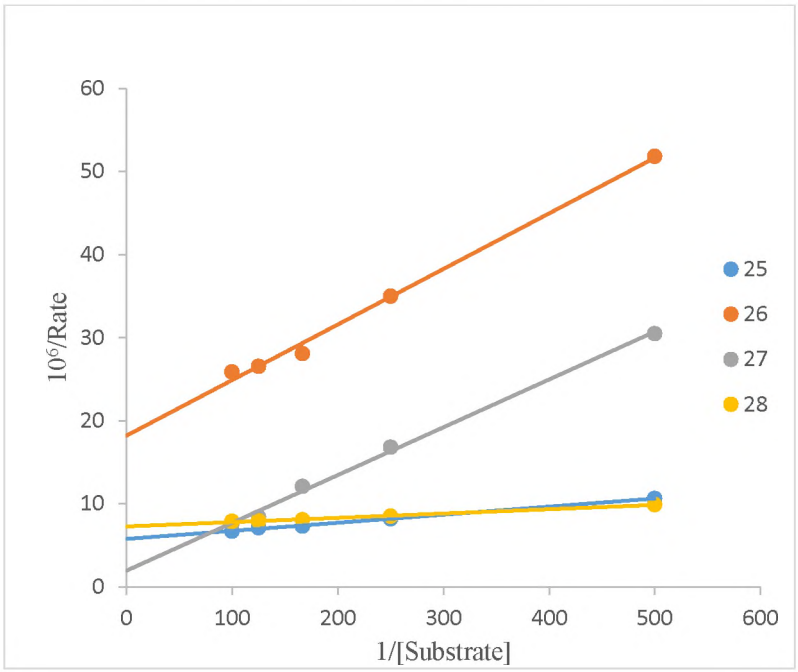

Fig. 5.21: Overlay of the Line-weaver Burk plots of complexes **25– 28.**

Detailed kinetic evaluation of the catecholase activity of complexes **25 – 28** leads to the observation of catalytic activities for all the complexes **25 – 28** in the range (1.86 -14.69 h^{-1}) with complex **27** displaying the highest activity. Results of the kinetic parameters from the Lineweaver Burk plots for complexes **25 – 28** are presented in Table 5.8.

Table 5.8. Kinetics parameters for the oxidation of 3, 5-DTBC catalysed by metal complexes of HL^7 (solvent: DMF).

Complex	K_M(M)	V_{max}(Ms^{-1})	k_{cat} (h^{-1})
25	$(1.67 \pm 0.08) \times 10^{-3}$	$(1.72 \pm 0.09) \times 10^{-7}$	6.19 ± 0.30
26	$(3.46 \pm 0.15) \times 10^{-3}$	$(5.18 \pm 0.30) \times 10^{-8}$	1.86 ± 0.09
27	$(2.35 \pm 0.12) \times 10^{-2}$	$(4.08 \pm 0.21) \times 10^{-7}$	14.69 ± 0.71
28	$(7.12 \pm 0.40) \times 10^{-4}$	$(1.38 \pm 0.06) \times 10^{-7}$	4.96 ± 0.22

The high catalytic activity of **27** compared to others within the series may be due to the presence of the chloride ions which represents excellent leaving groups.

The discussion of catecholase activity of Cu(II) and Fe(III) of a new Mannich base 2-((4-(2-hydroxy-4-acetamidobenzyl)piperazin-1-yl)methyl)-5-phenylacetamide (HL^8). Complexes **29** and **30** are square planar while **30** and **31** are octahedral. **30** and **32** are isostructural. All metal complexes **29 – 32** of the new ligand HL^8 displayed moderately high catecholase activity with the enzymatic ability enhanced evenly by the substituent considering the nature of the solvent. As a representative of this series, the wavelength scan for the catecholase activity of complex **32** with 100 equivalents of 3,5-DTBC in DMF 1 h at an interval of 5 min is presented in Figure 5.22.

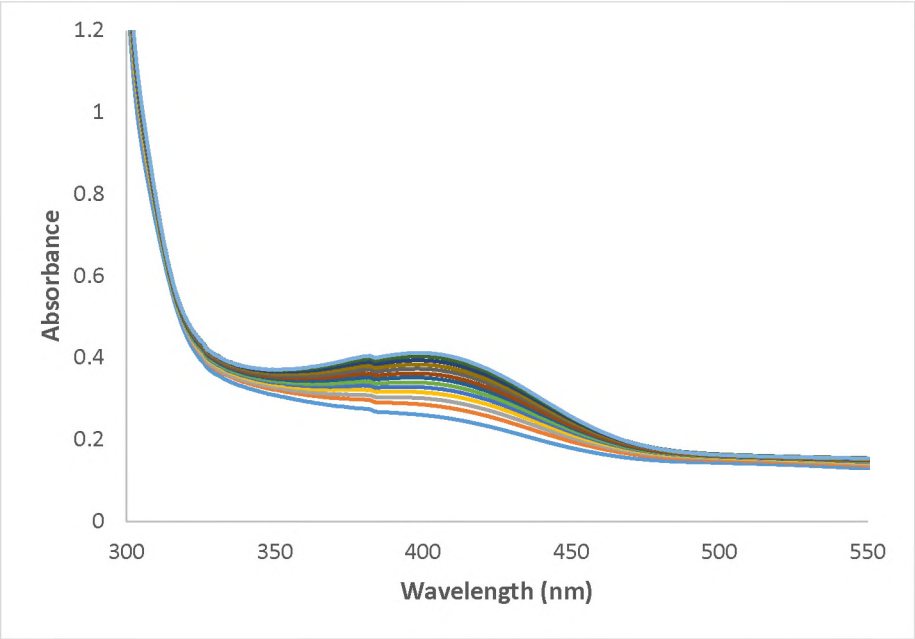

Fig. 5. 22: Wavelength scan for the catecholase activity of complex **32** in DMF with 100 equivalent of 3,5-DTBC for 1 h at an interval of 5 min.

Detailed kinetic studies were carried out with 20 – 100 equivalents of the substrate and the results are presented for the 100 equivalents in Figure 5.23, this is followed by the plot of the Lineweaver Burk equation presented in Figure 5.24.

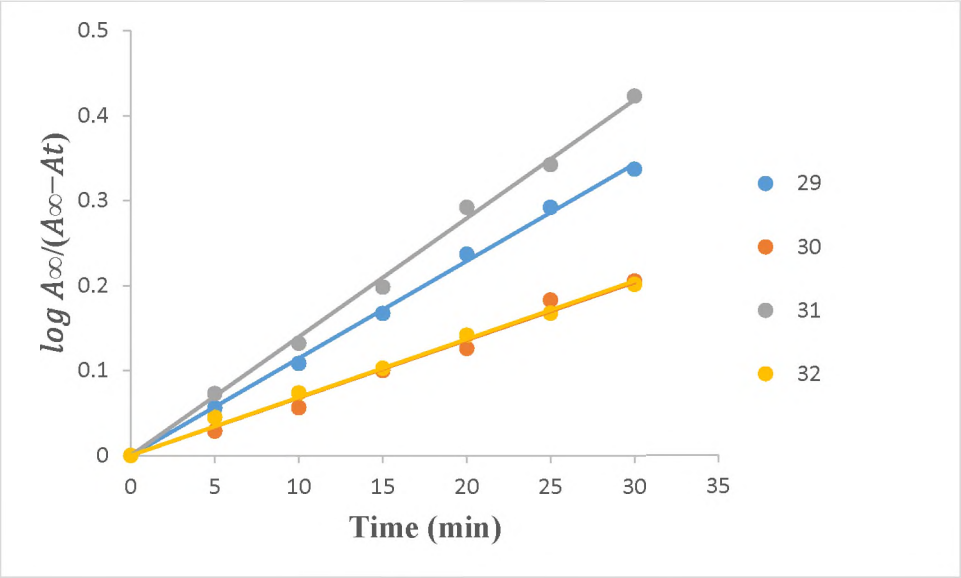

Fig. 5.23: Catecholase activity of complexes **29 – 32.**

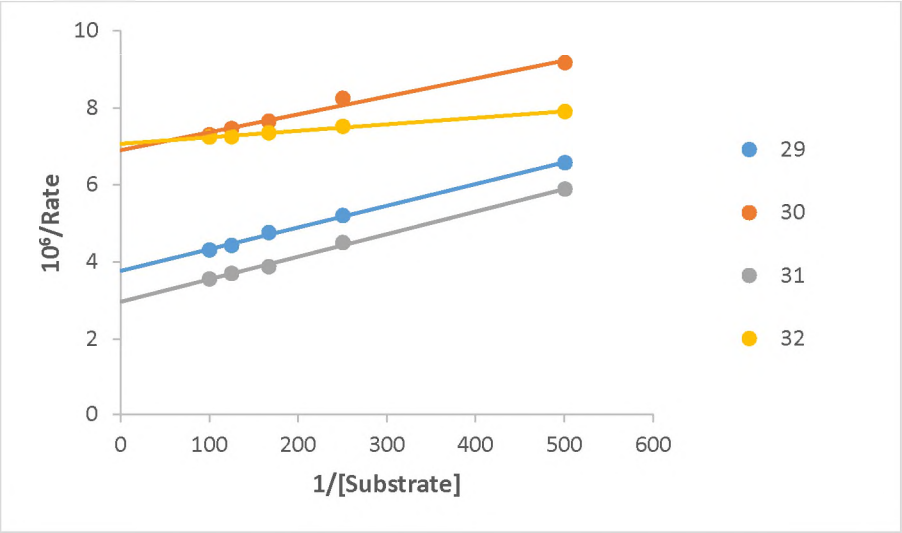

Fig. 5.24: Overlay of the Line-weaver Burk plots of complexes **29– 32.**

Evaluation of the kinetic parameters particularly k_{cat} which is important for the comparison of the metal complexes in order of their activity was done from the Lineweaver Burk plot and the result is presented in Table 5.9. Complex **31** is the most efficient catalyst in this set with a turnover rate of 12.96 h^{-1}. Good leaving groups (Cl^-) that are not bridged may be responsible for the higher turnover rates [39].

Table 5.9. Kinetics parameters for the oxidation of 3, 5-DTBC catalysed by metal complexes of HL^8 (solvent: DMF).

Complex	**K_M(M)**	**V_{max}(Ms^{-1})**	***k_{cat}*** **(h^{-1})**
29	$(1.50 \pm 0.06) \times 10^{-3}$	$(2.65 \pm 0.12) \times 10^{-7}$	9.54 ± 0.54
30	$(6.77 \pm 0.35) \times 10^{-4}$	$(1.45 \pm 0.08) \times 10^{-7}$	5.22 ± 0.22
31	$(1.97 +0.04) \times 10^{-3}$	$(3.36 \pm 0.14) \times 10^{-7}$	12.96 ± 0.71
32	$(2.38 \pm 0.12) \times 10^{-4}$	$(1.42 \pm 0.08) \times 10^{-7}$	5.12 ± 0.22

Catecholase activity of new Mannich base N-(4-hydroxy-3-((4-(acetamid-2-yl)acetamido-1-yl)methyl)phenyl)acetamide (HL^9). The Cu(II) and Fe(III) are isostructural with octahedral geometries and the thiocyanate complexes **34** and **36** are dinuclear and electrolytic (1:1) unlike their non-thiocyanate counterparts. The catalytic abilities of complexes **33 – 36** of new ligand HL^9 were determined using 20 – 100 equivalent of the substrate 3, 5-DTBC in DMF and the spectral scan involving complex **34** and 100 equivalents of 3,5-DTBC is displayed in Figure 5.25.

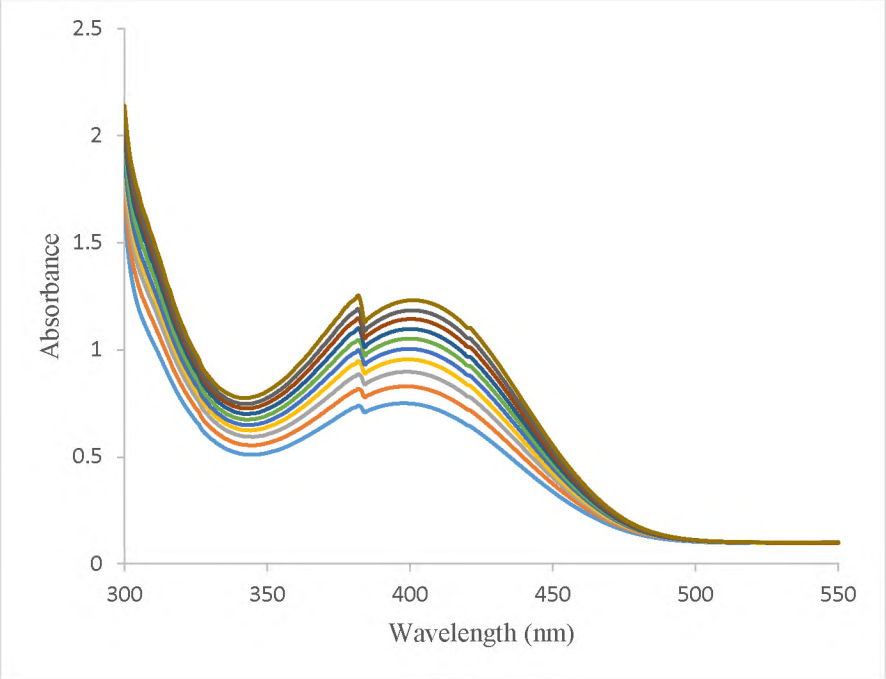

Fig. 5. 25: Wavelength scan for the catecholase activity of complex **34** in DMF with 100 equivalent of 3,5-DTBC for 1 h at an interval of 5 min.

Figure 5.26 is the result from the method of initial rates involving all the metal complexes and 100 equivalent of 3,5-DTBC.

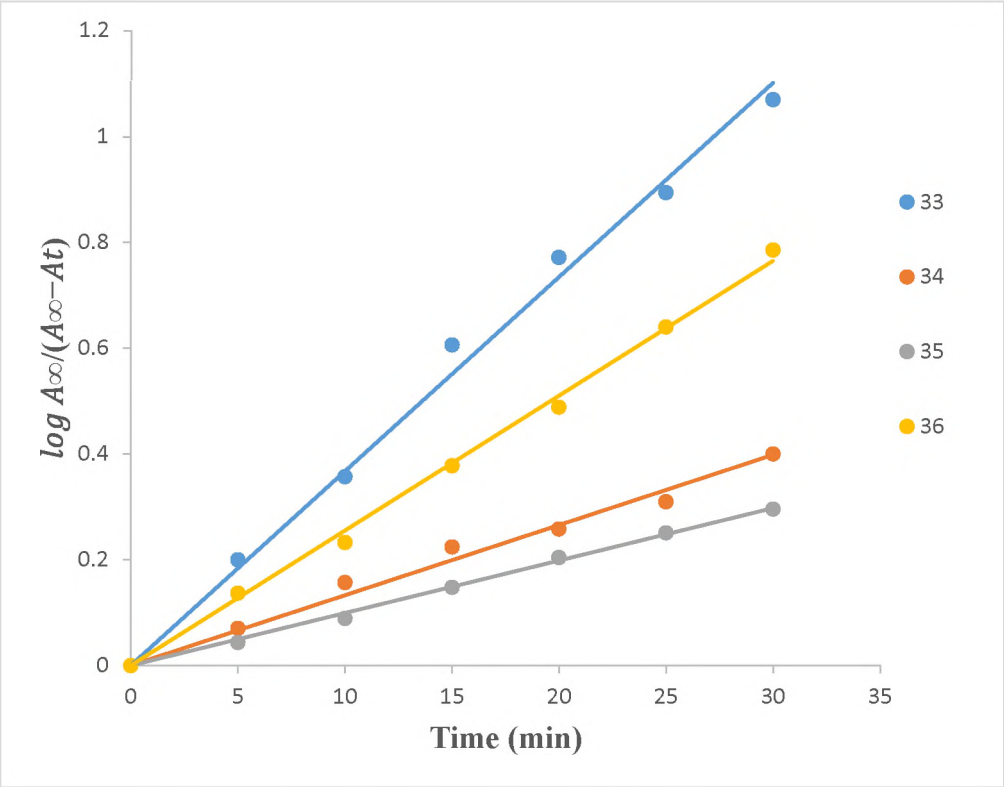

Fig. 5.26: Catecholase activity of complexes **33 – 36.**

This was followed by detailed kinetic evaluation by the method of initial rates and that led to the Lineweaver Burk plots presented in Figure 5.27. All the metal complexes were catalytically active with complex **35** the most active in this series with a turnover rate of 31.86 h^{-1}.

Determination of the kinetic parameters showed moderately high turnover rates recorded for the metal complexes as presented in Table 5.10. The thiocyanate containing metal complexes (**34, 36**) display lower turnover rates compared to the metal complexes (**33, 35**) without it as previously observed that thiocyanate metal complexes are generally poor candidates for catecholase activity.

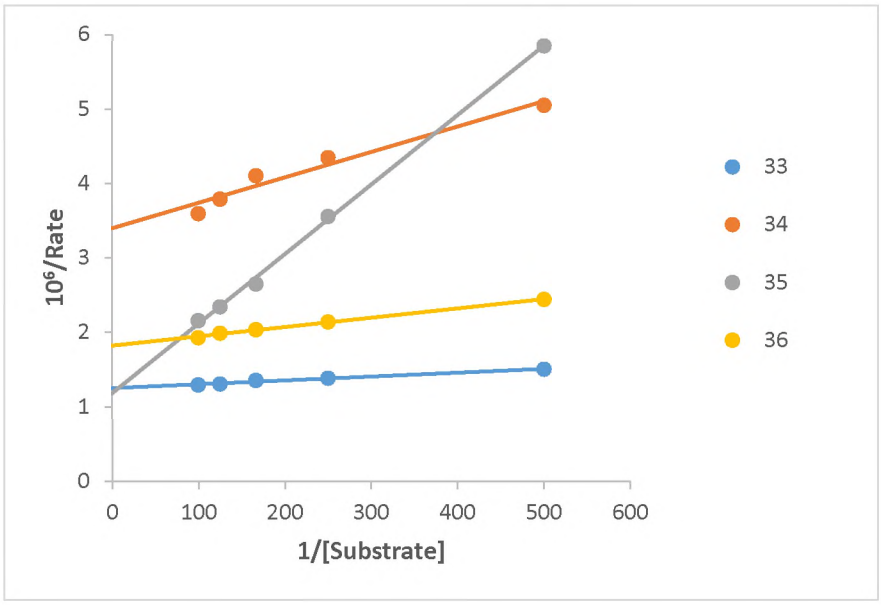

Fig. 5.27: Overlay of the Line-weaver Burk plots of complexes **33– 36.**

Also metal complexes of HL^9 display higher catecholase activity compared to those of HL^4 owing to the substituent effect of the acetamido at the para position to the hydroxyl group of the ligands. In addition, thiocyanate metal complexes of HL^9 are dinuclear compared to their mononuclear counterparts of HL^4. All these factors are responsible for the differing trend of catecholase activity.

Table 5.10. Kinetics parameters for the oxidation of 3, 5-DTBC catalysed by metal complexes of HL^9 (solvent: DMF).

Complex	**K_m(M)**	**V_{max}(Ms^{-1})**	**k_{cat} (h^{-1})**
33	$(4.03 \pm 0.22) \times 10^{-4}$	$(7.84 \pm 0.44) \times 10^{-7}$	28.22 ± 1.11
34	$(8.96 \pm 0.28) \times 10^{-4}$	$(2.63 \pm 0.11) \times 10^{-7}$	9.47 ± 0.52
35	$(8.25 \pm 0.49) \times 10^{-3}$	$(8.85 \pm 0.62) \times 10^{-7}$	31.86 ± 1.20
36	$(6.82 \pm 0.31) \times 10^{-4}$	$(5.48 \pm 0.12) \times 10^{-7}$	19.73 ± 0.89

Catecholase activity of Cu(II) and Fe(III) complex of a new Mannich base N-(4-hydroxy-3-((4-(4-nitrophenyl)piperazin-1-yl)methyl)phenyl)acetamide (HL^{10}). All the complexes **37** – **40** were obtained in ratio 1:1 (metal to ligand) except **38** the only dinuclear complex, also **37** and **39** are isostructural. The determination of catalytic abilities of complexes **37** – **40** was also carried out and all the metal complexes displayed catalytic abilities. The method of initial rate was employed to evaluate the catalytic abilities of the various metal complexes using 20 – 100 equivalent of the substrate. All the metal complexes displayed catalytic abilities. The catecholase activity plots of 100 equivalents of 3,5-DTBC are presented in Figure 5.28 and this was followed by the Lineweaver Burk plots presented in Figure 5.29.

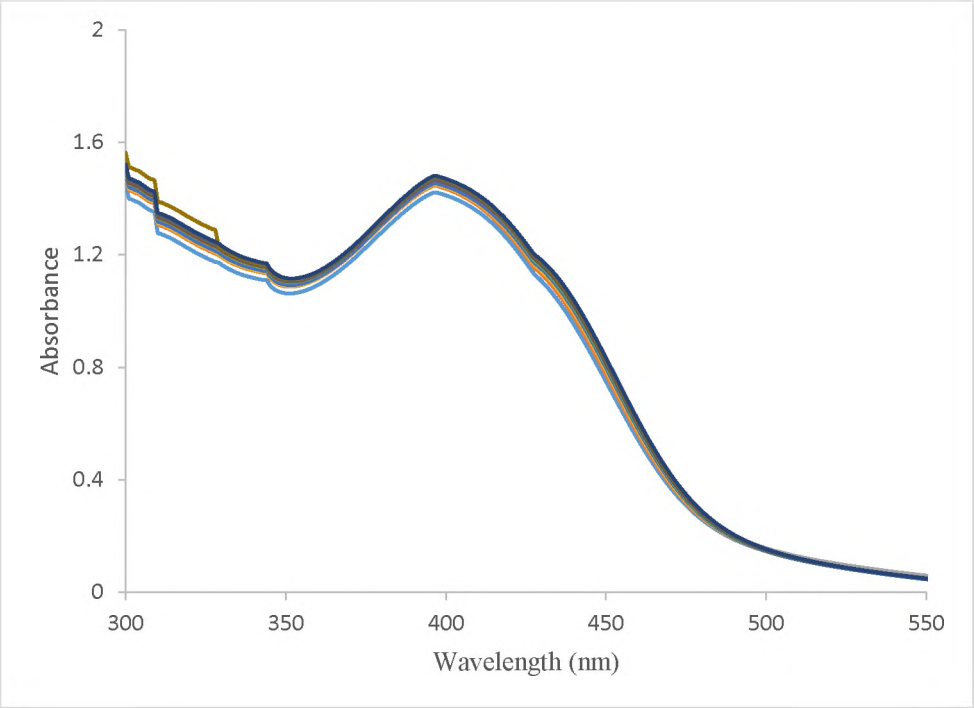

Fig. 5. 28: Wavelength scan for the catecholase activity of complex **39** in DMF with 100 equivalent of 3,5-DTBC for 1 h at an interval of 5 min.

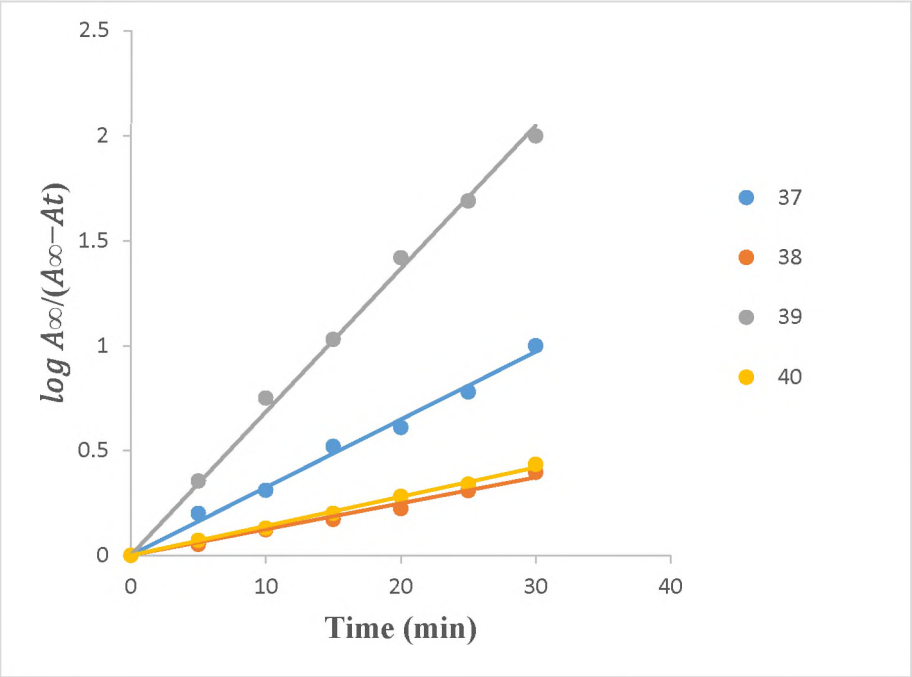

Fig. 5.29: Catecholase activity of complexes **37 – 40.**

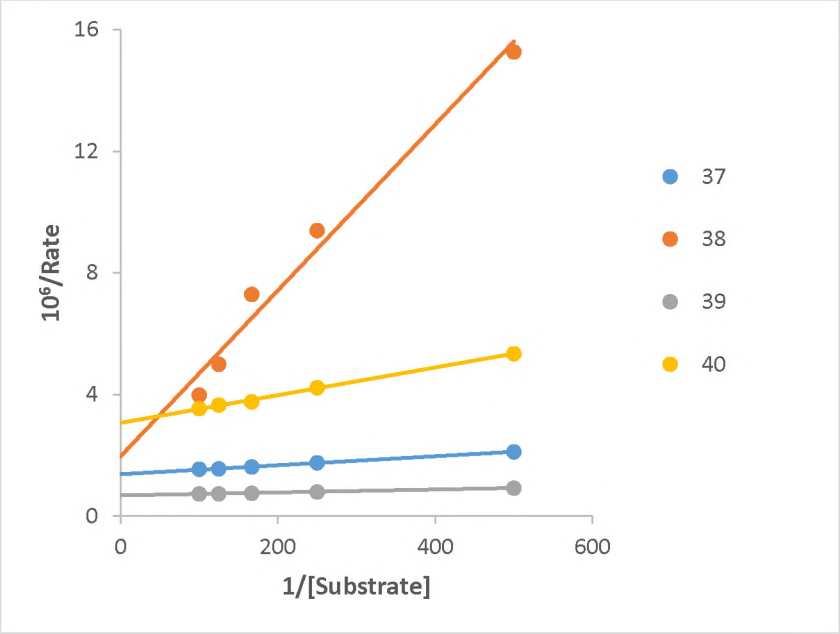

Fig. 5.30: Overlay of the Line-weaver Burk plots of complexes **37– 40.**

Detailed kinetic studied revealed that the iron(III) complex **39** is the best catalyst in the series judging from the turnover number (k_{cat}) of 52.96 h^{-1}. As previously observed, the thiocyanate

complexes have lower turnover rate compared to the metal complexes without it. The results from the Lineweaver Burk plots are presented in Table 5.11.

Table 5.11. Kinetics parameters for the oxidation of 3, 5-DTBC catalysed by metal complexes of HL^{10} (solvent: DMF).

Complex	K_M(M)	V_{max}(Ms^{-1})	k_{cat} (h^{-1})
37	$(1.67 \pm 0.09) \times 10^{-3}$	$(7.25 \pm 0.40) \times 10^{-7}$	26.10 ± 1.50
38	$(1.36 \pm 0.05) \times 10^{-2}$	$(5.00 \pm 0.22) \times 10^{-7}$	18.00 ± 1.10
39	$(6.99 \pm 0.40) \times 10^{-4}$	$(1.47 \pm 0.09) \times 10^{-6}$	52.96 ± 3.01
40	$(1.51 \pm 0.05) \times 10^{-3}$	$(3.31 \pm 0.11) \times 10^{-7}$	11.92 ± 0.62

5.3 Rationale for lower turnover rates (k_{cat}) in thiocyanate metal complexes

In summary, the values obtained for the k_{cat} in this study are in the range of 1.86 ± 0.09 to 112.32 ± 3.72 h^{-1} and these values are comparable to those previously reported in the literature for Cu(II) and other metal complexes [40 - 45]. Greater catecholase activity could possibly have been achieved with a less coordinating solvent. Reports from the literature have shown that solvents like DMF and DMSO that have high coordinating ability compared to methanol and acetonitrile retards the possibility of catechol–substrate adduct formation. This greatly slows down the rate determining step in the catalytic abilities of metal complexes [28, 46].

However as seen in Table 5.1, for Mannich bases this is not the case in the few studies so far conducted in coordinating solvents. Based on searches through the literature on the catalytic activity of Mannich base complexes of Cu(II) and Fe(III) this current study is a pioneering work in this field of comparative evaluation of the catalytic impact of thiocyanate moiety in such systems.

To simplify the correlation between the catalytic abilities of isostructural complexes, the selected compounds are grouped as follows: Isostructural complexes within a group or set and then a comparison of isostructural pairs of complexes based upon the ligand classes p-methylphenol (1 – 20) and p-acetamidophenol Mannich bases (21 – 40) in Tables 5.12 and 5.13. The metal complexes encountered in this study can be put into 6 groups (i) $M_a(L^n)_aCl_b.cH_2O$ (ii) $M_a(HL^n)_a(NCS)_aCl_b$ (iii) $M_a(L^n)_a(NCS)_aCl_b$ (iv) $M_a(HL^n)_aCl_b.cH_2O$ (v) $M_a(L^n)_a(NCS)_a.cH_2O$ (vi) $M_a(HL^n)_a(NCS)_a.cH_2O$ where a = 1 - 2 ; b = 1 – 4, c = 1 – 8.

Table 5.12. Isostructural Cu(II) and Fe(III) within a group.

Cluster	Compound	Formula	k_{cat}	Geometry	Comment
1	7	$[Fe(HL^2)Cl_3].CHCl_3$	6.02 ± 0.41	Oct.	8 more active than 7
	8	$[Fe(HL^2)(NCS)Cl_2].4H_2O$	12.00 ± 0.78	Oct.	
2	11	$[FeL^3Cl].H_2O$	112.32 ± 3.72	Oct.	11 more active than 12
	12	$[FeL^3(NCS)].5H_2O$	5.80 ± 0.41	Oct.	
3	13	$[Cu(HL^4)Cl_2]$	6.73 ± 0.33	Tri. byp.	13 more active than 14
	14	$[Cu(HL^4)(NCS)Cl].^1/_4CH_3CN$	3.81 ± 0.14	Tri. byp.	
4	17	$[CuHL^5Cl_2].^1/_3CHCl_3$	33.81 ± 1.65	Oct.	17 more active than 19
	19	$[Fe(HL^5)Cl_3].H_2O$	11.70 ± 0.52	Oct.	
5	18	$[Cu_2(HL^5)(NCS)_2]Cl_2$	60.84 ± 3.40	Sq. pl.	18 more active than 20
	20	$[Fe_2(HL^5)Cl_2(SCN)_2(H_2O)_2]Cl_2{}^x/_2$	17.53 ± 0.91	Oct.	
6	21	$[Cu(HL^6)_2Cl_2].H_2O.^1/_2CHCl_3$	56.52 ± 0.62	Oct.	21 more active than 22
	22	$[Cu(HL^6)_2(NCS)_2].2H_2O$	6.19 ± 0.41	Oct.	
7	25	$Cu(HL^7)Cl_2].H_2O.^1/_4CHCl_3$	6.19 ± 0.30	Sq. pl	25 more active than 26
	26	$[Cu(HL^7)(SCN)]Cl.3H_2O$	1.86 ± 0.09	Sq. pl.	
8	30	$[Cu_2(HL^8)(NCS)_2Cl_2].4H_2O$	5.22 ± 0.22	Sq. pl.	30 more active than 32
	32	$[Fe_2(HL^8)(NCS)_2Cl_2(H_2O)_4].Cl_2{}^1/_2X$	5.12 ± 0.22	Oct.	

Table 5.12 (continued)

Cluster	Compound	Formula	k_{cat}	Geometry	Comment
9	33	$[Cu(HL^9)Cl_2].4H_2O$	28.22 ± 1.11	Tri. byp.	35 more active than 33
	35	$[Fe(HL^9)Cl_3].6H_2O$	31.86 ± 1.20	Oct.	
10	34	$[Cu_2(HL^9)(NCS)_22H_2O]Cl_22H_2O$	9.47 ± 0.52	Sq. pl.	36 more active than 34
	36	$[Fe_2(HL^9)(NCS)_2(H_2O)_2Cl_2]Cl_2$ $6H_2O$	19.73 ± 0.89	Oct.	
11	37	$[Cu(HL^{10})Cl_2]$	26.10 ± 1.50	Sq. pl.	37 more active than 38
	39	$[Fe(HL^{10})Cl_3].CH_3OH$	18.00 ± 1.10	Oct.	

sq. pl. = square planar, Oct. = octahedral, Tri. byp. = trigonal bipyramidal, x = chloroform

For complexes derived from the same ligand, differences in reactivity can be explained in terms of geometry or anion from the coordination sphere of metal ion (conductivity). As the thiocyanate ion is a stronger binding ligand than the chloride ion or water molecule, its makes the coordination of substrate to the metal center less favourable and thus results in less active catalysts. Literature search has not revealed results for Cu(II) and Fe(III) complexes of Mannich bases on the comparative effect of replacing chlorides with thiocyanates on catecholase activity. This is found to be true for **11/12**, **13/14**, **21/22** and **25/26**, where the presence of thiocyanate in metal complexes reduced catecholase activity. Only in cluster **7/8** is the thiocyanate complex **8** (octahedral) more active than the chloride complex **7** and low activity is attributed to the five coordinate geometry of **7** which has been reported to do poorly in catalytic studies [29].

Secondly, we make a comparison of closely related Cu(II) and Fe(III) complexes of the Mannich bases of p-methylphenol including **17/19** and **18/20**, the Cu(II) complexes are more active than their Fe(III) counterparts. Whereas, results are less distinct in the metal complexes

of *p*-acetamidophenol Mannich bases which include **30/32** (Cu(II) complex is marginally more active), **33/35**, **34/36** (Fe(II) complexes are more active) **37/39** (Cu(II) is more active).

Considering the standard reduction potentials [47], Fe(III)/Fe(II) is more favourable than Cu(II)/Cu(I) but the presence of an electron donating group like Mannich bases will reverse this trend by making this process difficult. The instances of higher catalytic activity by Fe(III) over Cu(II) in **33/35** is attributed to geometry (octahedral versus trigonal bipyramidal) and **34/36** may be due to molar conductivity reasons [48]. Generally, there is a positive correlation between conductivity and catecholase activity. So in the case of **34/36**, since both are 1:1 electrolytes the reduction process is more favourable for **36** compared to **34** thereby leading to an increase in catecholase activity.

Table 5.13. Isostructural complexes for the two ligands classes.

Cluster	Compound	Molecular Formula	k_{cat}	Geometry	Comment
12	6	$[Cu(HL^{2})(NCS)Cl]$	7.42 ± 0.50	Sq. pl.	6 more active than 26
	26	$[Cu(HL^{7})(SCN)H_2O]Cl.2H_2O$	1.86 ± 0.09	Sq. pl.	
13	8	$[Fe(HL^{2})(NCS)Cl_2].4H_2O$	12.00± .78	Oct.	8 more active than 28
	28	$[Fe(HL^{7})(NCS)ClH_2O]Cl.^{3}/_{2}H_2O$	4.96 ± 0.22	Oct.	
14	13	$[Cu(HL^{4})Cl_2]$	6.73 ± 0.33	Tri. byp.	33 more active than 13
	33	$[Cu(HL^{9})Cl_2].4H_2O$	28.22± 1.11	Oct.	
15	17	$[CuHL^{5}Cl_2].^{1}/_{3}CHCl_3$	33.81 ± 1.65	Tri. byp.	17 more active than 37
	37	$Cu(HL^{10})Cl_2]$	26.10± 1.50	Tri. byp.	
16	19	$[Fe(HL^{5})Cl_3].H_2O$	11.70 ± 0.52	Oct.	39 more active than 19
	39	$[Fe(HL^{10})Cl_3].CH_3OH$	52.96 ± 3.01	Oct.	

Sq. pl. = square planar, Oct. = octahedral, Tri. byp. = trigonal bipyramidal

Five clusters are discussed herein of Cu(II) and Fe(III) complexes of the two different classes of ligands. Clusters **12**, **14** and **15** containing Cu(II) complexes revealed that the metal

complexes of p-methylphenol Mannich bases are more catalytically active than their p-acetamidophenol ones. The significant difference in catalytic activity of the complexes is that the *p*-substituent of the phenolic ring of the *p*-acetamidophenol Mannich base metal complexes have reduced catalytic activity due to the electron-donating para-substituent (CH_3CONH-) [49, 50]. If the reduction potential is too negative, the complex has decreased catalytic activity due to a more difficult reduction to copper(I), and a more positive reduction potential of the complex gives a higher catalytic activity since the donor atoms stabilize copper(I) [51]. This distinction has not been clear-cut as reports by Belle *et al.*[52] on dicopper(II) Schiff base complexes of (2,6-bis[(bis(2-pyridylmethyl)amino)methyl]-4-methylphenol) showed that modification on R-substituent induces a drastic effect on the catecholase activity: the presence of an electron donating group on the ligand increases this activity; the reverse effect is observed with an electron withdrawing group [52]. Clusters **14** and **16** in which metal complexes of p-acetamidophenol Mannich bases are more catalytically active than p-methylphenol counterparts is attributed to geometry (octahedral versus trigonal planar).

A more detailed explanation of this observation can be derived by considering the studies in the literature. Studies on metal complexes of other ligands including Schiff bases have yielded evidence to suggest that the presence of thiocyanate impacts negativity on the catecholase oxidase biomimetic abilities of their complexes using 3,5-DBTC as substrate [53, 54].

Reports from Barnes and Day [55] have suggested the perturbation of the d-orbital of the metal ions in the presence of thiocyanate group(s). They supported previous observation that coordination through sulphur causes less perturbation than coordination through the nitrogen of the thiocyanate ion because of their different arrangement in the spectrochemical series.

Also, Montazerozohori et al., in their study of various thiocyanate and azide complexes of new unsymmetrical Schiff bases of Zn, Cd and Hg noted that the thiocyanate complexes are quite

hard to reduce, electrochemically [56]. It is a known fact that reduction at the metal centre is a requirement for catecholase activity except for metals like nickel where a radical pathway mechanism has been postulated.

However, a positive inference can be drawn from the catalytic studies as the presence of thiocyanate afforded the formation of dinuclear complexes which sometimes exhibited increased catalytic efficiency compared to their mononuclear counterparts.

Biomimetic studies by Ramadan *et al.* [37] on cobalt Schiff bases on ascorbic acid and Pajan [57] work of cobalt complexes of Schiff bases on phenoxazinone synthase respectively have recently been reported. Their discussions included the impact of thiocyanate or isothiocyanate moieties on catalytic abilities that can provide some insight into what has been encountered in this research. Since all our metal complexes were derived from the same set of ligands, the higher reactivity in the absence of thiocyanate group in comparison to when present can only be explained in terms of lability of solvent or anion from the coordination sphere of the metal ion. As the thiocyanate ion is a stronger binding ligand than the of chloride ion or water molecule, it makes coordination of substrate to the metal center less favourable.

A leaving group, X (usually NCS or Cl) frequently must be dissociated to make a coordination site available for binding to 3,5-DBTC, O_2 or any reacting species during catalytic oxidation, and the important factor then is the strength of the metal-X bond itself. Coordination of Lewis-base, which is a better electron donor than halides, reduces the positive charge on the metal ion, weakening bonding between the metal ion and all other ligands. The effect is more pronounced for ligand in the trans- position to Lewis-base (trans influence) [58].

5.4 Identification and characterization of oxidation products by NMR spectroscopy

This procedure was carried out by making a further modification to the methods reported in the literature [59, 60]. The general catalytic procedure was followed using compounds (**18, 27**)

which demonstrated high catalytic ability as representatives of their respective groups. The reaction mixture was stirred for 48 hrs. The solvent was removed at the completion of the reaction. Then 7 mL of 1M HCl, saturated with NaCl, was added to the dry residue and the organic products were extracted with diethyl ether (3 × 30 mL). Precipitates were separated by the slow evaporation of the solvent, these were collected. Two staged column chromatography was carried out using chloroform and later diethyl ether as eluent. ^{1}H NMR spectroscopy was carried out using deuterated chloroform as solvent. The ^{1}H NMR spectrum of 3,5-DTBQ in $CDCl_3$ is given in Figure 5.31 below. Also, the coupling constant (J-value) are in agreement with those of meta-coupled protons.

^{1}H NMR ($CDCl_3$, 300 MHz): δ_H = 1.22 (s, 9H), 1.27 (s, 9H), 6.22 (d, J = 3.0 Hz, 1H), 6.92 (d, J = 3.0 Hz, 1H).

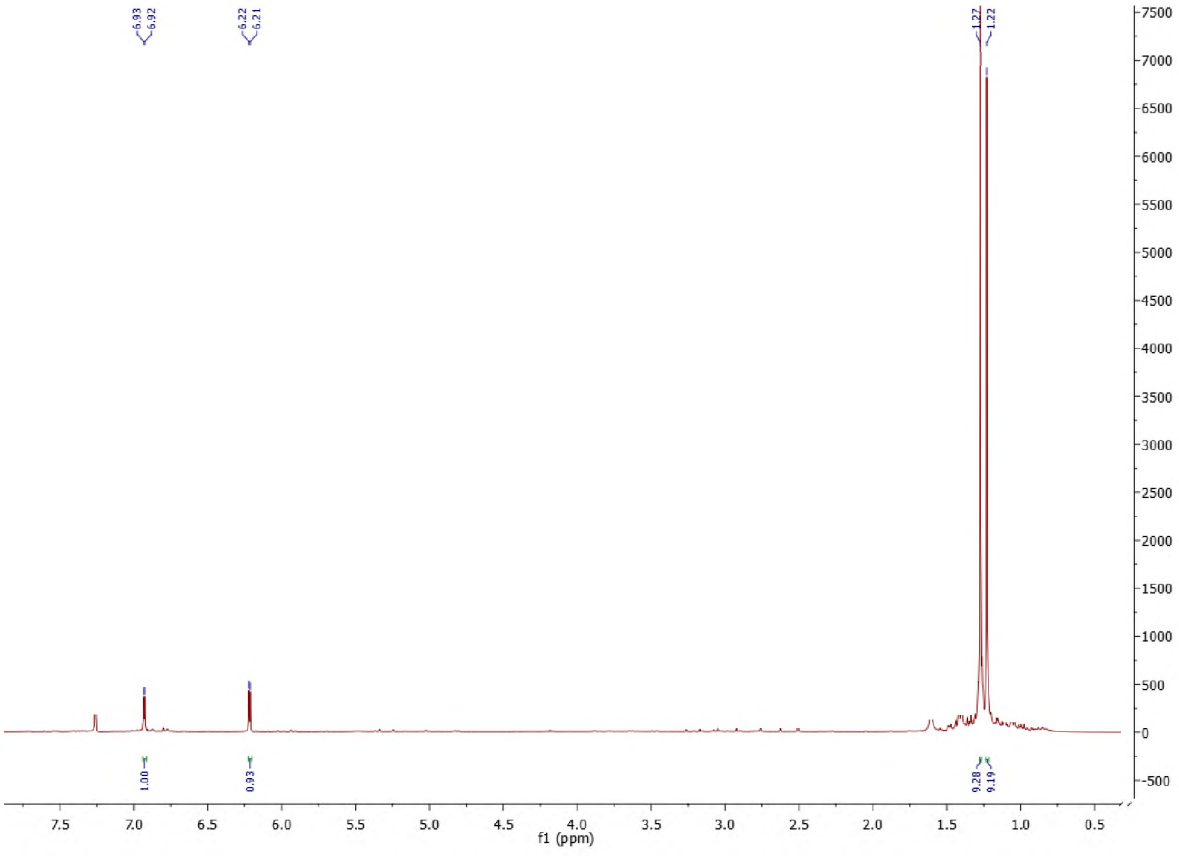

Fig. 5.31: ^{1}H NMR spectrum of 3, 5-DTBQ in $CDCl_3$.

Catechol oxidations assisted by copper ions usually result in either the production of o-quinones or ring-cleaved oxidation products like muconic acid or its derivative γ-lactone of the muconic acid ester [61]. However, it was found that the highly substituted catechols, like

DTBC, produce only quinones. This is due to the high redox potential of DTBQ [63]. In this study constituents of catalytic mixtures were identified by ^{1}H NMR to be DTBQ which is the principal reaction product after the formation/conversion of o-semiquinone as previously reported by Louloudi *et al.* [59].

These experiments show the formation of a stable radical at room temperature as reported from the ^{1}H NMR spectrum. The identification of an o-semiquinone radical in the catalytic mixture is consistent with our NMR findings where the observed paramagnetically broadened ^{1}H NMR signals can be attributed to the protons of this radical [63, 64]. EPR has previously also been used to establish the presence of the semi quinone radicals [65]. In general, the DTBQ formation as well as the o-semiquinone radical formation catalyzed by the present dicopper systems show similarities to the oxidation activity of the dicopper center of tyrosinase [60].

5.5 Spectrophotometric detection of H_2O_2 in the oxidation reaction

Hydrogen peroxide is an important product in the oxidation of the catalytic substrate, its identification from the reaction medium was carried out by adopting a method previously described [66, 67].

Reaction mixtures were prepared as in the kinetic experiments and the compounds (**18, 27**) demonstrated high catalytic activity as representatives of their respective groups. After 1 h of reaction an equal volume of water was added and the quinone formed was extracted three times with dichloromethane. The aqueous layer was acidified with H_2SO_4 to pH = 2 to stop further oxidation, and 1 mL of a 10% solution of KI and three drops of 3% solution of ammonium

molybdate were added. The presence of hydrogen peroxide is detected by the occurrence of the reaction;

$H_2O_2 + 2I^- + 2H^+ \rightarrow 2H_2O + I_2$, and with an excess of iodide ions, the triiodide ion is formed according to the reaction $I_{2(aq)} + I^- \rightarrow I_3^-$

The formation of I_3^- was monitored spectrophotometrically due to the development of the characteristic I^{3-} band ($\lambda = 353$ nm, $\varepsilon = 26000\ M^{-1}\ cm^{-1}$).

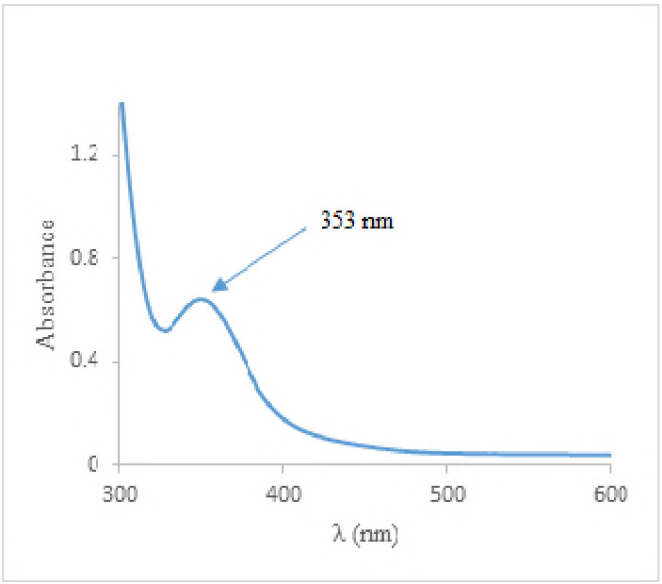

Fig. 5. 32: Spectrophotometric development of the characteristic I_3^- band.

References

1. W. S. Pierpoint, Biochem. J., **1969**, 112, 609 – 616.
2. J. W. Cary, A.R. Lax, W.H. Flurkey, Plant Mol. Biol., **1992**, 20, 245 – 253.
3. B.J. Deverall, Nature, **1961**, 189, 311 – 315.
4. P. Baruah, T. Swain, J. Sci. Food Agric., **1959**, 10, 125 – 129.
5. K. W. Wellington, P. T. Kaye, G. M. Watkins. Arkivoc, **2009**, 14, 301 – 313.
6. I. Szilagyi, L. Horvath, I. Labadi, K. Hernadi, I. Palinko, T. Kiss, Cent. Eur. J. Chem. **2006**, 4, 118 – 134.
7. R. Sanyal, S. K. Dash, S. Das, S. Chattopadhyay, S. Roy, D. Das, J. Biol. Inorg. Chem., **2014**, 19, 1099 – 1111.
8. P. Kar, R. Haldar, C. J. Gomez-García, A. Ghosh, Inorg. Chem., **2012**, 51, 4265 – 4273.
9. J. Mukherjee, R. Mukherjee, Inorg. Chim. Acta, **2002**, 337, 429 – 438.
10. C. S-Chuan, W. H-Hsiang, Inorg. Chim. Acta, **2002**, 340, 105 – 113.
11. K. W. Wellington, P. T. Kaye, G. M. Watkins, Arkivoc, **2008**, 17, 248 - 264.
12. R. Modak, Y. Sikdar, S. Mandal, S. Goswami, Inorg. Chem. Comm., **2013**, 37, 193 – 196.
13. A. Neves, L.M. Rossi, A.J. Bortoluzzi, A.S. Mangrich, W. Haase, R.J. Werner, Braz. Chem. Soc., **2001**, 12,747 – 754.
14. T. P. Camargo, F. F. Maia, C. Chaves, B. de Souza, A. J. Bortoluzzi, N. Castilho, T. Bortolotto, H. Terenzi, E. E. Castellano, W. Haase, Z. Tomkowicz, R. A. Peralta, A. Neves, J. Inorg. Biochem., **2015**, 146, 77 – 88.
15. A. Neves,A. J. Bortoluzzi, R. Jovito, R. A. Peralta, B. de Souza, B. Szpoganicz, A. C. Joussef, H. Terenzi, P. C. Severino, F. L. Fischer, G. Schenk, M. J. Riley, S. J. Smith, L. R. Gahan, J. Braz. Chem. Soc., **2010**, 21, 1201-1212.
16. F. Zippel, F. Ahlers, R. Werner, W. Haase, H.-F. Nolting, B. Krebs, Inorg. Chem., **1996**, 35, 3409 – 3419.
17. N. Singh, M.S. Hundal, G. Hundal, M.M. Ripoll, Tetrahedron, **2005**, 61, 7796 – 7806.
18. I.A. Koval, C. Belle, K.S.C. Philouze, A.A. Schuitema, P. G. Jean-Louis Pierre, J.J. Reedijk, J. Biol. Inorg. Chem., **2005,** 10, 739 – 750.
19. R. Sanyal, P. Kundu, E. Rychagova, G. Zhigulin, S. Ketkov, B. Ghosh, S.K. Chattopadhyay, E. Zangrando, D. Das, New J. Chem., **2016**, 40, 6623 – 6635.
20. K. A. Johnson, R. S. Goody, Biochem, **2011**, 50, 8264 – 8269.
21. H. Lineweaver, D. Burk, J. Am. Chem. Soc., **1934**, 56, 658 – 666.

22. A. Neves, L. M. Rossi, A. J. Bortoluzzi, B. Szpoganicz, C. Wiezbicki, E. Schwingel, Inorg. Chem., **2002**, 41, 1788−1794.
23. I. Majumder, P. Chakraborty, S. Das, H. Kara, S. K. Chattopadhyay, E. Zangrando, D. Das, RSC Adv., **2015**, 5, 51290 – 51301.
24. P. Chakraborty, J. Adhikary, B. Ghosh, R. Sanyal, S. K. Chattopadhyay, A. Bauza, A. Frontera, E. Zangrando, D. Das, Inorg. Chem., **2014**, 53, 8257−8269.
25. R. Sanyal, S. Ketkov, S. Purkait, F. A. Mautner, G. Zhigulinc, D. Das, New J. Chem., **2017**, 41, 8586 – 8597.
26. C-H. Kao, H-H. Wei, Y-H. Liu, G-H. Lee, Y. Wang, C-J. Lee, J. Inorg. Biochem., **2001**, 84, 171 – 178.
27. S. Anbu, M. Kandaswamy, Polyhedron, **2011**, 30, 123 – 131.
28. P. Chakraborty, I. Majumder, H. Kara, S. K. Chattopadhyay, E. Zangrando, D. Das, Inorg. Chim. Acta, **2015**, 436, 139 – 145.
29. J. Ackermann, F. Meyer, E. Kaifer, H. Pritzkow, Chem. Eur. J. **2002**, 8, 247 – 258.
30. A. Biswas, L. K. Das, M. G. B. Drew, G. Aromí, P. Gamez, A. Ghosh, Inorg. Chem., **2012**, 51, 7993 – 8001.
31. S. K. Dey, A. Mukherjee, New J. Chem., **2014**, 38, 4985 – 4995.
32. J. Mukherjee, R. Mukherjee, Inorg. Chimica Acta, **2002**, 337, 429 – 438.
33. A. Guha, T. Chattopadhyay, N. D. Paul, M. Mukherjee, S. Goswami, T.K. Mondal, E. Zangrando, D. Das, Inorg. Chem., **2012**, 51, 8750 – 8759.
34. R. Marion, N. M. Saleh, N. Le Poul, D. Floner, O. Lavastre, F. Geneste, New J. Chem., **2012**, 36, 1828–1835.
35. C-T. Yang, M. Vetrichelvan, X. Yang, B. Moubaraki, K. S. Murray, J. J. Vittal, Dalton Trans., **2004**, 113–121.
36. A. Neves, L. M. Rossi, A. J. Bortoluzzi, B. Szpoganicz, C. Wiezbicki, E. Schwingel, Inorg. Chem., **2002**, 41, 1788−1794.
37. M. Mitra, A. K. Maji, B.K. Ghosh, P. Raghavaiah, J. Ribas, R. Ghosh, Polyhedron, **2014**, 67, 19 – 26.
38. R. Kuttner, H. Wagreich, Achives Biochem. Biophy., **1953**, 80 – 87.
39. A. M. Ramadan, S. Y. Shaban, M. M. Ibrahim, J. Coord. Chem., **2011**, 64, 3376 – 3392.
40. J. Reim, R. Werner, W. Hasse, B. Krebs, Chem. Eur. J., **1998**, 4, 289 - 298.
41. X. Wang, J. Ding, J.J. Vittal, Inorg. Chim. Acta, **2006**, 359, 3481 - 3490.
42. P. Gentschev, N. Möller, B. Krebs, Inorg. Chim. Acta, **2000**, 300, 442 - 452.

43. E. Monzani, G. Battaini, A. Perotti, L. Casella, M. Gullitti, L. Santigostini, G. Nardin, L. Randaccio, S. Geremia, P. Zanello, G. Opromolla, Inorg. Chem., **1999**, 38, 5359 – 5369.
44. M. Thirumavalavan, P. Akilan, M. Kandaswamy, K. Chinnakali, G. S. Kumar, Inorg. Chem., **2003**, 42, 3308 – 3317.
45. M. Velusamy, M. Palaniandavar, M. Velusamy, M. Palaniandavar, Inorg. Chem., **2003**, 42, 8283 – 8293.
46. S. Majumder, S. Sarkar, S. Sasmal, E. C. Sanudo, S. Mohanta, Inorg. Chem., **2011**, 50, 7540 – 7554.
47. S. G. Bratsch, J. Phys. Chem. Ref. Data, **1989**, 18, 1 – 21.
48. J. Adhikary, P. Chakraborty, S. Das, T. Chattopadhyay, A. Bauza, S.K. Chattopadhyay, B. Ghosh, F. A. Mautner, A. Frontera, D. Das, Inorg. Chem., **2013**, 52, 13442−13452.
49. M.J. Mac Lachlan, M.K. Park, L.K. Thompson. Inorg. Chem., **1996**, 35, 5492 – 5499.
50. R. Mahalakshmy, R. Venkatesan, P. Sambasiva Rao, R. Kannappan, T.M. Rajendiran. Transition Met. Chem., **2004**, 29, 623 – 629.
51. K. S. Bharathi, S. Sreedaran, H. Priya, A. K. Rahiman, K. Rajesh, L. Jagadish, V. Kaviyarasan, V. Narayanan, J. Coord. Chem., **2009**, 62, 1356 – 1372.
52. C. Belle, C. Beguin, I. Gautier-Luneau, S. Hamman, C. Philouze, J. L. Pierre, F. Thomas, S. Torelli, Inorg. Chem., **2002**, 41, 479 – 491.
53. M. Das, R. Nasani, M. Saha, S. M. Mobin, S. Mukhopadhyay, Dalton Trans., **2015**, 44, 2299 – 2310.
54. P. Adak, C. Das, B. Ghosh, S. Mondal, B. Pakhira, E. Sinn, A. J. Blake, A. E. O'Connor, S. K. Chattopadhyay, Polyhedron, **2016**, 119, 39 – 48.
55. J.C. Barnes, P. Day, J. Chem. Soc., **1964**, 3886 – 3892.
56. M. Montazerozohori, K. Nozarian, H.R. Ebrahimi, J. Spec. Volume **2013**, Article ID 718149, http://dx.doi.org/10.1155/2013/718149
57. A. Panja, Polyhedron, **2014**, 80, 81 – 89.
58. G.H. Olive, S. Olive. Coordination and Catalysis, 1st Edn, Chap. 7, Verlag Chemie, Weinheim, New York (1977)
59. M. Louloudi, K. Mitopoulou, E. Evaggelou, Y. Deligiannakis, N. Hadjiliadis, J. Mol. Cat. A: Chemical, **2003**, 198, 231 – 240.
60. M. Mitra, P. Raghavaiah, R. Ghosh, New J. Chem., **2015**, 39, 200 – 205.
61. D.A. Rockcliffe, A.E. Martell, Inorg. Chem., **1993**, 32, 3143 – 3152.
62. D.A. Rockcliffe, A.E. Martell, J. Mol. Catal. A: Chemical, **1996**, 106, 211 – 221.

63. C.G. Pierpont, C.W. Lange, Prog. Inorg. Chem., **1994**, 41, 331.
64. A. De, D. Dey, H. R. Yadav, M. Maji, V. Rane, R M. Kadam, A. R. Choudhury, B. Biswas, J. Chem. Sci., **2016,** 128(11), 1775 – 1782.
65. M.M. Wick, L. Byers, E. Frei, Science, **1977**,197, 468 – 469.
66. A. I. Vogel, (1961)Textbook of quantitative inorganic analysis, Longmans, Green and Co. Ltd, London, 3rd edn, p. 366.
67. E. Monzani, L. Quinti, A. Perotti, L. Casella, M. Gullotti, L. Randaccio, S. Geremia, G. Nardin P. Faleschini and G. Tabbi, Inorg. Chem., **1998**, 37,553 – 562.

CHAPTER SIX

CONCLUSIONS AND FUTURE WORK

6.1 Research overview

In this research work, two classes of Mannich base ligands arising from p-acetamidophenol and p-methylphenol have been successfully synthesized and characterised, also four crystal structures have been reported. In addition, the Cu(II) and Fe(III) metal complexes of the ligands have been synthesized and characterised with the replacement of chloro ligands by thiocyanate or isothiocyanate substitution. The spectral properties of the metal complexes were studied and their catalytic properties investigated as catecholase biomimics.

Finally, biomimetic activity of the metal complexes of the Mannich bases synthesised was also investigated.

Highlights of the research are outlined below.

- A series of Mannich bases were obtained from p-methylphenol and secondary amines by refluxing in ethanol. The reactions are highly energy driven and require reflux for long hours; up to 24 hours. The phenomenon of polymorphism was encountered in one of the ligand series that was examined by various spectro-analytical techniques.
- A second series of acetamidophen-Mannich bases were synthesized. The synthetic process was milder than those above requiring only reflux in isopropanol over steam baths.
- The successful syntheses of the Cu(II) and Fe(III) complexes were achieved with protonating agent employed in the preparation of the metal complexes of the latter metal ion. All the complexes were characterised by various spectroscopic and analytical techniques.
- The successful introduction of thiocyanate groups into the coordination environment of the metal ion was successfully achieved as proven by data from infrared spectroscopy.

- Investigations into the potential catalytic activity of the metal complexes were successfully carried out with detailed kinetic examination of the catalytic process. The use of the substrate 3,5-DTBC (3,5-di-tert-butyl catechol) showed that the complexes are proven candidates in the field of biomimetics. Also, kinetic parameters (including V_{max}, K_M and k_{cat}) were comparable or sometimes higher than those previously reported in the literature.
- Finally, the presence of thiocyanate appear to lower the catalytic abilities of the metal complexes except in cases where the metal complexes are obtained as binuclear. This observation has lent credence to previously reported observations that the activation of molecular oxygen requires the presence of two metal ions in close proximity.

6.2 Future work

Future work is needed in the area of a detailed understanding of the catalytic pathway of these metal complexes and extending their applications. Possible continuations of the research work are outlined below.

- The catalytic pathway of the metal complexes needs to be examined in depth employing other methods like ESI-MS which are complementary to those earlier described in this research work.
- An investigation of the most active complexes should be conducted in various solvents of poor coordinating activity to compare the solvent behaviour of Mannich bases with those of Schiff bases.
- Investigation of catalytic promiscuity through the study of the catalytic abilities of these metal complexes to mimic dioxygenases, monooxygenases and tyrosinase would be a worthwhile endeavour.
- An investigation on the impact of bridging and non-bridging groups like azide, acetates and phosphines could be pursued in future.

- Optimising synthesis to target isostructural comparisons of the metal complexes in the mismatched series should be conducted.
- Since some of the ligands here prepared are novel, their bis-Mannich-bases should be synthesised.
- Finally, a number of Mannich bases and their metal complexes have been synthesised in this work. It would be interesting to have their biological activities investigated.